Energy & Environmental Science

REVIEW

View Article Online
View Journal | View Issue

Cite this: *Energy Environ. Sci.*, 2015, **8**, 3442

ZnO cathode buffer layers for inverted polymer solar cells

Zhiqiang Liang,[ab] Qifeng Zhang,[b] Lin Jiang*[a] and Guozhong Cao*[b]

Received 14th August 2015,
Accepted 28th September 2015

DOI: 10.1039/c5ee02510a

www.rsc.org/ees

This article provides an overview of the design, fabrication and characterization of the most widely used cathode buffer layers (CBLs) constructed using pristine zinc oxide (ZnO), doped-ZnO, and ZnO-based composites as well as the surface modified ZnO-based CBLs for the improvement of power conversion efficiency (PCE) and long-term device stability of inverted polymer solar cells (PSCs). To achieve high PCE in inverted PSCs, the selection of an appropriate material to form high quality CBLs so as to optimize the electron collection and transport is particularly important. ZnO has been the most extensively studied material for CBL of inverted PSCs in view of its relatively high electron mobility, optical transparency, ease of being synthesized with low cost solution methods at low temperature, versatile morphologies, and being environmentally stable. It is pointed out in this review that the electronic processes at the interface between the ZnO CBL and polymer active layer play an important role in determining the solar cells performance. This review attempts to deliver better understanding with regard of the impacts of (1) morphology, (2) thickness, (3) nanostructures, (4) doping, (5) surface modification and (6) composition/hybrids of ZnO CBLs on the inverted PSCs performance. Well understanding the interfacial processes in PSCs is believed also a benefit to the emerging perovskite solar cells in view of their similar energy levels and device structures.

Broader context

The photovoltaic technology of converting sunlight into electricity has been acknowledged as a promising way to meet the growing energy needs and the increasing concerns about carbon dioxide emission from the consumption of fossil fuels. In recent years, inverted polymer solar cells (PSCs) have attracted considerable attention due to their combined advantages of high power conversion efficiency, good stability, rapid energy payback time (EPBT), low-cost, and compatible with flexible substrate and roll-to-roll manufacturing. For the inverted PSCs, the device performance is strongly dependent on the optical and electrical properties of cathode buffer layers (CBLs) as well as the condition of the interface between CBLs and the active layer. Engineering the CBLs and the interface thereof has been considered as an essential issue for the next-stage development of PSCs towards high efficiency and good long-term stability. In this review, we focus on the rapid progress of the most widely used CBLs constructed using ZnO. The fabrication and characterization of CBLs with pristine ZnO, doped-ZnO, and ZnO-based composites and the surface modification of ZnO-based CBLs are described in detail, with the attempt to reach suggestions with regard to the strategies for fabricating inverted PSCs with high efficiency and long term device stability of inverted PSCs, so as to pave ways for their practical applications.

1. Introduction

Harnessing the abundant and renewable solar energy has been recognized as a promising way to address the quickly growing world's energy consumption and the increasing concerns about rapid increase in green-house gas emissions from the consumption of fossil fuels as the primary energy sources. Therefore, solar energy utilization is currently a leading research area for a CO_2-free and renewable energy supply. Many approaches have been proposed and studied extensively to harvest solar energy including solar thermal energy, photocatalytic and photo-electrochemical water splitting, and solar cells.[1–9] Among these technologies, the photovoltaic technology of converting sunlight directly into electricity is considered as one of the most promising and mature technologies.[7–10] Although silicon or other inorganic semiconductor solar cells and thin-film solar cells have been the most used solar cell systems because of their advantages of high efficiency and reliability, the high cost and slow energy payback time of these solar cells have limited

[a] *Institute of Functional Nano & Soft Materials Laboratory (FUNSOM), Jiangsu Key Laboratory for Carbon-Based Functional Materials & Devices, Collaborative Innovation Center of Suzhou Nano Science and Technology, Soochow University, Suzhou, Jiangsu 215123, China. E-mail: ljiang@suda.edu.cn*
[b] *Department of Materials Science and Engineering, University of Washington, Seattle, WA 98195-2120, USA. E-mail: gzcao@u.washington.edu*

their widespread applications. In recent years, polymer solar cells (PSCs) have attracted extensive interest as a potential alternative to conventional silicon-based solar cells, mainly due to their inherent advantages of being low-cost, and compatible with a flexible substrate and solution-based roll-to-roll processing technique.[8,9,11–14] In addition, the rapid energy payback time (EPBT) and low carbon emissions are also the major motivation for PSCs in future energy marketplace.[15,16]

Conventional PSC device architecture consists of a bulk-heterojunction (BHJ) active layer sandwiched between a transparent conducting electrode, such as indium tin oxide (ITO) glass, and a low-work-function metal electrode (which usually uses the Al material). The BHJ active layer is achieved by a blend of the p-type polymer donor and n-type fullerene acceptor materials dissolved in common solvent, and subsequent phase segregation results in the formation of two interpenetrated percolated networks during the annealing process after spin-coating. In such active layers, only excitons formed within a distance of ~20 nm from the p-type polymer donor/n-type fullerene derivative acceptor interface can reach the interface and then dissociate into free charge carriers.[13,17–19] The design criterion for the BHJ is to maximize the donor/acceptor interfacial area to provide possibly more exciton dissociation sites and form two interpenetrated continuous charge transport pathways in each material towards the corresponding electrodes.[13,17,18] Another outstanding merit of BHJ-based polymer solar cells is that the composite active

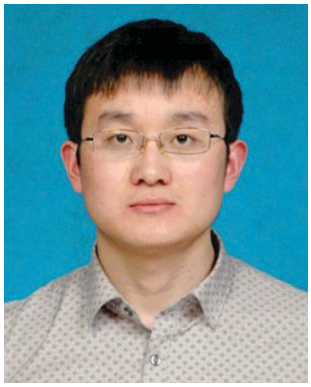

Zhiqiang Liang

Zhiqiang Liang is a lecturer at the Institute of Functional Nano & Soft Materials (FUNSOM), Soochow University, China. He received his MS and PhD degrees from Harbin Institute of Technology (Harbin, China), and BS from Anhui Polytechnic University (Anhui, China). He was awarded a scholarship under the State Scholarship Fund and worked as a joint PhD student at the Department of Materials Science of the University of Washington in the United States from 2010 to 2012. His current research is focused on the synthesis of nanomaterials and the application of nanomaterials in optoelectronic devices. Zhiqiang Liang can be reached at zqliang@suda.edu.cn.

Qifeng Zhang

Qifeng Zhang is currently working at the University of Washington as a Research Assistant Professor. His research interests involve engineering applications of nanostructured materials on electrical devices including solar cells, UV light-emitting diodes (LEDs), field-effect transistors (FETs), and gas sensors. His current research is focused on the synthesis of nanomaterials and the application of nanomaterials in electronic and optoelectronic devices, such as dye-sensitized solar cells (DSCs) and organic/inorganic hybrid solar cells. Qifeng Zhang can be reached at qfzhang@u.washington.edu.

Lin Jiang

Lin Jiang is a professor at the Institute of Functional Nano & Soft Materials (FUNSOM), Soochow University, China, a position she has held since 2012. She received her BS and PhD degrees in chemistry from Jilin University, Jilin, China, in 2000 and 2005, respectively. She was awarded the Alexander von Humboldt Research Fellowship in 2006 and worked at the Physical Institute of the University of Münster in Germany from 2006 to 2009. In 2009, she became a senior research fellow at the School of Materials Science and Engineering in Nanyang Technological University, Singapore. Lin Jiang can be reached at ljiang@suda.edu.cn.

Guozhong Cao

Guozhong Cao is a Boeing-Steiner Professor of Materials Science and Engineering, Professor of Chemical Engineering, and Adjunct Professor of Mechanical Engineering at the University of Washington, Seattle, WA. He received his PhD degree from Eindhoven University of Technology (the Netherlands), MS from Shanghai Institute of Ceramics of Chinese Academy of Sciences, and BS from East China University of Science and Technology (China). He has published over 300 SCI journal papers, authored and edited 7 books, and presented over 200 invited talks and seminars. His current research is focused mainly on chemical processing of nanomaterials for energy related applications including solar cells, lithium-ion batteries, and supercapacitors. Dr Cao can be reached at gzcao@uw.edu.

layer can be processed from a solution in a single step, making the fabrication of devices fully compatible with the roll-to-roll processing techniques.[13,18,20] Thus, the concept of BHJ was considered to establish the cornerstones of polymer solar cells.[21] In recent years, significant progress has been achieved on the improvement of the performance of PSCs.

The state of the art power conversion efficiencies (PCEs) of single junction PSCs with conventional structure exceeding 9%,[22–24] and higher than 10%[25] for tandem PSCs have been achieved in small area devices, which promises them a bright future in commercialization.

However, in spite of high PCEs, the PSCs with conventional architecture have suffered from some drawbacks that hinder the solar cells from practical applications. One of the major drawbacks of the conventional structure PSCs is the lack of long-term stability when exposed to air.[26–29] This is, on one hand, because the use of a low-work-function metal (*e.g.*, Al) such as cathode, which is sensitive to air and moisture and leads to the oxidization of the cathode quickly. On the other hand, in the conventional structure PSCs, the acidic PEDOT:PSS interfacial layer directly contacts the ITO glass and can etch the ITO resulting in a degradation of the device performance.[26–28,30] This has inspired the emergence of inverted structure polymer solar cells, in which the nature of charge collection is reversed.[12,31–33] Fig. 1a is a schematic showing an inverted polymer solar cell with a stacked structure of a transparent electrode (*e.g.*, ITO, FTO and AZO), an interfacial layer named as the cathode buffer layer (CBL), a BHJ active layer, an anode buffer layer (ABL) usually made of PEDOT:PSS, and a metal electrode with high-work-function such as Ag and Au. The structure of conventional PSCs is also schematically presented in Fig. 1b for comparison. It should be noted that in literature, the CBL is also named as the electron selective layer (ESL), the electron collection layer (ECL) or the electron transport layer (ETL), and the ABL is named as the hole selective layer (HSL), the hole collection layer (HCL) or the hole transport layer (HTL). For the sake of clarity and ease in presentation, the CBL and the ABL are used in this review unless specified otherwise.

In the inverted device architecture, the contact between the ITO and PEDOT:PSS is avoided, and meanwhile Al for the top electrode adopted in conventional PSCs is replaced with an air stable high-work-function metal, such as Au or Ag.[31,34] As a result, the inverted PSCs exhibit greatly improved ambient

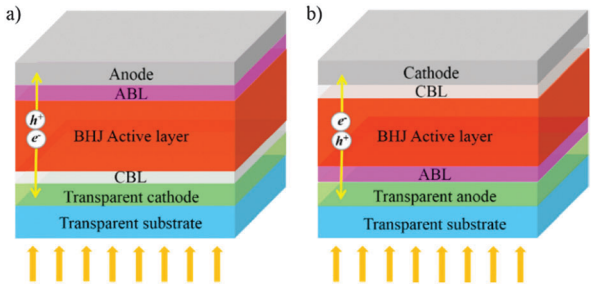

Fig. 1 Schematic illustration of device structures of (a) inverted and (b) conventional PSCs with bulk heterojunction active layers.

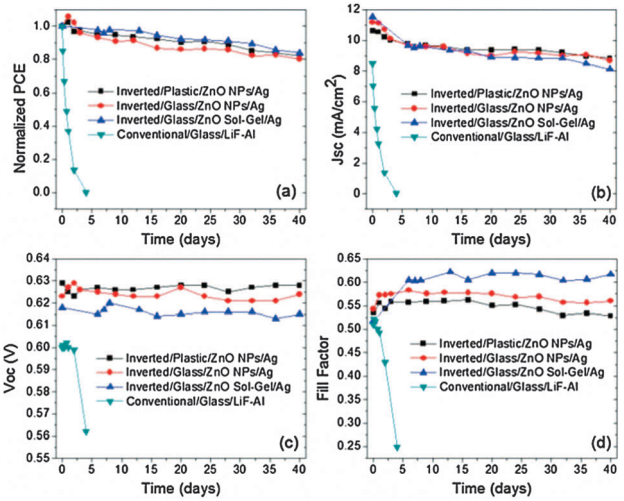

Fig. 2 Device performance of unencapsulated inverted PSCs with ZnO CBLs and conventional PSCs stored 40 days in air under ambient conditions. (a) Normalized PCE, (b) short circuit current density (J_{sc}), (c) open circuit voltage (V_{oc}), and (d) fill-factor (FF).[32] Adapted with permission from ref. 32 Copyright 2008 AIP Publishing LLC.

stability as compared to the PSCs with a conventional structure (Fig. 2), overcoming one big hurdle for possible widespread applications of PSCs.[32,33,35–38] Moreover, in the case of inverted solar cells, the high-work-function metal anode, such as Ag, can be prepared using either the coating or printing technology. These technologies are compatible with all solution processing methods and can therefore greatly simplify the fabrication process and lower the manufacturing cost of solar cells.[39–41] Another advantage of the inverted geometry is that it possesses higher flexibility in terms of the design of multi-junction or tandem solar cells compared to the conventional one.[13,25] In addition, the vertical phase separation mechanism, which describes the P3HT prone to accumulate on top of the electrode and the fullerene derivative at the bottom, also makes the inverted device configuration more advantageous compared to the normal configuration.[21,34,42–44] Despite the inverted PSCs having a lot of apparent merits, one shortcoming of the inverted device geometry is that the PCE is usually inferior to those of conventional PSCs in the initial stages of the study for inverted PSCs. But the study in recent years has overturned this situation and demonstrated that inverted PSCs can possess both long-term stability and high PCEs.[25,45–50] It has been reported that, through device engineering and using of new polymers, the state of the art PCEs of single junction inverted PSCs exceeding 10% have been achieved in small area devices, which are comparable to and even exceed the efficiencies of conventional ones.[47,49,51–54]

The study of the high PCE, stability and the roll-to-roll process has become three major directions in polymer solar cells.[25,30,55,56] The inverted PSCs seem to be the best candidates that meet the requirements for high efficiency, good stability, low cost and being compatible with the existing roll-to-roll process.[12,34,55,56]

The working mechanism of inverted PSCs can be described as follows. Under illumination, photo-generated excitons diffuse to the donor–acceptor (such as P3HT:PCBM) interface, where the

excitons dissociate due to a driving force in view of the energy level difference between the donor and the acceptor. The separated electrons will diffuse through the acceptor layer and are collected by the CBL, and ultimately reach the cathode electrode.[37] The CBLs in inverted devices are to (1) form an electron selective and transport interlayer, (2) block the reverse holes flowing from the donor polymer to the cathode, (3) adjust the energetic barrier between the active layer and the cathode, and (4) prevent the chemical or physical reaction between the active layer and the cathode. To achieve high power conversion efficiency in inverted polymer solar cells, the selection of an appropriate material to form the high quality CBL so as to optimize the electron collection and transport is particularly important. The key requirements for an ideal CBL include being good at electron extraction and transport, having a suitable energy level that facilitates electron transport, and having high transparency, good compactness, and high stability.

Recently, inorganic–organic organometal perovskite solar cells have emerged and are acknowledged as a new promising photovoltaic technology with respect to their tremendous progress in power conversion efficiency and potentially low-cost. In the past two years, the PCEs of perovskite solar cells have advanced from 15% to 19% and have now exceeded 20% on the basis of both planar and mesoscopic cell configurations.[57–66] However, perovskite solar cells also face the device stability problems, and this will determine their practical applications.[57,67–69] Similar to the polymer solar cells, it has been found that the selection and modification of a suitable interface layer could substantially improve the efficiency and stability of perovskite solar cells.[68,70–73] Therefore, the fundamental understanding of the rapid progress of interfacial engineering made in polymer solar cells would be beneficial to the development of perovskite solar cells, in addition to advancing the polymer solar cell itself. Compared to the existing photovoltaic (PV) technologies, perovskite solar cells exhibit very short energy payback time (EPBT).[74,75] Although perovskite solar cells are the youngest number in the PV family, they may become the most environmentally sustainable PV technology due to their potential for high efficiency, rapid EPBT and stable performance.[74,75]

Over the past few years, many semiconducting metal oxides (MOs) including zinc oxide (ZnO),[29,31,33,37,76,77] zinc tin oxide (ZTO),[78] titanium sub-oxide (TiO_x),[35,36,79–82] aluminum oxide (Al_2O_3),[83] and niobium pentoxide (Nb_2O_5)[84] have been studied to serve as the CBL in inverted PSCs. Besides the metal oxides, several polymers, such as hydrophilic conjugated 2,7-carba-zole-1,4-phenylene alternating copolymers PCP-NOH or PCP-EP,[85] cationic biopolymer poly(2-(dimethylamino)ethyl methacrylate) (PDMAEMA),[86] poly(amido amine) (PAMAM, generation 2),[86] poly(ethyleneimine) (PEI)[87] and conjugate polyelectrolyte poly-[(9,9-bis(3′-(*N*,*N*-dimethylamino)propyl)-2,7-fluorene)-*alt*-2,7-(9,9-ioctylfluorene)] (PFN),[45,51,88] and PFPA1[89] have also been studied for inverted PSCs to work as efficient CBL materials. In addition, some other materials such as ZnS,[90] CdS,[91,92] cesium carbonate (Cs_2CO_3),[93–96] $SrTiO_3$,[97] $SrTiO_3$:ZnO composites,[98] MoO_3–Al composites,[99] In_2S_3,[100,101] ionic liquid-functionalized carbon nanoparticles (ILCNs),[102] sodium hydroxide (NaOH),[103] zwitterions,[104] amino acid (serine),[105] amino-functionalized fluorene oligomers,[106] ionic liquids (ILs),[53] and the low work function metals (such as Al, Mg and Ca)[107] have also been investigated as CBLs in inverted PSCs. Another low work function metal, lanthanum (La), can also serve as a cathode interlayer material for PSCs with conventional structure.[108] Graphene as a promising two-dimensional nanomaterial with outstanding electronic, optical, thermal, and mechanical properties has also been used in inverted PSCs to serve as the CBL.[109–111]

For inverted PSCs, the device performance critically relies on the type of the CBL material and the condition of the interface between the CBL and the BHJ active layer. Among the materials mentioned above, ZnO is the most extensively investigated one for CBLs in the inverted PSCs, mainly due to its suitable energy levels, high electron mobility, good transparency, environmental stability and low cost.[13,29,31,32,37,55,76,112,113] The energy levels of ZnO (conduction band bottom and valence band top) are at around −4.4 eV and −7.8 eV, respectively. Such band positions allow ZnO to function well for electron collection and hole blocking. The relatively high electron mobility of ZnO makes it a suitable material for cathode buffer layers to reduce the charge recombination. The good transparency in the whole visible spectrum benefits in lowering the optical loss and the band edge cut-off of ZnO at around 375 nm can block UV light and accordingly protect the organic materials from photodegradation under UV light irradiation.[33,43] For single junction inverted PSCs, the state of the art PCEs of ~10% have been achieved by using ZnO or ZnO-based CBLs.[46,47,49,52,53,114] Another merit of ZnO as the CBL material is that it can be easily processed *via* a solution method with subsequent thermal treatment at relatively low temperatures. This makes the ZnO fully compatible to all solution roll-to-roll fabrication on flexible plastic substrates which is the predominant advantage of polymer solar cells.[29,55,115–118] Almost all of the reported inverted PSCs fabricated using the roll-to-roll processing technique are based on ZnO thin layers as CBLs.[40,41,56,116,119,120] Due these features and merits mentioned above, ZnO has been identified as a good material to serve as the CBL in inverted PSCs.

Shirakawa *et al.* were the first group to demonstrate the application of a ZnO film as the cathode interfacial layer in an organic photovoltaic cell with a stacked structure of ITO/ZnO/C60/PAT6/Au.[17] The first inverted polymer solar cells based on a sol–gel processed ZnO thin film on ITO as the CBL and a P3HT:PCBM BHJ active layer was pioneered by White and co-workers in 2006.[31] Significant progress has been made in the past few years in this area, with the research focused mainly on the preparation method and modification of ZnO buffer layers. However, due to the use of different polymers for the construction of solar cells and different methods for the fabrication of the cathode buffer layer, it is hard to make a fair comparison of the effects of the cathode buffer layer. In recent years, many papers have reviewed the photovoltaic materials of active layers and electrode buffer layers, cell architectures, interfacial layer engineering, and the device operation mechanisms of polymer solar cells.[7,8,12–14,19,25,30,37,44,55,56,121–127] However, as one of the most extensively used CBL in inverted PSCs,

so far no paper has provided a comprehensive review on the progresses and perspectives of ZnO and ZnO based CBLs. This review article intends to fill this gap and provide a comprehensive overview of the design, fabrication, and characterization of ZnO, doped-ZnO, and ZnO-based composite CBLs as well as their surface chemistry and morphology modification for inverted PSCs. The development of ZnO cathode buffer layers will make an important contribution to the fabrication of PSCs with high power conversion efficiency and long-term stability at a large scale for their practical applications.

2. ZnO cathode buffer layers in inverted PSCs

2.1 ZnO as a good fit for CBLs in inverted PSCs

In the polymer solar cells with inverted geometry, a ZnO film inserted between the BHJ active layer and the cathode can function as a CBL to extract and transport electrons, and simultaneously block the reverse flow of holes from the donor polymer to the cathode. The good fit of ZnO as a CBL in inverted PSCs first of all originates from its suitable energy levels. Fig. 3 shows a schematic diagram of the energy levels and the transport directions of electrons and holes in an inverted structure solar cell consisting of a ZnO cathode buffer layer and a P3HT:PCBM active layer. It can be seen that, on one hand, the conduction band bottom of ZnO at −4.4 eV is lower than the lowest unoccupied molecular orbital (LUMO) of the fullerene derivative acceptor (for example, −3.8 eV and −3.74 eV for PCBM and ICBA, respectively), meaning that ZnO CBLs can help in extracting and collecting electrons in the fullerene derivative acceptor.[37,128] It has been reported that the electron transport from PCBM to ZnO does not result in a significant energy loss.[31] On the other hand, the valence band top of ZnO at ~−7.8 eV is lower than the highest occupied molecular orbital (HOMO) of the polymer donor (for example, −5.0 eV for P3HT). As a result, the reverse flow of holes from the polymer donor to the ITO cathode is blocked by the great energy barrier at the P3HT/ZnO interface.

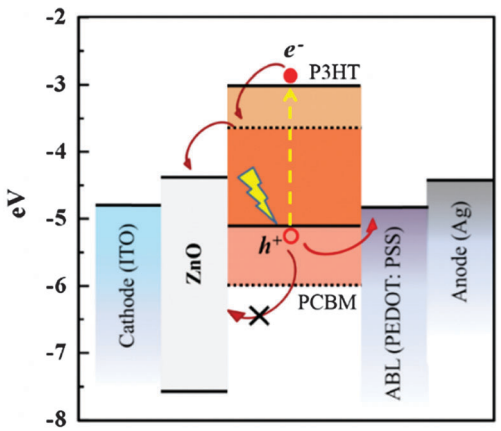

Fig. 3 Schematic illustration of the energy level and the main charge transportation of an inverted PSC with the ZnO CBL and P3HT:PCBM active layer.

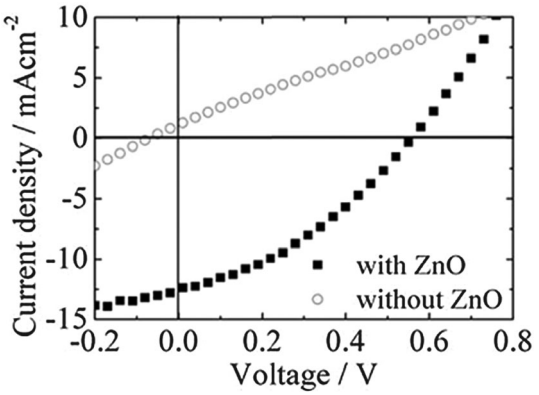

Fig. 4 The *J*–*V* curves of the inverted PSCs with and without ZnO CBL.[77] Adapted with permission from ref. 77 Copyright 2010 The Royal Society of Chemistry.

This means that the ZnO CBL can prevent the generation of leakage current at the polymer/ITO interface. That is why the inverted PSCs with ZnO CBLs have been found to dramatically improve photovoltaic performance compared to those without a ZnO CBL.[33,43,77,129,130]

In a study done by Liu *et al.*, it was reported that the devices with and without ZnO CBLs presented different shapes of the *J*–*V* curve, as shown in Fig. 4.[77] Such a difference in the *J*–*V* curve was attributed to the converse directions of charge transport, suggesting the function of ZnO CBLs in transporting electrons and blocking holes.[77] Yang *et al.* have also studied inverted PSCs constructed with solution processed ZnO thin films as a CBL, PsiF-DBT:PCBM blend as a BHJ active layer, a MoO_3 thin film as an anode buffer layer (ABL), and an Au electrode as an anode.[33] It was found that, due to the use of ZnO, the series resistance (R_S) of solar cells decreased from 56 Ω cm^2 to 13 Ω cm^2 and the shunt resistance (R_{SH}) increased from 600 Ω cm^2 to 1400 Ω cm^2 giving rise to a dramatic enhancement in the solar cell PCE, which increases from 1.67% to 3.80%. A high R_{SH} means a low current leakage or energy loss across the solar cell.[33,131] Table 1 shows a summary of device characteristics of representative inverted PSCs with or without ZnO CBLs. The values shown in brackets are obtained for the solar cells without CBLs, exhibiting much lower efficiencies than those using CBLs for the reason of severe charge recombination. These results are great evidence that the ZnO films can efficiently work as hole-blocking layers to prevent the current leakage.

2.2 Fabrication of ZnO cathode buffer layers

The performance of inverted PSCs can be significantly affected by the method used for the preparation of ZnO CBLs, which influences the morphology, thickness, crystallinity, and the optical and electrical properties of the resulting CBL. Various methods have been employed for the fabrication of ZnO thin films to serve as the CBL in inverted PSCs. In general, the fabrication methods for ZnO CBLs can be grouped into: (1) solution processing, mostly the sol–gel method,[29,31,33,38,76,132–142] (2) solution method derived from pre-fabricated ZnO NP suspensions or aqueous ZnO hydrate,[32,77,119,143–146] (3) atomic layer deposition (ALD),[129,147–151]

Table 1 Non-exhaustive survey of inverted PSCs with or without ZnO CBLs. The photovoltaic parameters are compared to those measured for a reference cell (values in parentheses) without ZnO CBLs

Device architecture	J_{sc} [mA cm^{-2}]	V_{oc} [V]	FF [%]	PCE [%]	Ref.
ITO/ZnO/P3HT:PsiF-DBT/MoO_3/Au	5.03 (4.23)	0.90 (0.81)	60 (39)	3.80 (1.67)	33
ITO/ZnO(SP)/P3HT:PCBM/WO_x/Al	10.03 (8.91)	0.48 (0.41)	53 (50)	2.56 (1.76)	43
ITO/ZnO(ED)/P3HT:PCBM/WO_x/Al	10.08 (8.91)	0.55 (0.41)	66 (50)	4.00 (1.76)	43
ITO/ZnO/P3HT:PCBM/MoO_3/Ag	11.9 (8.5)	0.59 (0.33)	0.6 (0.31)	4.18 (0.57)	129
ITO/ZnO/P3HT:PCBM/MoO_3/Au	12.05 (10.9)	0.59 (0.40)	49.8 (39.8)	3.54 (1.74)	156
ITO/ZnO/P3HT:PCBM/PEDOT:PSS/Ag	8.41 (6.86)	5.65 (4.26)	53.9 (29.2)	2.56 (0.85)	162
ITO/ZnO/PCDTBT12:$PC_{71}BM$/MoO_3/Al	9.78 (9.57)	0.98 (0.59)	57.7 (46.4)	5.53 (2.62)	130
ITO/ZnO/PTB7:$PC_{71}BM$/MoO_x/Ag	14.64 (16.16)	0.75 (0.48)	64.75 (45.27)	7.11 (3.48)	48

(4) spray pyrolysis,[43,152,153] (5) metal organic chemical vapor deposition (MOCVD),[154] (6) mist pyrolysis chemical vapor deposition (MPCVD),[155] (7) radio-frequency sputtering (RF),[156] (8) magnetron sputtering,[157,158] (9) fine-channel mist-spray coating,[159] (10) chemical bath deposition (CBD),[160] and (11) electro-deposition (ED).[43] Among these methods, the solution processing and deposition methods have been the most popular ways to make ZnO CBLs for inverted PSCs, due to their high-quality, ease of preparation at a relatively low temperature, without requiring any vacuum instrument and low cost.

2.2.1 ZnO CBLs fabricated with sol–gel processing. The sol–gel method using a mixture of zinc acetate [$Zn(OAC)_2$] and 2-ethanolamine in methoxyethanol (MEA) as precursors is a widely used approach for the fabrication of ZnO CBLs for inverted PSCs. ZnO thin films obtained using this method present good surface quality, excellent optical transmittances and electrical properties. Moreover, this is a low-cost process that does not involve any expensive and/or vacuum instruments.[29,132,161] In addition, the features of low temperature and solution processing make the sol–gel method compatible to roll-to-roll manufacturing for the fabrication of inverted PSCs on flexible plastic substrates, which is one of the important advantage of PSCs.[29,55,115]

In the sol–gel method, the post heat treatment process is adopted to convert the spin-coated gel film to crystalline ZnO and is a factor which can significantly affect the optical and electrical properties of ZnO films as well as the photovoltaic performance of the inverted PSCs. First, the heat treatment temperature is required to be higher than the boiling points of the solvents (2-methoxyethanol and MEA at 125 °C and 170 °C, respectively) to get the solvents completely evaporated.[161,163] Second, it has been demonstrated that, when heated in air, $Zn(OAC)_2$ begins to thermally decompose at 190 °C, its thermal decomposition completed at around 310 °C, and the formation of crystalline ZnO at the temperature between 300 °C and 400 °C. A higher annealing temperature ranging from 400–500 °C is identified as the most efficient temperature for the thermal decomposition of $Zn(OAC)_2$ to form crystalline ZnO.[164]

The electron mobility of sol–gel processed ZnO films as well as the device performance of inverted PSCs based on these ZnO films as the CBL would be promoted by improving the crystallinity of ZnO. However, there have been conflicting reports of the optimized annealing temperature of sol–gel processed ZnO CBLs for inverted PSCs in the literature.[29,33,38,137,142,165,166] The optimal annealing temperature reported in the literature range from 100 °C to 450 °C.[26,30,35,134,140,160,161] Zhang *et al.* reported that the inverted PSCs using sol–gel processed ZnO CBLs exhibit a clear improvement in the device performance upon increasing the ZnO sintering temperature from 100 °C to 350 °C.[137] It was observed that R_S of the inverted devices decreased with an increased sintering temperature and it reached a minimal value when the sintering temperature increased from 100 °C to 350 °C, as a result an improved device performance (PCE = 2.58%) was achieved. Such a performance improvement was ascribed to the improved ZnO quality in view of a relatively high sintering temperature, which effectively promoted the electron mobility of sol–gel processed ZnO films by improving the crystallization of ZnO. However, the need of a high annealing temperature above 300 °C hampers the advantage of PSCs compatible with flexible substrates, such as polyethylene terephthalate (PET), which usually cannot withstand a high temperature treatment process. Additionally, the high annealing temperature processes will also lead to the degradation of the conductivity of the cathode (*i.e.*, ITO) and thus degrades the device performance.[137,166]

In order to overcome these constraints, the sol–gel derived ZnO CBLs annealed at a relatively low temperature have been studied.[29,33,38,137,166] Sun *et al.* fabricated sol–gel derived ZnO CBLs obtained at the temperatures of 130 °C, 150 °C and 200 °C.[29] They found that the ZnO films annealed at 200 °C were able to function as an efficient electron transporting layer in inverted solar cells, leading to a PCE as high as 6.33% for the inverted devices constructed with the PCDTBT:$PC_{70}BM$ active layer. In addition, the inverted devices based on those low temperature (130 °C, 150 °C and 200 °C) annealed ZnO buffer layers exhibit a promising long-term stability. For example, the PCEs retain above 70% of their original value even after being exposed to air at room temperature for more than 30 days (without encapsulation).[29] In sharp contrast, for the unencapsulated solar cells with the PCDTBT:$PC_{70}BM$ active layer and in the conventional structure, the PCE decreases significantly under the same conditions.[29]

Some research revealed that the ZnO films annealed at 200 °C were amorphous instead of being crystalline, and as a result their electron transporting properties ($\sim 1.3 \times 10^{-4}$–2.6×10^{-5} cm^2 V^{-1} s^{-1}) are not as good as those of the crystalline ZnO (~ 1 cm^2 V^{-1} s^{-1}).[33,38,142] However, it seems because the electron mobility of this amorphous ZnO is comparable to that of most organic materials for PSCs, the device

performance is not apparently affected by the relatively poor conduction of amorphous ZnO.[33] By using the low temperature annealed amorphous ZnO CBL and PTB7-F20/$PC_{71}BM$ blend active layers, Park *et al.* prepared inverted PSCs and reached a J_{sc} of 13.93 mA cm^{-2}, a V_{oc} of 0.71 V, a FF of 0.65, and a PCE of 6.42%, plus long-term stability.[142] Recently, Jagadamma *et al.* reported the use of sol–gel driven amorphous ZnO CBLs annealed at a lower temperature ($\sim$100 °C) for inverted PSCs to minimize the degradation to flexible plastic substrates.[140] They demonstrated that the sol–gel driven amorphous ZnO layers annealed at such a low temperature delivered the solar cell performance comparable to the best devices based on ZnO films prepared at substantially higher temperature. In their results, the inverted PSCs based on these amorphous ZnO CBLs and constructed using low band-gap polymer donors on glass/flexible PET substrates show performances of PTB7:$PC_{71}BM$ (PCE: 6.5% (glass)/5.6% (PET)) and PBDTTPD:$PC_{71}BM$ (PCE: 6.7% (glass)/5.9% (PET)).[140] More recently, Morvillo *et al.* investigated the performance of the inverted PSCs based on sol–gel deposited ZnO CBLs annealed at different temperatures (100, 150, 200, 250 and 300 °C) for 5 or 10 min.[166] They found that the sheet resistance of the ITO increased linearly with the increase of annealing temperatures and times, which, in turn, contributes to the reduction of the FF and the PCE of the corresponding devices. As a result, the highest PCE (7%) was achieved for the device fabricated using a ZnO CBL annealed at 150 °C for only 5 min. Therefore, recently, most of the sol–gel processed ZnO CBLs adopted heat treatment at a relative low temperature ($<$200 °C) due to the comparable performance and compatible with the solution processing technique of inverted PSCs fabricated on flexible substrates.

During the post annealing process, the annealing environment, such as humidity and vacuum, can also affect the electrical properties of ZnO CBLs to some extent.[167] Lin *et al.* found that a thermal treatment (150 °C) of the solution processed ZnO CBLs in a vacuum could help further reduce the defects and increase the electron mobility in the low temperature processed ZnO film (up to 0.36 cm^2 V^{-1} s^{-1}), and thus improve the electron extraction in inverted PSCs.[167] Besides the annealing temperature and annealing environment, the concentration of the ZnO precursor is another key factor largely affecting the quality of ZnO CBLs derived from a sol–gel route. In general, a relatively low sol concentration ($\sim$0.1–0.3 M) is more prone to yield a ZnO film with high quality, reflecting on denser films, lower surface roughness, and higher transmittance.[38,132,137,167] This is because a low sol concentration can form small nano-sized ZnO colloids and small grain sizes. As a result, the inverted devices based on dense ZnO CBLs exhibit a low reverse current and contact resistance between the ZnO layer and the active layer owing to the full coverage of the ITO surface and an intimate contact between the ZnO and the active layer, and as a result the overall R_S is reduced, giving rise to enhanced photovoltaic performance.[132,137] On the contrary, a relatively high sol concentration ($\sim$0.5–0.75 M) is usually prone to result in a ZnO film with larger surface roughness and even voids. The rough surface and the existence of voids in ZnO buffer layers would result in an increase in R_S, due to the inferior contact between the ZnO buffer layer and the photoactive layer.[37,132,137] However, it has also been demonstrated that ZnO buffer layers having both dense and smooth surfaces and a large surface area could be obtained by using a slow ramp annealing method to heat treat the wet gel film derived from the ZnO sol with relatively high concentrations (*i.e.*, 0.75 M).[138,139] It was explained that a low heating rate in the ramp annealing process provided sufficient time for the gel particles to structurally relax and pile up, resulting in a dense and undulated film.[138,139] More recently, it was reported that the type of ZnO precursor could also affect the properties of the sol–gel processed ZnO CBL, and thus impacts the device efficiency and stability.[168] It has been reported that the inverted PSCs with ZnO layers derived from diethylzinc are more stable than the devices with ZnO layers prepared by decomposing zinc acetate under long term illumination.[168] The difference in device stability was attributed to the different chemical nature of ZnO surfaces, specifically the presence of interstitial zinc (Zn_i) defects at the ZnO surface and their subsequent interactions with the adjacent active layer. It was explained that the ZnO layers derived from diethylzinc (deZn) possessed less Zni defects than the ZnO layers deposited from zinc acetate ($Zn(OAC)_2$).[168] Overall, to achieve a high quality ZnO CBL using the solution processed sol–gel method, the type of ZnO precursor as well as the concentration, and the post heat treatment temperature and environment should be considered comprehensively.

2.2.2 ZnO CBLs derived from pre-fabricated ZnO nanoparticle suspensions or aqueous ZnO hydrate. Besides the sol–gel method, another widely used solution processing method to deposit ZnO CBLs is spin-coating the pre-fabricated ZnO nanoparticle (NP) suspensions or colloids, synthesized using a hydrolysis and condensation of zinc acetate dihydrate under low temperature.[12,32,77,119,143–146,169] The resulting ZnO NPs demonstrated good electron mobility ($\sim$0.066 cm^2 V^{-1} s^{-1}) even though no additional post-thermal treatment was applied.[170] Hau *et al.* prepared ZnO NP CBLs (50 nm in thickness) with a dense and homogenous surface (Fig. 5) by spin-coating pre-fabricated colloidal ZnO NPs.[12,32] They found that the inverted devices with the ZnO NP CBLs exhibited performance comparable to that of devices based on sol–gel processed dense ZnO CBLs treated at a high temperature (400 °C). Qin *et al.* found that there were a large number of hydroxyl (–OH) groups formed on the ZnO NPs synthesized by hydrolysis and condensation of zinc acetate dehydrate.[146] It was suggested that the surface hydroxyl groups could depredate the photoactive layer by elevating the photocatalytic activity of ZnO, and hence deteriorate the device performance. Fortunately, the hydroxyl groups could be effectively detached from the ZnO NPs by annealing at a low temperature, $\sim$150 °C.[146] The low temperature treatment and the scalable processing capability make the colloidal ZnO NPs well compatible with the solution processing technique for inverted PSCs fabricated on flexible substrates. Krebs *et al.* have successfully employed the solution processed ZnO NP layers as CBLs for the complete roll-to-roll printing process to manufacture inverted PSCs on a large scale.[41,116] Recently, Spyropoulos and

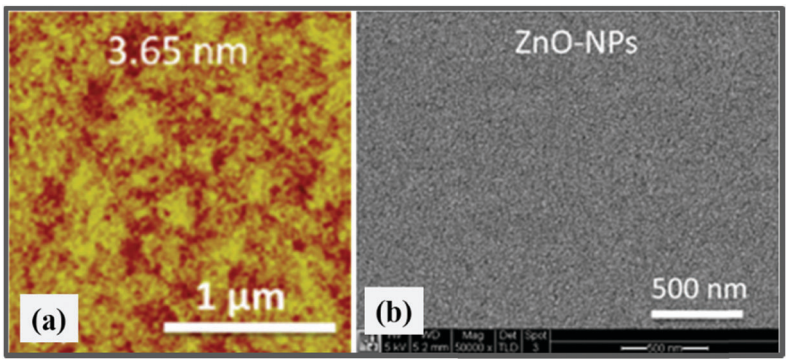

Fig. 5 (a) AFM and (b) SEM images of ZnO NP thin films.[169] Adapted with permission from ref. 169 Copyright 2010 American Chemical Society.

co-workers reported the fabrication of flexible organic tandem solar modules with a PCE as high as ~6% by using ZnO NP CBLs combined high throughput roll-to-roll compatible processing.[120]

However, the ZnO NPs in suspension are not very stable and are sensitive to the moisture. Therefore, an appropriate ligand is usually required to be attached onto the NPs to stabilize them to avoid aggregation. To prevent the aggregation of ZnO NPs and to fabricate ZnO films with a smooth surface are important for the achievement of high performance inverted PSCs.[108,132–134,171] Therefore, a major challenge of this method is to achieve spatial distribution of individual NPs and gain high electron mobility without the high temperature annealing process.[172–174] The improvement of spatial distribution of ZnO NPs by using polymeric or organic molecules as a matrix/surfactant has been reported by several groups.[144,172–174] However, it should be noted that the removal of the surfactant material from ZnO films is required to optimize the properties of ZnO CBLs as well as the device performance, due to the fact that surfactant materials may reduce the electron transport by introducing additional resistance.[172,173] Besides the surfactant, the solvent of the ZnO NP solution also plays an important role in the ZnO NP dispersion and the morphology of ZnO NP films. Li *et al.* reported the study of the control of ZnO NP aggregation in solution by adjusting the solvent ratio (chloroform *vs.* methanol).[171] They found that when the ratio of chloroform : methanol was 1 : 1 (v/v), the superior dispersity of ZnO NPs in solution and a consequent ZnO film with compact and homogeneous surface could be obtained. As a result, a remarkable PCE of 8.54% in inverted PSCs based on the PTB7:$PC_{71}BM$ active layer was achieved. Besides the use of colloidal ZnO NPs, Chen *et al.* achieved ultrathin (~4 nm) ZnO CBLs by spin coating an aqueous zinc oxide hydrate ($ZnO{\cdot}xH_2O$) solution.[175] They demonstrated that a post annealing temperature can be as low as 80 °C due to the low energy metal-ammine dissociation and hydroxide condensation/dehydration chemistry. The inverted devices with the ultrathin ZnO CBLs and PCDTBT:$PC_{71}BM$ photoactive layers show a high PCE, up to 6.48%, which is comparable to those devices based on ZnO CBLs deposited by the sol–gel process using zinc acetate and annealed at 200 °C.[175]

2.2.3 ZnO CBLs fabricated using the atomic layer deposition method. Besides the above-mentioned solution approaches, there are several other methods for the fabrication of ZnO CBLs, including atomic layer deposition (ALD),[129,148–150] spray pyrolysis,[43,152,153] metal organic chemical vapor deposition (MOCVD),[154] mist pyrolysis chemical vapor deposition (MPCVD),[155] radio-frequency sputtering (RF),[156] magnetron sputtering,[157,158] and fine-channel mist-spray coating.[159] Among these methods, the ALD technique is regarded as a very promising approach for fabricating the ZnO CBLs for inverted PSCs in view of the capability of ALD in producing a high surface quality film at a relatively low temperature and controlling the film thickness precisely.[148]

Wang *et al.* deposited the ZnO CBL on the plastic substrate, ITO/PEN, using the ALD method at low temperatures (45 °C and 80 °C) for flexible inverted PSCs.[129] They found that the devices with ZnO grown at 80 °C presented enhanced photovoltaic performance compared to the devices with ZnO grown at 45 °C, for the reason that the former achieved a smoother and more hydrophobic surface than the latter. The authors suggested that the smoother and more hydrophobic surface of ZnO was beneficial to the contact quality between the ZnO and the active layer, thus leading to reduced series resistance and improved electron transport to the ITO electrode. It is worth pointing out that, besides the morphology, the ALD temperature also affects the electrical properties of the grown ZnO films.[176] Chang and Tsai found that both the electron mobility and electron concentration of the ZnO CBL increased with increasing deposition temperature for the reason of increased crystallinity.[149] In their results, the best inverted device was achieved by using a ZnO CBL (60 nm in thickness) deposited at 90 °C and exhibited a PCE of 4.1%, high R_{SH}, and low R_S.[149] An atmospheric atomic layer deposition (AALD) method was also developed to grow ZnO thin layers in ambient atmosphere to avoid the slow and vacuum-based process in conventional ALD.[150] It has been demonstrated that the AALD ZnO layers possessed compact surface, high electron mobility (3.4 ± 0.1 cm^2 V s^{-1}) and good transmittance to visible light. As a result, the inverted BHJ P3HT:PCBM PSCs with AALD ZnO CBLs exhibited a PCE of 3.6% and good device stability in air. Compared with the conventional ALD route, such an AALD method allows the ZnO layer to be deposited more rapidly in air, and thus has higher potential for implementation in a throughput roll-to-roll process.

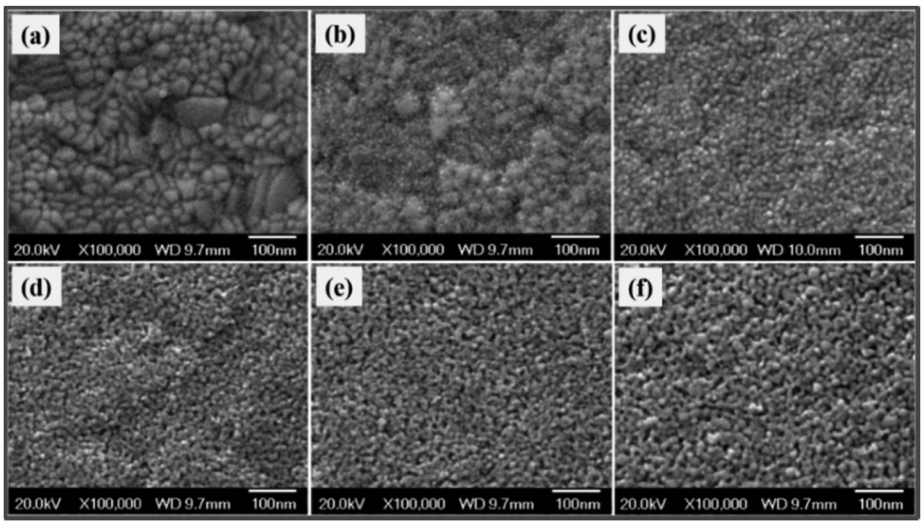

Fig. 6 The SEM images of ZnO layers derived from sol concentrations of (a) 0.02, (b) 0.05, (c) 0.1, (d) 0.3, (e) 0.6, and (f) 1 M, respectively.[132] Adapted with permission from ref. 132 Copyright 2012 Wiley-VCH Verlag GmbH & Co. KGaA.

2.3 The impacts of the morphology of ZnO CBLs on the performance of inverted PSCs

The photovoltaic performance of the inverted PSCs depends critically on the electrical properties of the interface between the ZnO CBL and the active layer. The condition of the interface is largely related to the contact quality and the contact area.[13,37,132,177] Therefore, the control of the morphology of ZnO CBLs is an important aspect to tune the contact quality so as to achieve the full potential of inverted PSCs.

In a work done by Liang *et al.*,[132] the ZnO CBL was prepared using a sol–gel method and its morphology was controlled by adjusting the concentration of the precursor sol. Fig. 6a–f exemplify the morphological change when the concentration of the precursor sol changes from 0.05 to 1 M. The PCE of 3.3% was obtained for the device with the P3HT:PCBM active layer and based on a dense and homogenous ZnO film driven from 0.1 M sol (Fig. 6c); such an efficiency is 32% higher than that for the device made using a rough ZnO film derived from a 1 M sol. The PCE enhancement arises from the higher FF while J_{sc} only increases slightly and V_{oc} remains almost unchanged. R_S, series resistance, was found to increase by increasing the surface roughness and the content of voids in ZnO films. According to these experimental observations, Liang *et al.* suggested that the dense ZnO CBL with a homogenous surface allowed the formation of an intimate contact between the ZnO CBL and the BHJ photoactive layer, however a rough surface including voids led to an inferior contact and an increase in the contact resistance.[132] In addition, the uniform coverage of the ZnO CBL derived from 0.1 M sol is crucial for separating the ITO cathode from contacting the active layer, and blocking the reverse flow of holes from the active layer to the ITO electrode. These results demonstrated that the ZnO layer with a dense and homogenous surface benefited from establishing a better contact between the ZnO and the active layer, resulting in the low R_S of the device.

Besides the compactness, the surface area of ZnO CBLs, which is mainly determined by the morphology, is another important issue that impacts the device performance by affecting the interfacial area between the CBL and the active layer and therefore affecting the electron collection efficiency.[43,138,139,151] Sekine *et al.* first reported the use of unique nano-ridge (also named as nano-ripple) ZnO films having both a large surface area and a dense surface in inverted PSCs to serve as a CBL (Fig. 7a).[139] By adopting sol–gel processing and using a ramp annealing method at a rate of 50 °C min^{-1} from room temperature to 275 °C, they fabricated the nano-ridge ZnO films with a peak height of around 120 nm and a valley to valley distance of about 500 nm, as shown in Fig. 7b and c.[139] It was suggested that

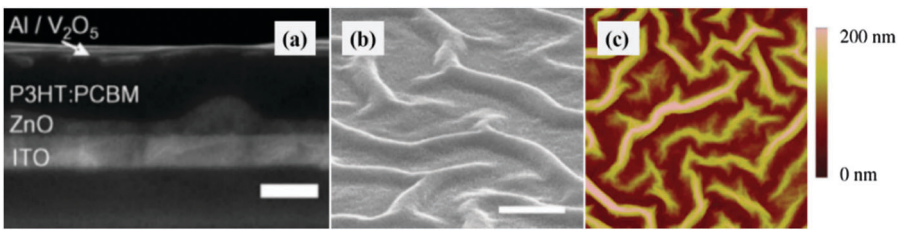

Fig. 7 (a) Cross sectional SEM image of the inverted PSC, scale bar: 200 nm and (b) SEM image of the ZnO nano-ridge film, scale bar: 500 nm, and (c) AFM image of the ZnO nano-ridge film showing a 5 μm × 5 μm surface area.[139] Adapted with permission from ref. 139 Copyright 2009 Elsevier.

the low heating rate of the ramp annealing method provided sufficient time for the gel particles to structurally relax and pile up, resulting in a dense and undulated film.[139] In their results, the inverted solar cells fabricated based on nano-ridge films showed an average PCE of 3.87%, while the devices with planar films only showed an efficiency of 3.06%. The enhancement resulted in a low leakage current due to the improvement in the electron collection efficiency and the hole blocking capability of the nano-ridge film, resulting in higher FF, while V_{oc} and J_{sc} were found to remain almost unchanged. The better charge extraction was thought to result from the large surface area of the ZnO nano-ridge film, which makes the device possess a large ZnO/BHJ active layer interfacial area for electron collection and shortens the travelling distance of charges. Meanwhile, the ZnO nano-ridge film is also very dense, making it effective in blocking the hole from transporting from the active layer to the ITO cathode, and thus reducing the charge recombination and leading to a low leakage current.

To meet the full potential of ZnO nano-ripple CBLs for high performance inverted PSCs, the ripple size and density should be controlled. By adding ZnO nanoparticles in zinc acetate solutions and using a ramp annealing method, Lim *et al.* prepared ZnO nano-ripple films with controlled ripple size and density (Fig. 8).[138] It has been found that the surface structure of ZnO nano-ripples with ~70 nm high nano-ripples gives the highest PCE of ~ 3.2%. They demonstrated that the homogenous surface and a higher contact area between ZnO and the active layer contributed to the enhanced photovoltaic performance of the inverted PSC. Besides adding ZnO NPs, it has been found that the ripple morphology can also be tuned *via* controlling the concentration of the $Zn(OAC)_2$ sol–gel solution, annealing ramp rate, and the spin-coating parameters.[140,142,178–180] This is because the surface morphology of the sol–gel derived ZnO thin films depends largely on the solvent drying kinetics.[142]

Although many reports have demonstrated that the ripple morphology of ZnO CBLs could result in a high contact area between the ZnO and the active layer and thus enhanced the solar cell performance, there are some other reports showing that the ripple ZnO CBLs with a large surface area however harm the device performance compared to the smooth ZnO layers.[140,179] Ma *et al.* reported that nano-ripple ZnO CBLs with a high surface roughness could lead to high surface energy and a small donor/acceptor (D/A) interfacial area in the active layer deposited on the top of ZnO CBLs, and thus lower the J_{sc}.[179] In addition, it has been suggested that the large surface area of ZnO CBLs could also result in more trap-assisted recombination at the active layer/ZnO interface compared to the case of smooth ZnO CBLs, and accordingly reduces the FF of solar cells. As a result, the best inverted PSCs were produced with the smoothest ZnO layer which gives the largest D/A interfacial area, and the lowest ZnO/active layer interfacial area.[179] The different or even contrary effect of the large surface area of nano-ripple ZnO CBLs on the device performance may be because the dominant factors influencing on the device performance, such as surface area, surface energy and surface defect, are different in various research studies. Therefore, to fully achieve the potential of the nano-ripple ZnO CBLs possessing a large surface area, the surface defects of the nano-ripple ZnO should be passivated and the surface energy should be optimized.

Besides the 3D ZnO nano-ridge films, there are several other ZnO films with a large surface area fabricated to serve as CBLs in inverted PSCs. Schumann *et al.* reported that the preparation of ZnO CBLs using spray-pyrolysis (SP) and electro-deposition (ED) methods achieved different surface morphologies.[43] In their work,

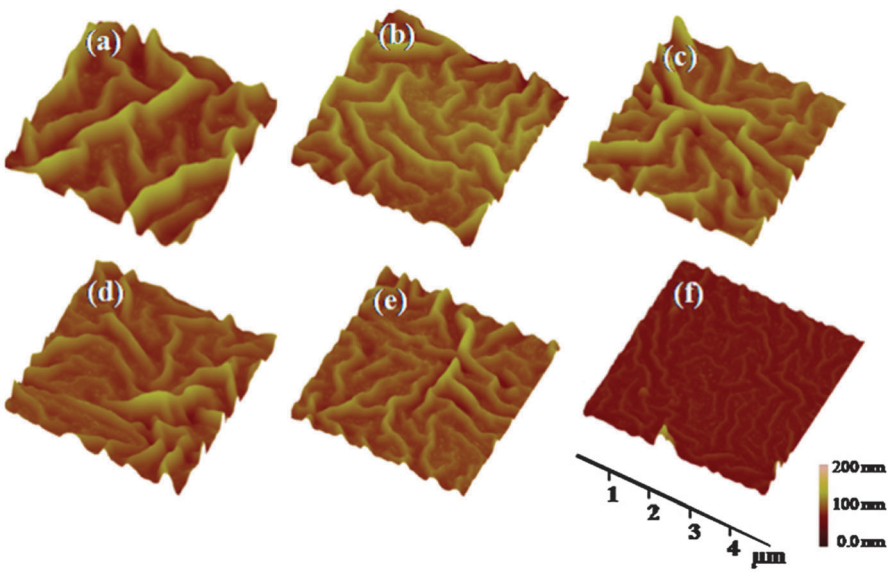

Fig. 8 AFM images of (a) a ZnO layer spin-coated using bare zinc sol. (b–f) ZnO layers were spin-coated using mixtures of ZnO nanoparticles and ZnO sol. The amount of ZnO nanoparticles added to 21 ml of ZnO sol was 0.25, 1, 3, 5 and 10 mg ZnO NPs for (b–f), respectively. All of the ZnO layers were heated to 350 °C with a heating rate of 23 °C min^{-1}.[138] Adapted with permission from ref. 138 Copyright 2011 Elsevier.

the interfacial area between the ZnO and the BHJ active layer was adjusted by controlling the surface roughness of ZnO CBLs. They demonstrated that the J_{sc} increased by increasing the ZnO/BHJ active layer contact area which provided a larger interface for electron extraction and transport. It should be noted that, in Schumann' work, the gaps in ZnO films seem to be wide enough and allow the blend of polymer/fullerene to infiltrate easily and thus obtain an intimate contact. Shin *et al.* fabricated ZnO CBLs with a large surface area by utilizing a mist pyrolysis chemical vapor deposition (MPCVD) method at a low temperature of 180 °C.[155] It was also demonstrated that a large ZnO CBL surface area might enlarge the interfacial area between the active layer and ZnO CBLs, leading to an effective increase in the number of electrons transferred from the active layer to the ZnO CBL. From these reports, we can conclude that the morphology of ZnO CBLs for inverted PSCs should meet the following requirements: (i) having a dense and homogenous surface, (ii) being able to provide a large surface area, and (iii) allowing the polymers to well contact with the ZnO layer.

2.4 The effects of the thickness of ZnO CBLs on the performance of inverted PSCs

The thickness of ZnO CBLs can affect the device performance by changing the optical transmittance, electrical conduction, and even the work function of CBLs, and thus imposes a profound impact on the photovoltaic performance of the inverted PSCs. Stubhan *et al.* reported that increasing the thickness of ZnO CBLs from 30 to 126 nm could result in a drop of solar cell PCE from 2.5% to 1.5%.[162] It was explained that the efficiency decrease arose from the low conduction of thick ZnO CBLs, which resulted in an increase of the series resistance (R_S) from 1 Ω cm^2 to 3.2 Ω cm^2. Cheun *et al.* have also studied the effects of the thickness of ZnO CBLs by varying the thicknesses from 0.1 to 100 nm using an atomic layer deposition (ALD) technique.[148] They demonstrated that the device performance strongly depended on the thickness of ZnO CBLs and there was a critical value for the thickness, which was at around 10 nm. For ZnO CBLs with thickness below this critical value the device demonstrated poor performance and the current–voltage (J–V) curves presented an ''S-shaped'' kink. For devices with ZnO layers from 10 nm and up to 100 nm in thickness, the ''S-shaped'' kink completely disappeared, and the thickness difference of ZnO CBLs only caused a little variation in the PCE and FF. Such a ''S-shaped'' J–V curve was suggested to be a result of the low conductivity of such ultra-thin ZnO layers, which had a large surface-to-bulk ratio and might cause considerable defects at grain boundaries; these defects act as electron traps reducing the electrical conduction of the CBL.[41,148] Recently, a number of studies have ascribed the low conductivity of ZnO layers to the presence of oxygen at the grain boundaries or at the surface.[41,128,181,182] A similar phenomenon of ''S-shaped'' kink in the J–V curve in inverted devices with ultrathin ZnO CBLs (several nanometers) has also been found in Liang's[132] and Sharma's[179] work. In addition, the film thickness and the preparation method are two main factors affecting the coverage of ZnO buffer layers. A full and conformal coverage of ZnO layers is crucial to separate the cathode from the active layer, and block the reverse flow of holes from the active layer to the cathode.[132,140,183,184] For the ZnO buffer layer derived from the sol–gel method, it has been found that a very thin ZnO layer (a few nanometers in thickness) is difficult to achieve a full coverage on the ITO surface, and thus leaving a portion of uncovered ITO in direct contact with the active layer forming current leakage pathways.[132,140,184] Therefore, for ZnO buffer layers derived from the sol–gel method, a certain thickness (around ten nanometers) is necessary to obtain a full coverage on the cathode.

Cheun *et al.* found that, when the thickness of ZnO layers increased from 10 nm to 100 nm, similar grain sizes and surface morphology were observed, resulting in little variation in the device performance.[148] More recently, Hu *et al.* fabricated ZnO CBLs with varying thicknesses (from 0 to 1500 nm) and different surface morphology and work function.[154] They found that, when using a P3HT:PCBM active layer, the optimized inverted device with a ZnO thickness of 80 nm showed a PCE of 2.93% using a P3HT:PCBM active layer. Based on the UPS spectra, Loser *et al.* found that both the valence band (VB) and the conduction band (CB) shifted slightly when the thickness of the ZnO layer increased from 3.0 to 42 nm.[185] In their results, the device performance only slightly varies as the ZnO thickness changes. Overall, a few tens of nanometers of the ZnO layer is suitable to obtain a uniform and dense surface so as to fully cover the cathode surface and completely separate the cathode from contacting the active layer and thus blocking the reverse hole flow, while not harming its electrical properties, transmittance, and mechanical robustness. It has been demonstrated that the inverted PSCs with different thicknesses of ZnO CBLs exhibit good long-term device stability, which is much better than that of the inverted PSCs without ZnO CBLs as well as that of various conventional PSCs.[38]

The transmittance of CBLs is another important factor that affects the device performance by influencing the light harvest of the BHJ photoactive layer.[76,132,135,155] In order to obtain a high device performance, the light absorption of the active layer should be maximized. In inverted PSCs, incident light comes from the transparent cathode side (*i.e.*, ITO or FTO) where the CBL was prepared on. Therefore, a CBL with high transmittance in the visible region is important in order to make the active layer gain high optical absorption of the active layer. The transmittance of ZnO films not only depends on the film thickness, but is also affected by the crystal size, defects and crystallinity, which are related to the preparation methods and post-treatment parameters.[186–188] High quality ZnO thin films possess an excellent transparency in the whole visible range and give rise to minimize optical losses. Through an optimization of the heat treatment process, Liang *et al.* fabricated high transparent ZnO layers on the ITO cathode with the thickness ranging from several nm to ~55 nm using a sol–gel process.[132] They found that the transmittance of ITO/ZnO layers increased with increasing ZnO thickness, and is even higher than the bare ITO when the ZnO thickness is over 10 nm (Fig. 9). The transmittance enhancement of ITO/ZnO layers was attributed to the antireflection

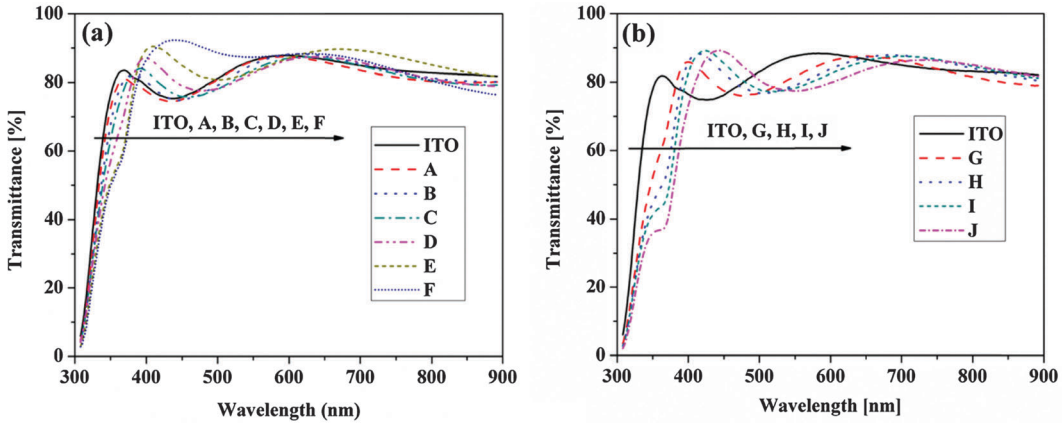

Fig. 9 The transmittance spectra of bare ITO and ITO coated with ZnO layers. (a) ZnO layers derived from (A) 0.02, (B) 0.05, (C) 0.1, (D) 0.3, (E) 0.6 and (F) 1 M sol, respectively; (b) ZnO CBLs derived from 0.1 M sol and by spinning (G) 3, (H) 5, (I) 7 and (J) 10 times, respectively.[132] Adapted with permission from ref. 132 Copyright 2012 Wiley-VCH Verlag GmbH & Co. KGaA.

effects caused by the ZnO coating on the surface of the ITO substrates, originating from the good transparency and appropriate refractive index ($n \sim 2$) of ZnO films.[38,141,189] Therefore, the high transmittance of ITO/ZnO layers will certainly benefit to the light absorption of the active layer in inverted PSCs. In addition, in Fig. 9, it can be seen that the sharp absorption edge of the transmittance spectra of ZnO modified ITO exhibits a gradual red shift toward ~380 nm (corresponding to an energy gap, ~3.2 eV of ZnO) by increasing the ZnO film thickness.[38,132,141] The band edge cut-off of ZnO at ~380 nm can help in blocking the UV light and thus protecting the organic materials from the photo-degradation induced by UV light.[33,43]

In Liang's work, a new parameter, "relative optical transmittance" (T_R), was put forward to quantify the overall effect of the transmittance of ZnO CBLs on the optical absorption of the given photoactive layer in inverted PSCs. The T_R was calculated using the following formula:[132]

$$T_R = \frac{\int_{\lambda_2}^{\lambda_1} I_\lambda t_\lambda d\lambda}{\int_{\lambda_2}^{\lambda_1} I_\lambda d\lambda}$$

where t_λ is the measured transmittance spectra of the ITO/ZnO buffer layer at λ wavelength, I_λ is the measured absorption spectra intensity of the active layer at λ wavelength, and $\lambda_1 \sim \lambda_2$ is the measurement arrange, usually corresponding to 300–900 nm.

According to the definition of "relative optical transmittance", T_R reflects the influence of ZnO CBL transmittance on the optical-absorption of the active layer. The higher T_R means less optical loss and higher optical-absorption of the photo-active layer, leading to better device performance. In Liang's work, although the transmittance of ITO/ZnO CBLs decreased at UV and increased at the wavelength of around 450 nm by increasing the thickness of ZnO films, the calculated T_R presented very small variation.[132] This indicates that the change in the transmittance of ZnO CBLs in their work just makes a negligible impact on the light harvest of the photo-active layer and device performance. In other words, the light harvest and the device performance are only affected when there is an obvious change in the transmittance of ZnO CBLs. Kyaw *et al.* reported that the improvement in optical transmittance of ZnO CBLs led to an increase in the J_{sc} of devices from 5.986 to 8.858 mA cm^{-2} without sacrificing the V_{oc} and FF of the solar cell.[76] Recently, it has been demonstrated that the light-absorption of the active layer can also be enhanced by the ZnO nano-ripple structure due to its good light-scattering properties, which contribute to increasing the J_{sc} of the device.[178,190,191] From these results, we can see that the charge extraction at the ZnO/active layer interface and the photovoltaic performance of the inverted devices are a combined effect relating to both the thickness and morphology of the ZnO layer.

3. Doping of ZnO CBLs in inverted polymer solar cells

In inverted PSCs, the thickness of ZnO CBLs is typically only a few tens of nanometers in order to ensure good conductivity so as to reduce the serial resistance and improve device performance.[38,162] However, such a thin CBL makes the devices suffer from low mechanical robustness and reduced protective properties against a chemical or physical reaction between the active layer and the electrode.[162,192] Therefore, such a thin ZnO CBL imposes a challenge for the manufacture of PSCs with scalable processes, such as the roll-to-roll manufacturing.[47,162,192] Doping is an efficient way to enhance the conductivity of ZnO so as to overcome the thickness limitation. Through doping, an increase in the electrical conductivity of ZnO CBLs and the photovoltaic performance of inverted PSCs has been observed.[162,192–197] The group-III elements, such as boron (B),[154] aluminum (Al),[162,192,195,197–199] gallium (Ga)[193,200] and indium (In)[194] have been intensively investigated for the doping of ZnO CBLs. It was explained that group-III elements could work as an n-type dopant for ZnO to replace Zn sites and generate free electrons. Besides aluminium and group-III elements, group-II elements (alkaline earth), such as magnesium (Mg), strontium (Sr) and barium (Ba) doped ZnO (named as MZO, ZnSrO and ZnBaO, respectively)

Table 2 Non-exhaustive survey of inverted PSCs including a doped ZnO CBL. The photovoltaic parameters are compared to those measured for a reference cell (values in parentheses), when available, based on pristine ZnO CBLs

Device architecture	J_{sc} [mA cm^{-2}]	V_{oc} [V]	FF [%]	PCE [%]	Ref.
ITO/AZO/P3HT:PCBM/PEDOT:PSS/Ag	8.36 (8.41)	0.569 (0.565)	50.8 (53.9)	2.42 (2.56)	162
ITO/AZO/P3HT:PCBM/PEDOT:PSS/Ag	8.97 (8.33)	0.54 (0.56)	55.0 (56.5)	2.65 (2.62)	192
ITO/AZO/P3HT:PCBM/NiO_x/Ag	6.78		38	1.36	198
ITO/AZO-NP/P3HT:PCBM/PEDOT:PSS/Ag	9.23	0.602	51.9	2.88	202
ITO/AZO/P3HT:PCBM/WO_3/Al	10.22	0.56	48.81	2.79	199
ITO/AZO/P3HT:PCBM/PEDOT:PSS/Ag	11.02 (10.73)	0.59 (0.58)	58.40 (53.73)	3.78 (3.32)	203
ITO/AZO(flat)/P3HT:PCBM/MoO_3/Ag	9.21	0.61	42.3	2.38	191
ITO/AZO(textured)/P3HT:PCBM/MoO_3/Ag	10.74	0.60	42.2	2.72	191
ITO/AZO/P3HT:$PC_{60}BM$/MoO_x/Ag	8.7	0.61	68.3	3.54	47
ITO/AZO/PBDTTPD:$PC_{70}BM$/MoO_x/Ag	12.5	0.87	62	6.7	47
ITO/AZO/PBDTTT-C-T:$PC_{70}BM$/MoO_x/Ag	16.0	0.76	66	7.6	47
ITO/AZO/PBDTTT-C-T-EFT:$PC_{70}BM$/MoO_x/Ag	17.7	0.80	70.7	9.94	47
ITO/AZO/PTB7:$PC_{70}BM$/MoO_x/Ag	17.1 (16.9)	0.74 (0.73)	70.6 (66.6)	8.86 (8.24)	47
FTO/IZO/P3HT:PCBM/MoO_3/Ag	9.935 (8.392)	0.605 (0.613)	55 (57)	3.30 (2.94)	194
ITO/InZnO/PTB7-Th:$PC_{71}BM$/MoO_3/Ag	16.32 (15.32)	0.79 (0.79)	70.0 (67.1)	9.03 (8.12)	49
ITO/InZnO-BisC60/PTB7-Th:$PC_{71}BM$/MoO_3/Ag	17.24	0.80	74.1	10.22	49
ITO/GZO/P3HT:PCBM/MoO_3/Au	11.7 (6.3)	0.42 (0.41)	39.7 (35.7)	1.95 (0.92)	193
ITO/GZO/PCDTBT:$PC_{71}BM$/MoO_3/Al	10.46 (8.85)	0.90 (0.86)	59.03 (50.27)	5.56 (3.72)	200
ITO/GZO/PTB7:$PC_{71}BM$/MoO_3/Al	14.96 (14.14)	0.75 (0.74)	64.95 (50.44)	7.34 (5.31)	200
ITO/BZO/P3HT:PCBM/MoO_3/Al	11.31 (8.95)	0.538 (0.565)	54 (58)	3.26 (2.93)	154
ITO/ZMO/PTB7:$PC_{71}BM$/MoO_3/Ag	16.78 (14.64)	0.74 (0.75)	66.99 (64.75)	8.31 (7.11)	48
ITO/MgZnO/P3HT:PCBM/MoO_3/Ag	9.7 (9.2)	0.577 (0.515)	56.8 (44.9)	3.17 (2.13)	203
ITO/MgZnO/P3HT:ICBA/MoO_3/Ag	9.9 (9.6)	0.828 (0.727)	67.0 (55.5)	5.48 (3.88)	203
ITO/ZnO-C60/PTB7:$PC_{71}BM$/MoO_3/Ag	15.41 (13.75)	0.73 (0.70)	73.0 (69.0)	8.21 (6.65)	114
ITO/ZnO-C60/PTB7-Th:$PC_{71}BM$/MoO_3/Ag	15.73 (14.02)	0.80 (0.79)	74.3 (69.1)	9.35 (7.64)	114
ITO/ZnO-BisC60/PTB7-Th:$PC_{71}BM$/MoO_3/Ag	16.88 (15.32)	0.79 (0.79)	72.0 (67.1)	9.60 (8.12)	49

layers have also been introduced into inverted PSCs.[48,201] Besides the metals, the fullerene derivatives have been used to dope ZnO for forming an efficient CBL in inverted PSCs.[49,114] The photovoltaic performance of inverted devices based on these doped ZnO CBLs in literature is summarized in Table 2.

Among the various doping methods, aluminium doping is a well-known approach to enhance the conductivity of ZnO layers for inverted PSCs. This seems to be because the doping of ZnO with aluminium can be easily processed and the aluminium-doped ZnO (AZO) possesses better electrical properties than that of an intrinsic ZnO (i-ZnO) reference.[162,192] It has been reported that the inflection (S-shaped) *I–V* curve of inverted PSCs could be removed by introducing an AZO CBL.[195–197] Stubhan *et al.* and co-workers studied the thickness dependence of the performance of inverted PSCs based on both i-ZnO and AZO CBLs with thicknesses from ~30 to 120 nm.[162,192] They demonstrated that an increase of the thickness of AZO CBL from ~30 to more than 100 nm did not hamper the solar cell performance, while the devices based on 100 nm i-ZnO films suffered from severely decreased FF, V_{oc} and PCE due to an increase in the series resistance. Considering that a thick CBL has a relatively good mechanical strength robust which benefits the inverted devices to be fabricated using a roll-to-roll method, the authors suggested that the doping of ZnO with aluminium opens the possibility to incorporate a thick CBL into the inverted devices without sacrificing their efficiency. More recently, based on a facial and low temperature (125 °C) solution processed Al doped ZnO electron accepting/hole blocking layer, Jagadamma *et al.* reached high performance inverted PSCs yielding a remarkable PCE in excess of 10% on glass substrates and 8% on plastic substrates.[47] They found that the average PCE of inverted devices using the PTB7:$PC_{70}BM$ active layer decreased marginally from 8.8% to 8.1%, while the thickness of AZO CBLs increased from 22 nm to 75 nm. The very slight decrease of the device performance by increasing the AZO thickness indicates that a relatively thick AZO can serve as an efficient CBL material for inverted PSCs. A thicker CBL with better mechanical strength is more suitable for manufacturing PSCs by scalable processes, such as the roll-to-roll manufacturing.[47,162,192]

For the inverted PSCs with AZO CBLs, it is worth noting that the device performances are strongly affected by the crystallinity and stoichiometry of AZO.[192,203] This is because the electronic properties of AZO CBLs, such as the work function, conductivity, mobility as well as surface states, are massively determined by the stoichiometry of AZO.[153,163] Tsai and co-workers have investigated the effects of the Al content (from 0 to 12 mol%) on the electronic properties of AZO layers and device performances of inverted PSCs with a structure of ITO/AZO/P3HT:PCBM/PEDOT:PSS/Ag (Fig. 10a).[203] They found that the carrier concentration, mobility and resistivity of AZO thin films strongly depended on the Al molar ratio (Fig. 11), which further impacted the performance of inverted devices with AZO CBLs. In their results, to achieve the best device performance, the optimum Al content of AZO CBLs is 6 mol%. Compared with the devices based on pure ZnO layers, the device with optimum AZO CBLs exhibits highest PCE of 3.78%, enhanced by ~13.9% *via* improving J_{sc} from 10.73 to 11.12 mA cm^{-2} and FF from 53.7% to 60.8%.[203] At the optimum Al doping concentration, the authors demonstrated that the band structure of ZnO was modified with an upward energy shift in the Fermi level (Fig. 10b), which facilitates the electron collection and can also serve as an efficient hole blocking layer. It is believed that the tunable band-gap

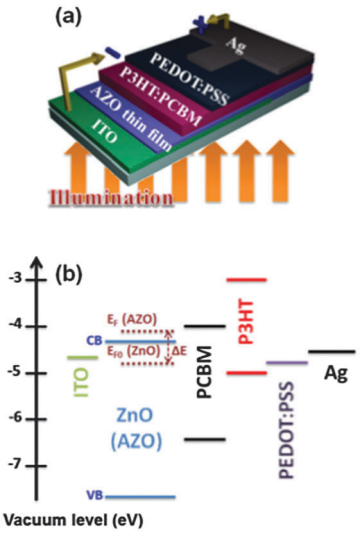

Fig. 10 (a) Schematic diagram of the inverted device structure with AZO CBLs and (b) band diagram of devices with pristine ZnO or AZO CBL.[203] Adapted with permission from ref. 203 Copyright 2013 AIP Publishing LLC.

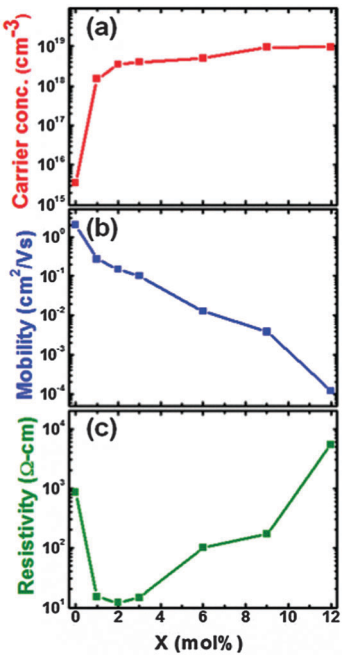

Fig. 11 (a) Carrier concentration, (b) mobility, and (c) resistivity of $A_xZn_{1-x}O$ (AZO) thin layers as a function of Al content (X, molar ratio).[203] Adapted with permission from ref. 203 Copyright 2013 AIP Publishing LLC.

combines with the increased carrier concentration and conductivity of AZO films *via* Al doping, and enhanced optical absorption of P3HT are the reasons of enhanced device performance.

Doping of ZnO with group-III elements such as boron (B), gallium (Ga), or indium (In) for doping ZnO CBLs is another effective way to improve the performance of inverted PSCs.[154,193,194,200] Kyaw *et al.* investigated the correlation between the device performance and indium contents of the sol–gel derived indium-doped ZnO (IZO) CBL in inverted PSCs.[194] Compared to the device with i-ZnO CBLs, the photovoltaic performance of the devices using appropriately doped IZO CBLs, especially in terms of J_{sc}, was enhanced, due to a combined effect of improvement in charge collection and higher optical transmittance of the electrode/IZO buffer layer stack. The device with 1 at% IZO CBLs showed a maximum PCE of 3.3% compared to the PCE of 2.94% for the device with i-ZnO CBLs. Gallium (Ga) has also been used as a dopant to enhance the electrical conductivity of ZnO CBLs. Shin *et al.* investigated the Ga-doped ZnO (GZO) CBL for the inverted PSCs.[193] By employing a GZO CBL, the PCE of the fabricated devices was improved by about 110% compared to the devices with i-ZnO CBLs, which was ascribed to the higher electron conductivity and smooth surface morphology of the ZnO film with Ga doping.

The doping of ZnO with group-II elements (alkaline earth), such as magnesium (Mg), strontium (Sr) and barium (Ba), doped ZnO (named as MZO, ZnSrO and ZnBaO, respectively) films have also been studied for inverted PSCs to serve as CBLs.[48,201] Pachoumi *et al.* reported an improved performance and stability of inverted PSCs by employing the sol–gel processed amorphous Sr and Ba doped ZnO CBLs prepared at a relatively low temperature.[201] The inverted PSCs based on Sr and Ba doped ZnO CBLs exhibited higher performance and better stability than the devices with pure ZnO CBLs. In addition, the common requirement of light soaking for reaching a maximum photovoltaic performance of inverted device based on i-ZnO CBLs was successfully circumvented. The improvements of device performance were attributed to the doping of ZnO with Sr or Ba reducing the electron trapping on the surface associated with oxygen absorption. The authors suggested that the Sr or Ba doping could effectively suppress/reduce the oxygen adsorption in mobile oxygen vacancy sites on the ZnO surface.[201]

For doped ZnO CBLs, the band gap structure is a key parameter that could affect the device performance. The band gap and energy level dependence on the doping content enables researchers to adjust the optical and electrical properties of the doped ZnO CBLs for achieving better device performance.[48,192,198] For example, it is well established that the substitutional doping of Mg^{2+} into the Zn site leads to an increase in the bandgap of ZnO.[48,204,205] By using Mg doped ZnO (ZMO) CBLs, Yin *et al.* fabricated inverted PSCs with high performance, as shown in Fig. 12a.[48] They developed a solution processed ZMO CBL with tunable band gaps and energy levels (Fig. 12b), good optical transmittance and electron transporting abilities. With an increase of the Mg content (x = 0.1–0.6), the CB edge value of ZMO CBLs are finely adjusted in the range of ~ -4.3 to -3.9 eV (inset in Fig. 12c) to approach the LUMO of $PC_{71}BM$. The corresponding band gap of ZMO films increased from 3.3 to 3.7 eV, which was confirmed by the gradual blue shift of the fundamental absorption edge as the Mg content increases (Fig. 12c). A favorable CB level of ZnO matching well with the $PC_{71}BM$ acceptor would improve the electron extraction/transportation in inverted devices. The electron mobility of ZMO films was found to be close to that of pure ZnO films, which is in favor of electron extraction/transportation in the inverted PSCs. Moreover, ZMO layers also exhibit a more hydrophobic

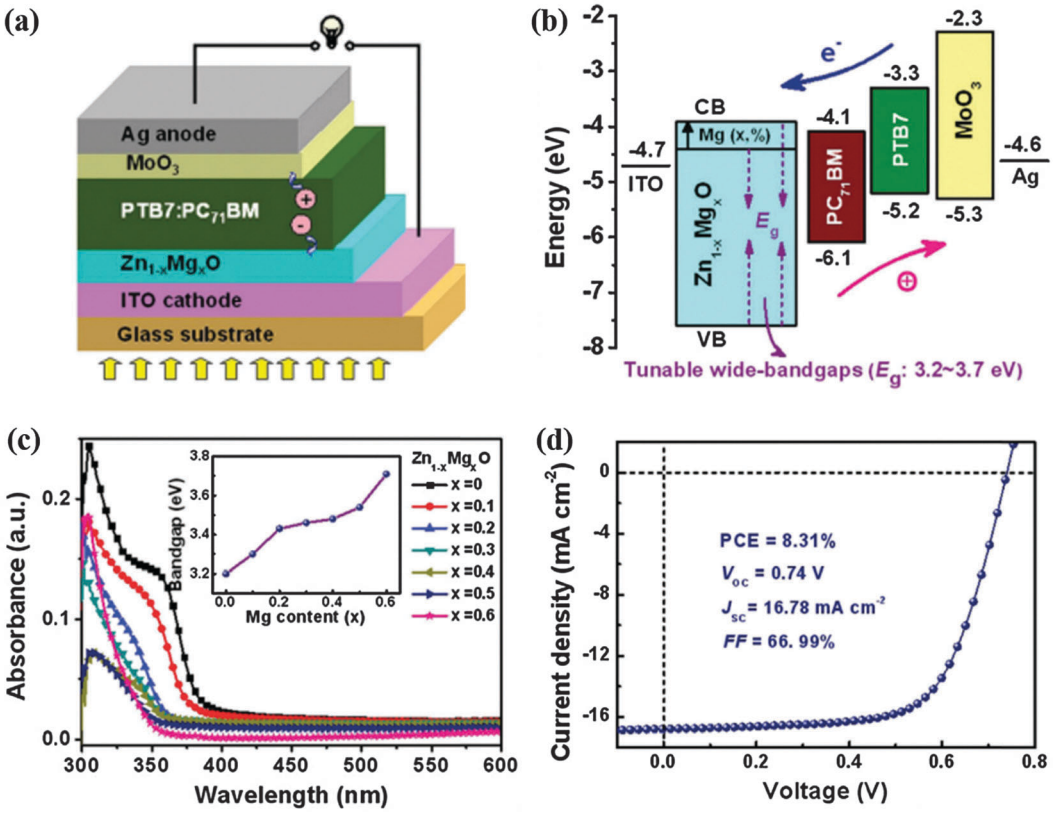

Fig. 12 (a) Schematic illustration of the device structure with ZnMgO CBLs. (b) Energy levels of the components in the inverted PSCs with various ZMO CBLs. (c) Optical absorption spectra of ZMO films. The inset shows an increase in the bandgap of ZMO films with the increase of Mg content (x). (d) J–V curve of the device with the ZMO (x = 0.3) CBL.[48] Adapted with permission from ref. 48 Copyright 2014 Wiley-VCH Verlag GmbH & Co. KGaA.

surface than ZnO, benefiting to form a high quality contact between the organic active layer and inorganic metal oxide CBLs. As a result, by incorporating the optimized ZMO layers derived from a 0.2 M precursor solution, the inverted PSCs with the structure ITO/ZMO/PTB7:$PC_{71}BM$/MoO_3/Ag exhibit preferable PCEs exceeding 8% (up to 8.31–8.35%, as shown in Fig. 12d), which are much higher than those of devices with an i-ZnO CBL (PCE = 7.1%) under the same conditions.[48] Macleod and co-workers have also reported an improved PCE in inverted PSCs when a sol–gel processed Mg–ZnO is used in place of ZnO as CBLs.[205] It has been found that, as the Mg content increased, the FF and V_{oc} increased substantially for both the devices based on P3HT:PCBM and P3HT:ICBA systems. The maximum PCEs were achieved when the Mg content in the precursor was 10 mol%, and subsequently decreased for higher Mg content due to decay in J_{sc}. They have also found that the increase in Mg content led to a decrease in the work function and an increase in the bandgap. The increased bandgap in Mg–ZnO is ascribed to a downshift in the valence band maximum, rather than an upshift in the conduction band minimum. The improved device performances were partially ascribed to the reduced recombination caused by substituting Zn with Mg. However, it has been suggested that the mechanisms for the improvement of inverted devices with Mg doped ZnO CBLs remain an open question.[205] More systematic investigation needs to be done to elucidate the dominating factors with regard to the improvement in the performance of inverted PSCs when using Mg–ZnO CBLs.

Besides the above-mentioned metals, fullerene derivatives have also been used to dope ZnO for forming high quality CBLs in inverted PSCs.[49,114] Liao *et al.* reported a fullerene derivative doped ZnO (ZnO-C60) nanofilm as the CBL of inverted PSCs.[114] For the inverted device with ZnO-C60 CBLs, the PCE remarkably improved from 7.64% to 9.35% for the PTB7-th:$PC_{71}BM$ active layer, from 6.65% to 8.21% for PTB7:$PC_{71}BM$, and from 5.26% to 6.60% for P3HT:ICBA, compared to the devices with pristine ZnO CBLs. It has been demonstrated that the ZnO-C60 CBL can enhance the electron collection by producing a fullerene derivative rich cathode surface and promote electron conduction at the interface and in the bulk of ZnO-C60. The high content of fullerene at the surface of ZnO-C60 CBLs offers a better contact with the fullerene derivative in the active layer, and thus facilitates electron collection. In another work also done by Liao *et al.*, a dual-doped ZnO with indium and fullerene derivative (BisNPC60-OH) was fabricated by sol–gel processing and applied as CBLs in inverted PSCs (Fig. 13).[49] They found that this dual doped ZnO, InZnO-BisC60, buffer layer showed dual and opposite gradient dopant concentration profiles, being rich in fullerene derivative at the cathode surface in contact with the active layer and rich in indium at the cathode surface in contact with the ITO surface (Fig. 13b). For the InZnO-BisC60 film, the surface conductivity was improved by a factor of 270

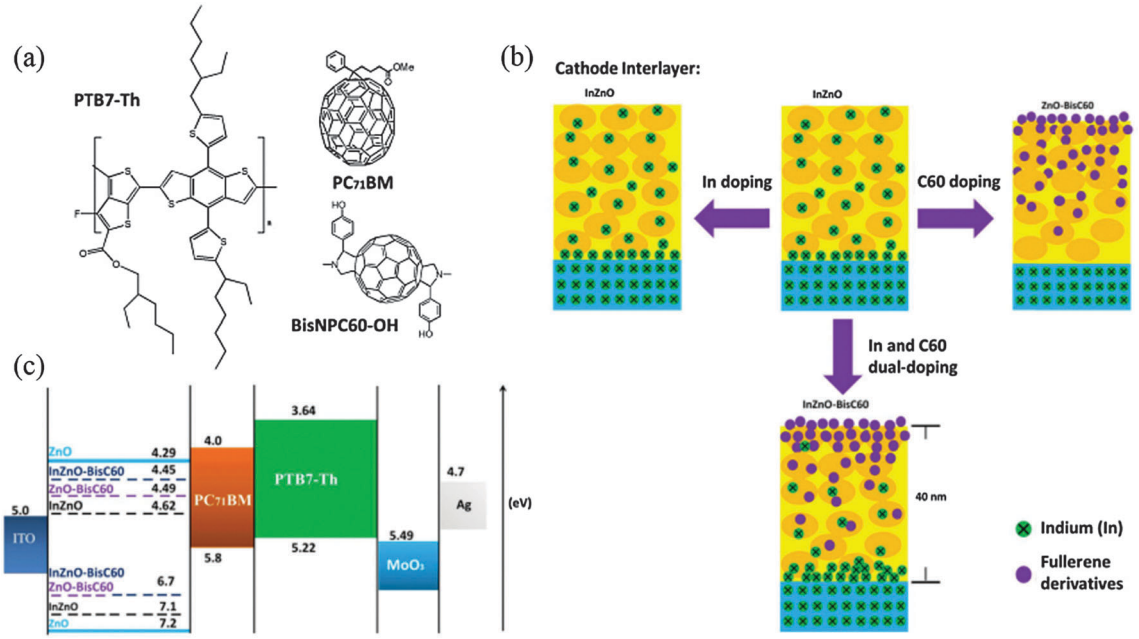

Fig. 13 (a) Chemical structures of PTB7-Th, $PC_{71}BM$ and BisNPC60-OH, (b) schematic illustration of the proposed cathode interlayer from the XPS depth profile; (c) energy level diagrams for ZnO, InZnO, ZnO-BisC60 and InZnO-BisC60 determined from ultraviolet photoelectron spectroscopy (UPS) and UV-Vis results and for all the components in the inverted PSCs.[49] Adapted with permission from ref. 49 Copyright 2014 Nature Publishing Group.

(from 0.015 to 4.06 S cm^{-1}), and the electron mobility was enhanced by a factor of 132 (from 8.25×10^{-5} to 1.09×10^{-2} cm^2 V^{-1} s^{-1}). As a result, with this InZnO-BisC60 film as the CBL, the PTB7-Th–$PC_{71}BM$ inverted device exhibited a preferable PCE, 10.31%, significantly higher than the 8.25% for pristine ZnO.

4. One dimensional ZnO nanostructures for inverted polymer solar cells

For polymer solar cells, the bulk-heterojunction (BHJ) active layer was considered to establish the cornerstones of a device with high performance. This is because the structure of the BHJ can maximize the donor/acceptor interfacial area to provide possibly more exciton dissociation sites and form continuous pathways for the transport of electrons and holes.[13,18,21] However, there are still some shortcomings of the BHJ active layer that limit the photovoltaic performance of polymer solar cells. One of the limitations is that the very thin thickness of the BHJ active layer leads to low optical absorption and thus non-ideal device performance.[206–208] The use of a very thin active layer is, on one hand, because the photo-generated charges in the active layer need to transport in the percolation network of the polymer donor and the acceptor, and on the other hand the carrier mobility in polymers is relatively low.[206,209] The charge recombination in a thick active layer will increase because of an increase in the diffusion length of carriers, leading to a decrease in device performance. Thus, the optimal thickness of the active layer is determined by a trade-off between maximizing the optical absorption and meanwhile allowing the charges to transport efficiently from the BHJ active layer to the electrode. It has reported that an optimal active layer thickness is typically about only ~100–200 nm.[185,206–208]

Research effort on the methods of light absorption enhancement has been driven by these limitations, including using photonic crystals,[210] plasmonic enhancement,[211–214] and textures.[215,216] Besides the methods mentioned above, another way to enhance the light harvesting of the photoactive layer is to increase the effective thickness of the photoactive layer and meanwhile avoid the increase of charge recombination in the case of a thick active layer.[217,218] To increase the effective thickness of the photoactive layer, the use of a vertically aligned one dimensional (1D) ZnO nanostructure in PSCs to provide a direct electron transport pathways so as to enhance charge carrier collection and transport has been investigated.[213,214] Fig. 14 shows a schematic diagram of inverted PSCs with a 1D ZnO nanostructure. In the case of inverted PSCs with ZnO nanorods (NRs), after the charge

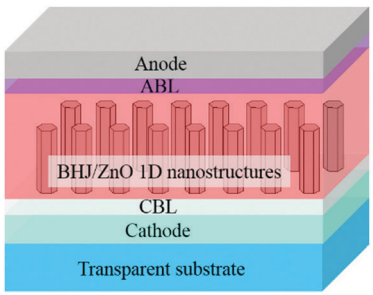

Fig. 14 Schematic diagram of the inverted PSC structure with 1D ZnO nanorods.

Table 3 Non-exhaustive survey of photovoltaic parameters of inverted PSCs including a 1D ZnO nanostructure. The photovoltaic parameters are compared to those measured for a reference cell (values in parentheses), when available, without the 1D ZnO nanostructure layer

Device architecture	J_{sc} [mA cm^{-2}]	V_{oc} [V]	FF [%]	PCE [%]	Ref.
ITO/ZnO NF/P3HT:PCBM/Ag	10.00	0.475	43	2.0	234
ITO/ZnO NR/P3HT:PCBM/Ag	9.60 (9.0)	0.57 (0.52)	50 (38)	2.7 (1.8)	217
ITO/ZnO NR/PCBM:P3HT/VO_x/Ag	10.4 (10.6)	0.58 (0.57)	65 (50)	3.9 (3.0)	222
ITO/ZnO NR/PCBM:P3HT/Ag	11.7	0.53	58	3.58	218
ITO/ZnO NR/P3HT:PCBM/Ag	6.62	0.36	49	1.16	223
ITO/ZnO NR-N719/P3HT:PCBM/Ag	8.89	0.57	41	2.00	223
ITO/ZnO(buffer layer)/ZnO NR/P3HT:PCBM/Ag	14.99 (9.59)	0.48 (0.49)	34 (35)	2.44 (1.64)	224
ITO/ZnO NR/P3HT:PCBM/PEDOT:PSS/Ag	6.28	0.432	44.76	1.19	225
ITO/ZnO NR/P3HT:PCBM/Ag	10.13	0.51	45	2.35	226
ITO/ZnO NR-PCBM/P3HT:PCBM/Ag	11.67	0.55	50	3.2	226
ITO/AZO/ZnO NW/P3HT:PCBM/PEDOT:PSS/Ag	10.02	0.55	53	2.94	231
ITO/ZnO NR/P3HT:PCBM/MoO_x/Au	9.917 (3.250)	0.266 (0.220)	37.126 (36.212)	0.979 (0.259)	227
FTO/ZnO nanopillars/P3HT:PCBM/Ag	7.29 (5.46)	0.40 (0.25)	35 (27)	1.02 (0.37)	235
ITO/ZnO NW + ZnO NPs/P3HT:PCBM/MoO_3/Ag	13.75 (9.48)	0.57 (0.56)	52 (64)	4.1 (3.41)	232
ITO/ZnO NR/P3HT:PCBM/MoO_3/Al	9.02	0.555	44.2	2.15	220
ITO/ZnO NR/P3HT:PCBM/MoO_3/Ag	5.70	0.509	38	1.11	228
ITO/ZnO NR/P3HT:PCBM:*x*-3-HF/Ag	11.56	0.59	44.63	3.05	229
FTO/ZnO nanopillars/P3HT:PCBM/MoO_3/Ag	8.55 (5.46)	0.44 (0.25)	45 (27)	1.71 (0.37)	236
ITO/ZnO NW/P3HT:PCBM/MoO_3/Ag	9.4 (9.1)	0.55 (0.54)	66.1 (59.7)	3.5 (2.9)	221
ITO/ZnO NR/P3HT:ICBA/PEDOT:PSS/Ag	8.34 (7.73)	0.793 (0.802)	61.12 (61.42)	4.04 (3.80)	230
ITO/ZnO NR/PBDTTT-C-T:$PC_{71}BM$/MoO_x/Ag	18.4 (13.5)	0.733 (0.788)	58.0 (50.6)	7.80 (5.40)	238
ITO/ZnO NR/PTB7:$PC_{71}BM$/MoO_x/Ag	16.5 (16.0)	0.709 (0.708)	66.7 (63.7)	7.80 (7.24)	238

separation at the polymer and fullerene interface, the photogenerated electrons at the LUMO level of fullerene transfer to the conduction band of ZnO. Then, the electrons quickly move to the cathode electrode along the ZnO NRs, in view of high electron mobility of ZnO NRs ($\sim$15 cm^2 V^{-1} s^{-1} along the *c*-axis)[219] which is several orders of magnitude higher than what are typically found in most of the organic semiconducting materials.[7,217,220] For the devices with ZnO NRs, the average distance from the generation sites of charge carriers to the surface of the ZnO electron collection layer would be shorter than that in the solar cells without ZnO NRs, and as a result the charge recombination can be effectively reduced.[217,221] To date, 1D ZnO nanostructures, such as nanorods (NRs),[217,220,222–230] nanowires (NWs),[221,231–233] nanofibers (NFs),[234] and nanopillars,[235,236] and 2D vertically aligned nanowall arrays,[230,237] combined with dense ZnO films have been employed to fabricate the inverted PSCs. Table 3 summarizes the photovoltaic parameters of inverted devices by using 1D ZnO nanostructures. Fig. 15 presents the SEM images of several typically vertically aligned 1D ZnO nanowires used in inverted PSCs.

Olson *et al.* demonstrated for the first time that the inverted PSCs fabricated with the blend of a P3HT:PCBM and 1D ZnO nanostructure prepared using a solution method, and a PCE of 2.03% was obtained.[234] Kazuko *et al.* investigated the effect of the length of ZnO NRs on the performance of inverted PSCs.[217] They found that the PCE and FF of devices were improved from 1.8% and 0.38 to 2.7% and 0.50, respectively, while the I_{sc} and V_{oc} remained almost constant when the length of ZnO nanorods increased from 0 to 350 nm. The improvement in PEC was mainly ascribed to the enhancement in FF, resulting from introducing ZnO nanorods as direct pathways for more efficient electron transport and collection. It has been demonstrated that the ZnO NR array in the ZnO NR/P3HT:PCBM system mainly works as an electron collector/transport pathway, rather than an acceptor material to form heterojunctions with the donor polymer in view of a much larger interface between the P3HT and PCBM than the interface between the P3HT and ZnO NRs.[77,217,239] In conventional and inverted PSCs, holes are also commonly limiting charge carriers. Although ZnO nanorods may not improve the hole transport, the extraction and transport away from electrons would reduce the probability of electron–hole recombination.

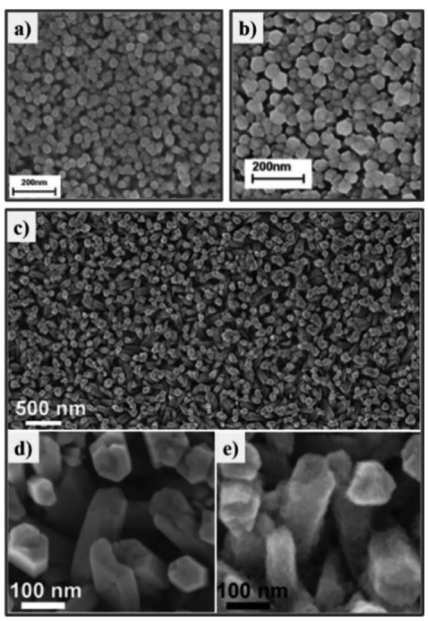

Fig. 15 SEM images of 1D ZnO nanostructures employed in inverted PSCs. (a) Top view of ZnO nanorods.[226] Adapted with permission from ref. 226 Copyright 2010 Elsevier. (b) Hydrothermal two-growth ZnO nanorods.[238] Adapted with permission from ref. 238 Copyright 2015 Elsevier. FE-SEM micrographs of (c) ZnO nanowires and magnified view of (d) as-electrodeposited and (e) ZnO nanoparticle modified ZnO nanowires.[232] Adapted with permission from ref. 232 Copyright 2011 The Royal Society of Chemistry.

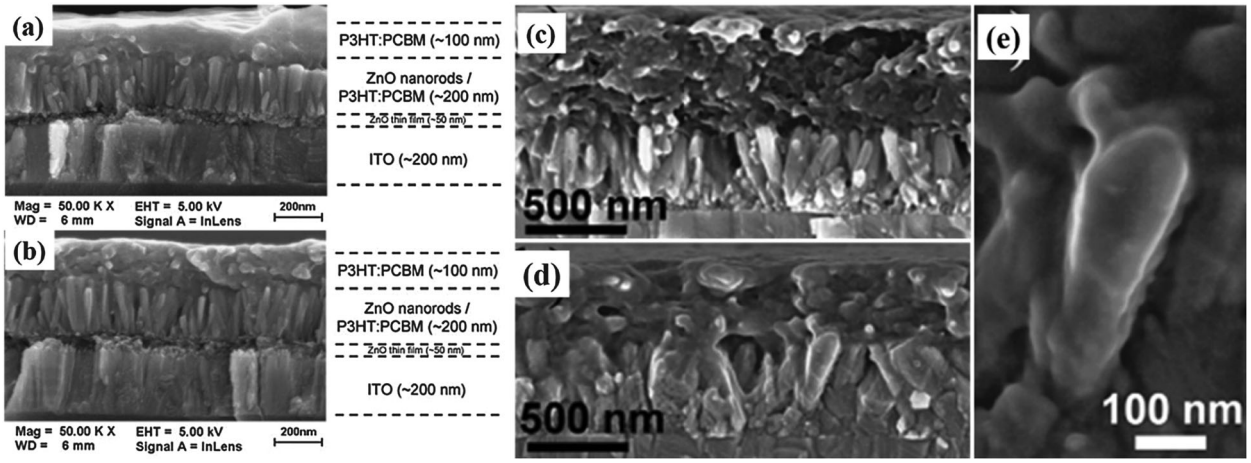

Fig. 16 Cross-sectional SEM images of inverted devices (a) with and (b) without a fullerene interlayer.[226] Adapted with permission from ref. 226 Copyright 2010 Elsevier. Cross-sectional FE-SEM micrographs of inverted devices with (c) unmodified ZnO nanowires, (d) ZnO NP modified ZnO nanowires, and (e) the higher magnification view of the ZnO nanowire well covered by the P3HT:PCBM blend.[232] Adapted with permission from ref. 232 Copyright 2011 The Royal Society of Chemistry.

In order to fully achieve the potential of 1D ZnO nanostructures in inverted PSCs, an electrical coherence at the organic photoactive layer and ZnO interface needs to be provided. Therefore, the infiltration of polymers into the space between ZnO NRs is a critical issue that greatly affects the device performance. Several methods have been developed to improve the contact between the active layer and ZnO nanostructures, including the surface modification of ZnO nanostructures and optimizing the post-treatment processes.[218,226,230,232] Fig. 16 shows the SEM images of the cross-section of inverted devices with the ZnO nanowire arrays with or without surface modification. Obviously, the surface modification of ZnO NPs effectively improved the infiltration of polymer and fullerene blends into the space of ZnO NRs.

Chou *et al.* reported that the device performance of inverted PSCs with ZnO NRs could be improved by increasing the polymer solidification time.[218] They suggested that the increase of the polymer solidification time made the polymer chains have enough time to self-organize, leading to the enhanced crystallinity of polymers and improved the infiltration of the photoactive layer into ZnO NP space. For the inverted device with the active layer up to 400 nm in thickness, the PCE of the device improved to 3.58% as a result of enhanced FF (58%).[218] Thitima *et al.* reported that the performance of inverted PSCs could also be improved by modifying the surface of the ZnO nanostructure with the N719 dye.[223] The dye interlayer covered on the surface of ZnO was thought to serve as a mediator to improve the electron transportation and injection from the polymer to ZnO. Huang *et al.* reported that the solution-processed PCBM interlayer could efficiently modify ZnO NRs and accordingly enhance the PCE from 2.35% to 3.2%.[226] They demonstrated that the PCBM interlayer enhanced the infiltration of the photoactive layer into the intervals between ZnO NRs (Fig. 16b) and may facilitate the self-organization of polymers.

Ajuria *et al.* investigated the functionalization of the ZnO nanowire (NW) surface with ZnO nanoparticles (NPs) with the consideration to improve the contact between ZnO and the P3HT:PCBM active layer.[232] It was found that, by modifying the ZnO NW array with a thin layer of ZnO NPs by immersing in a ZnO colloidal suspension, improved P3HT:PCBM blend penetration was achieved (Fig. 16d and e). A PCE as high as 4.1% was obtained for the inverted device based on ZnO NP-coated NWs and commercial P3HT:PCBM blend active layers. The ZnO NP modification was found to contribute to enhance the exciton dissociation and increase the charge lifetime by reducing charge recombination. More recently, Ho *et al.* fabricated ZnO NRs with controlled density and length by using a two-growth hydrothermal method (as shown in Fig. 15b).[238] Compared to the devices made with planar ZnO films, the PCEs of devices with the two-growth ZnO NRs are enhanced from 5.40% to 7.80% and from 7.24% to 8.01% for the PBDTTT-C-T:$PC_{71}BM$ and PTB7:$PC_{71}BM$ active layer, respectively. The improved device performances were ascribed to the morphology of two-growth ZnO NRs, which helps in achieving deeper and superior infiltration of the organic active layer.[238] From these results, we can conclude that, for 1D ZnO nanostructures applied in inverted PSCs, their length, density, surface morphology, and surface modification are key parameters that will significantly affect the penetration of polymers and fullerene blends and thereby affect the device performance.

5. Surface modification of ZnO CBLs

The performance of polymer solar cells is critically dependent on the properties of each layer and the interfacial contacts. For ZnO CBLs, without interface engineering, the inorganic ZnO CBL and surface defects may lead to a poor interfacial contact with the polymer based active layer and, thus, result in poor electron extraction, which is one of the main reasons leading to a relatively high charge recombination and series resistance (R_S).[240,241] Especially, in the case of ZnO CBLs prepared with widely used sol–gel processing or colloidal nanocrystals, the low-temperature and solution process often lead to high densities

of surface defects, such as dangling bonds, surface groups and charged oxygen molecules.[41,128,195,242] Such surface defects can act as recombination centres for photogenerated charge carriers, decreasing the photocurrent and power conversion efficiency as well as the device stability. It has been demonstrated that the deteriorated electrical properties at the interface between ZnO CBLs and organic active layers are caused by incompatible chemical interfaces and the formation of electron trapping states on the surface of ZnO layers.[243] A phenomenon commonly observed on the *J–V* curve of inverted PSCs when employing ZnO CBLs is the appearance of an inflection point, *i.e.* the so-called "S-shape" kink feature. It is believed to be due to the accumulation of charges at the ZnO/active layer interface.[144,148,197,201] Therefore, appropriate electrical contacts at interfaces between ZnO CBLs and BHJ active layers are highly desirable and essential to achieve a high power conversion efficiency and good stability of inverted PSCs. In this regard, many studies have focused on engineering the surface of ZnO CBLs to reduce the R_S of solar cells through improving the interfacial electrical properties, better aligning the energy-level and controlling the surface energy. There have been several efficient surface engineering methods to modify the surface of ZnO CBLs, such as ultraviolet (UV)[41,133,144,148,182,197,201] or UV-ozone treatment,[144,172] thermal and vacuum treatment,[167] and incorporation of the surface modification interlayer, such as the self-assembled monolayers (SAMs).[169,244–247]

5.1 UV illumination treatment of ZnO CBLs

UV or UV-containing light illumination treatment, also known as "light-soaking", is a common way to improve the electrical characteristics and optimize optimum photovoltaic performance of inverted devices with ZnO CBLs.[41,133,144,148,182,197,201] UV illumination can passivate the defect states, such as the negatively charged oxygen molecules trapped at the grain boundaries and the surface, and thus remove the electron extraction barrier and reduce carrier recombination at the ZnO/photoactive layer interface.[41,128,195] The metal-oxide/organic active layer interface is identified as the reason of the S-shaped *J–V* curve due to an electron extraction barrier.[181,182,197] Under dark conditions, electrons in the conduction band of the ZnO layer are trapped by the chemisorption of O_2 molecules (Fig. 17a, step (1)), and therefore form a depletion layer and band bending next to the surface (Fig. 17a, step (2)).[181,182] It has been suggested that both the depletion layer and the band bending can result in the formation of a barrier for the electron injection and extraction at the ZnO/BHJ active layer interface and are more pronounced in the case of small ZnO nanocrystals with a high surface-area-to volume ratio. Upon UV illumination, the electron–hole pairs are generated in ZnO, leading to neutralization of O_2 species and desorption of oxygen from the ZnO surface, as shown in Fig. 17a, steps (3)–(5).[181] The desorption of O_2 from the ZnO surface reduces the electron traps, and thus increases the concentration of mobile electrons.[182] As a result, the inflection point problem (S-shaped) on the *J–V* curve of the inverted devices incorporating ZnO CBLs could be solved by exposing the cells to UV illumination, leading to the device performance improvement (Fig. 17b).[41] The UV-ozone (UVO) treatment has also been investigated to modify ZnO CBLs.[144,172] Chen *et al.* found that the UVO treatment of ZnO NP films could effectively passivate the defect states leading to longer carrier life time of devices compared to the devices treated with UV light soaking.[144] By reducing the interfacial recombination *via* UVO treatment and employing a high performance PDTG-TPD:$PC_{71}BM$ active layer, the inverted PSCs with PCEs exceeding 8% were achieved. According to the PL measurement, it was proposed that the passivation mechanism under UVO treatment of ZnO films is correlated with the reduction of oxygen vacancies (V_O) in both the surface and bulk due to the penetration of oxygen in the porous NP films. As a result, the defect passivation in ZnO NP layers can help to reduce the carrier recombination at the ZnO/active layer interface, and thus enhance the device performances.[144] However, the UV exposure approach is limited in the case when the devices are based on substrates with low UV transmittance, UV blocking filters or UV to VIS down-conversion concepts.[197] Many active organic donor polymers must be protected from being exposed to UV light so as to achieve a reasonable device stability.[55,197,248] In order to alleviate the requirement for UV illumination, surface modification

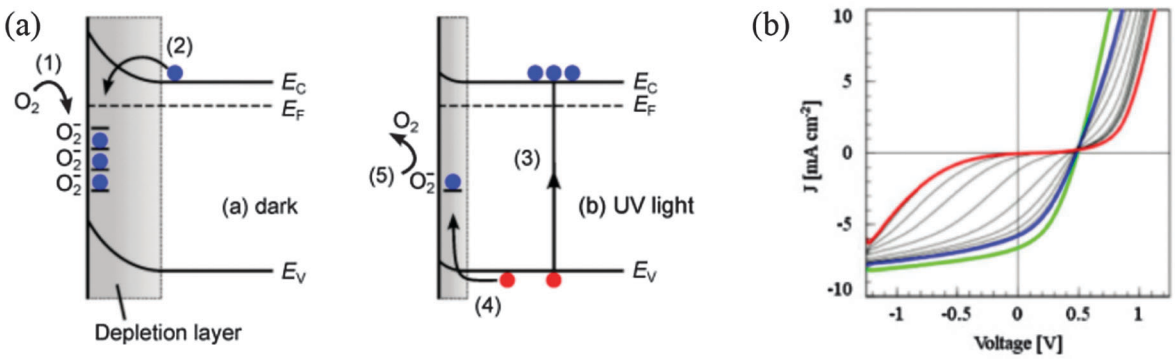

Fig. 17 (a) Schematic view of the oxygen absorption and desorption process in the n-type ZnO layer in the dark (left) and UV illumination (right).[181] Adapted with permission from ref. 181 Copyright 2014 American Chemical Society. (b) The evolution of *J–V* curves over time during UV illumination for a single inverted PSC with a ZnO NP layer.[41] Adapted with permission from ref. 41 Copyright 2010 Elsevier.

methods and the use of doped-ZnO CBLs are developed to improve the electronic properties of ZnO CBLs and the contact properties of the ZnO/organic active layer interface.

5.2 Fullerene based interlayer modification of ZnO CBLs

Modifying ZnO CBLs with a functional interlayer derived from fullerene derivatives (C60-SAM),[50,169,202,244,246,247,249] conjugated polyelectrolytes (CPEs)[250,251] and poly(ethyleneimine) (PEI)[87] is another representative method to enhance the electrical properties of the ZnO/BHJ active layer interface as well as the performance of inverted PSCs. Among these interfacial modification materials, fullerene derivatives (C60-SAM), which are very effective in acting as an interlayer for the modification of ZnO CBLs in inverted PSCs, are the most extensively investigated interfacial modification materials. Fig. 18 shows several cross-section schematics of the inverted devices with fullerene derivative modified ZnO CBLs. The improvement of photovoltaic parameters of inverted devices using surface modified ZnO CBLs with fullerene derivatives (C60-SAM) is summarized in Table 4.

C60-SAMs can be easily processed to form a modification layer on the surface of ZnO CBLs through either a solution immersion technique or a solution-based spin-coating method. The Jen group developed a series of C60-based SAM modifiers containing different anchoring groups (catechol, carboxylic acid, and phosphonic acid), linkage location, and functionalization (Fig. 18a).[169,244] They found that these C60-SAM functional layers could help in reducing the charge recombination at the ZnO/active layer interface, improve the morphology of the active layer, and enhance the charge selectivity, leading to high FF and J_{sc}. For instance, an average PCE of 4.5% (with the highest PCE of 4.9%) was achieved for the devices with a C60-SAM (SAMs [1], shown in Fig. 18a) modified ZnO CBL surface; such an efficiency is over 20% higher than those unmodified devices. Cheng *et al.* synthesized a PCBM-based and cross-linked n-type interlayer (C-PCBSD) (Fig. 18b) for the modification of ZnO CBLs.[246,249] This C-PCBSD interlayer was considered to have several positive impacts on the interfaces of the active layer, including improved exciton dissociation efficiency, reduced charge recombination, decreased interface contact resistance, and introduced vertical phase separation to reduce the bulk resistance of the active layer as well as passivating the local shunts of the ZnO CBL interface.[246,249] As shown in Fig. 18b, the authors suggested that, first, the C-PCBSD interlayer provided an extra P3HT/C-PCBSD interface area for ultrafast exciton dissociation; second, the LUMO energy level of C-PCBSD (3.8 eV) was located between the LUMO of P3HT (3.3 eV) and the conduction band of ZnO (4.4 eV), which makes the electrons to efficiently transport from the active layer to ZnO through C-PCBSD as an energetically favorable

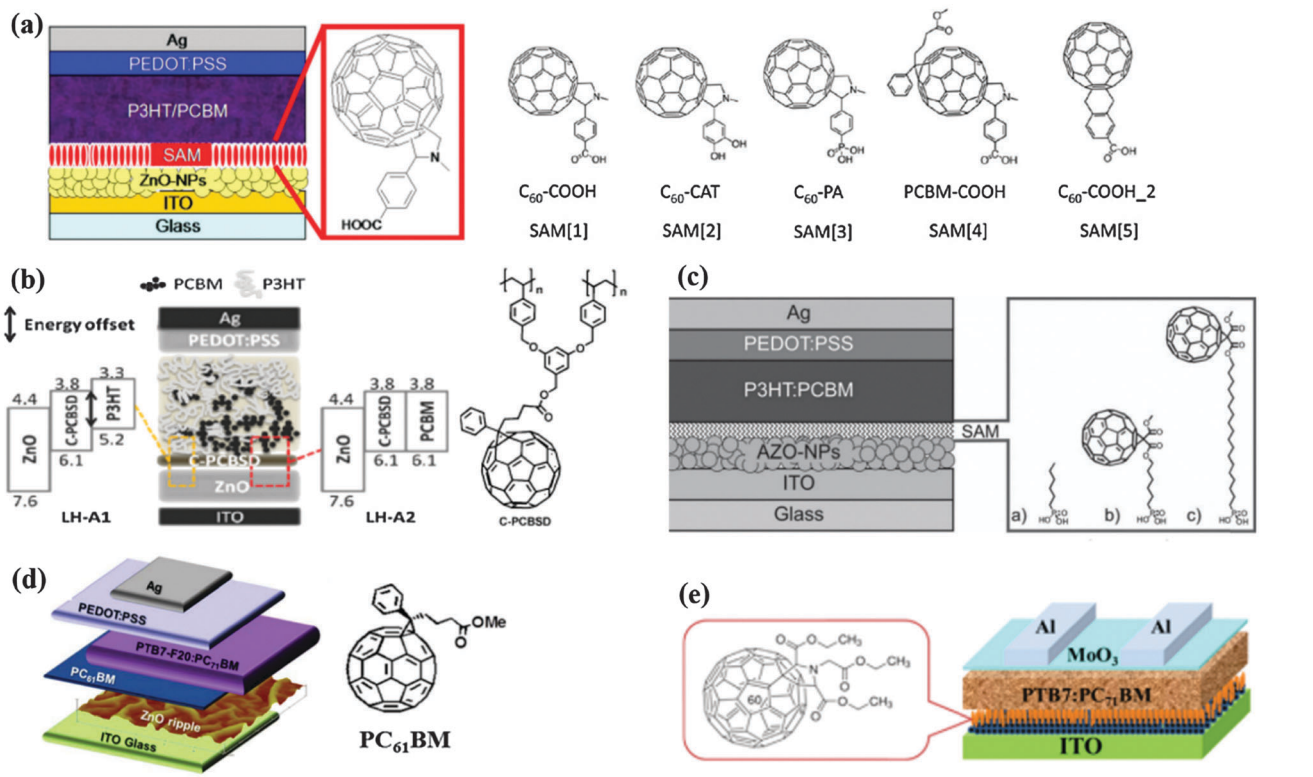

Fig. 18 Schematic illustrations of device structures and chemical structures of ZnO surface modification fullerene based interlayers including (a) fullerene self-assembled monolayer (C60-based SAM) modifiers containing different anchoring groups.[169,244] Adapted with permission from ref. 169 Copyright 2010 American Chemical Society and from ref. 244 Copyright 2008 AIP Publishing LLC. (b) Cross-linked fullerene (C-PCBSD) interlayers.[246] Adapted with permission from ref. 246 Copyright 2010 American Chemical Society. (c) Hosphonic acid anchored C60 SAMs.[202] Adapted with permission from ref. 202 Copyright 2012 Wiley-VCH Verlag GmbH & Co. KGaA. (d) $PC_{61}BM$.[247] Adapted with permission from ref. 247 Copyright 2014 Nature Publishing Group. (e) C60 pyrrolidine tris-acid ethylester (PyC60).[50] Adapted with permission from ref. 50 Copyright 2014 Elsevier.

Table 4 Non-exhaustive survey of inverted PSCs including modified ZnO CBLs with fullerene derivatives (C60-SAM). The photovoltaic parameters are compared to those measured for a reference cell (values in parentheses), when available, made with a pristine ZnO CBL

Device architecture	J_{sc} [mA cm^{-2}]	V_{oc} [V]	FF [%]	PCE [%]	Ref.
ITO/ZnO/SAM/PCBM:P3HT/PEDOT:PSS/Ag	12.0 (10.8)	0.63 (0.63)	60.6 (55.4)	4.54 (3.74)	244
ITO/ZnO/C60-SAM/P3HT:PCBM/Ag	10.25	0.62	66.6	4.20	143
ITO/ZnO/C60-COOH/PCBM:P3HT/PEDOT:PSS/Ag	11.12 (10.07)	0.61 (0.60)	64.0 (57.7)	4.36 (3.47)	169
ITO/ZnO/C60-CAT/PCBM:P3HT/PEDOT:PSS/Ag	10.86	0.61	62.4	4.13	169
ITO/ZnO/C60-PA/PCBM:P3HT/PEDOT:PSS/Ag	10.27	0.62	62.6	3.96	169
ITO/ZnO/PCBM-COOH/PCBM:P3HT/PEDOT:PSS/Ag	10.85	0.62	63.6	4.24	169
ITO/ZnO/C60-COOH_2/PCBM:P3HT/PEDOT:PSS/Ag	11.26	0.61	62.4	4.30	169
ITO/ZnO/C-PCBSD/P3HT:PCBM/PEDOT:PSS/Ag	12.8 (11.6)	0.60 (0.58)	58 (52)	4.4 (3.5)	246
ITO/ZnO/C-PCBSD/ICBA:P3HT/PEDOT:PSS/Ag	12.4 (10.6)	0.84 (0.82)	60 (55)	6.22 (4.81)	249
ITO/AZO-C6-C60/P3HT:PCBM/PEDOT:PSS/Ag	9.92 (9.23)	0.583 (0.602)	57.4 (51.9)	3.32 (2.88)	202
ITO/ZnO/PyC60/PTB7:$PC_{71}BM$/MoO_3/Al	16.04 (16.11)	0.753 (0.740)	72.5 (68.5)	8.62 (7.92)	50
ITO/ZnO-PC61BM/PTB7-F20:$PC_{71}BM$/PEDOT:PSS/Ag	17.042 (14.783)	0.684 (0.693)	66.0 (63.1)	7.698 (6.475)	247

downhill pathway.[246] As a result, the inverted devices based on C-PCBSD modified ZnO CBL with a P3HT:PCBM blend active layer gained an improvement in J_{sc} from 11.6 mA cm^{-2} to 12.8 mA cm^{-2}, and exhibited a PCE as high as 4.4%, which is much higher than 3.5% for a reference device with unmodified ZnO CBL.[246] An impressive high PCE of 6.2% has been achieved through introducing C-PCBSD modified ZnO CBLs into inverted devices based on the ICBA:P3HT blend active layer, leading to a 29% enhancement compared to the device with un-modified ZnO CBLs.[249] The improved device photovoltaic performance in terms of J_{sc} and FF of the devices with C-PCBSD modified ZnO CBLs was attributed to a high shunt resistance (R_{SH}) and a low series resistance (R_S) due to the decreased contact resistance and increased electron collection efficiency at the ZnO/C-PCBSD interface. Besides high PCE, the devices with C-PCBSD modified ZnO CBLs also demonstrated good device stability in air without encapsulation. In their results, the PCE of the unencapsulated devices with P3HT:PCBM active layers and based on bare ZnO CBLs retained 80% of their original value after being stored under ambient conditions for 35 days. In contrast, the device based on C-PCBSD modified ZnO CBLs exhibited a better long-term stability, retaining above 85% of its original value under the same conditions.[246] In sharp contrast, the device with a conventional structure (ITO/PEDOT:PSS/PCBM:P3HT/Ca/Al) and without encapsulation suffer a rapid decay in just two days. It was suggested that the coverage of a three-dimensional C-PCBSD network on the ZnO buffer layer might have passivated the hot spots generated in ZnO CBLs to suppress the leakage current, and thus improved the device lifetime.[246,249]

Stubhan *et al.* investigated the modification of the AZO buffer layer with phosphonic acid anchored SAMs (as illustrated in Fig. 18c).[202] They demonstrated that the phosphonic acid anchored SAM decorated AZO could increase R_{SH} and decrease the R_S of the device due to the improved charge transfer from the PCBM to AZO. The average PCE had been improved by approximately 15% from 2.9% to 3.3%. More recently, Cho *et al.* demonstrated that the PCBM itself could serve as an interfacial modification material (Fig. 18d).[247] They suggested that the PCBM layer between ZnO and the BHJ active layer can effectively quench the electron–hole recombination by reducing trapped charges at the ZnO surface, which resulted in a 16% increase in the PCE (up to 7.7%) compared to devices without an additional PCBM layer. The C60-based modifiers with weaker acids have been also explored to modify ZnO CBLs.[50,169,244] It has been found that the modifiers with ester units exhibit much weaker acidity and better affinity for the ZnO surface.[169] Li *et al.* developed a C60 pyrrolidine tris-acid ethylester (PyC60) with three ester groups to modify ZnO CBLs (Fig. 18e).[50] By using this PyC60 upper layer modified ZnO NP films as the CBL, high efficiency (average PCE of 8.62%) inverted PSCs based on the photoactive layer of the PTB7:$PC_{71}BM$ blend were achieved. The authors demonstrated that the PyC60 improves the morphology quality of ZnO/PyC60 films by filling in the voids of the ZnO layer and partly passivating the defects of ZnO NPs. It was indicated that the PyC60 could also improve the interfacial contact between the ZnO and the active layer, lowering the electron injection barrier. As a result, the ZnO/PyC60 CBL effectively decreased R_S and interfacial charge recombination, and increased electron injection and collection efficiency in the inverted PSCs.[50]

5.3 Non-fullerene based interlayer modification of ZnO CBLs

Non-fullerene based interlayers, such as mixed SAM,[241] poly(ethylene oxide) (PEO),[174] poly(ethyleneimine) (PEI),[87] ruthenium dye N719,[199] conjugated polyelectrolytes (CPEs),[250,251] HfO_2,[149] ionic liquids (Ils)[53] and ultrathin metal oxide layers[136,151,252,253] have also been studied to modify ZnO CBLs for further improving the performance of inverted PSCs. The improvement of photovoltaic parameters of inverted devices by using non-fullerene based interlayer modified ZnO CBLs in literature are summarized in Table 5.

Bulliard *et al.* reported a mixed SAM to control the surface energy of the ZnO buffer layer.[241] They found that, by changing the surface composition of two different SAMs (Fig. 19a), the surface energies of the ZnO CBL were tuned over a wide range of values (between 40 mN m^{-1} and 70 mN m^{-1}) with negligible changes in its work function.[241] They suggested that a surface treatment to obtain an intermediate surface energy above the neutral range favors the competition between lateral and vertical phase separation, resulting in morphology with desirable domain size. By tuning the surface energy of ZnO CBLs in a given range, the PCE increased from 3.27% to 3.70%. Yoo *et al.* developed

Table 5 Non-exhaustive survey of inverted polymer solar cells including modified ZnO CBLs with non-fullerene based interlayers. The photovoltaic parameters are compared to those measured for a reference cell (values in parentheses), when available, made with a pristine ZnO CBL

Device architecture	J_{sc} [mA cm^{-2}]	V_{oc} [V]	FF [%]	PCE [%]	Ref.
ITO/ZnO/mixed-SAM/P3HT:PCBM/MoO_3/Ag	9.65	—	—	3.70	241
ITO/ZnO/TiO_2/P3HT:PCBM/Ag	9.81 (9.04)	0.58 (0.59)	46 (47)	2.65 (2.53)	136
ITO/ZnO/P3HT:PCBM/PEDOT:PSS/Au	11.89 (11.14)	0.59 (0.59)	64.1 (61.8)	4.5 (4.1)	149
ITO/ZnO/PFN-Br/PBDT-DTNT:$PC_{71}BM$/MoO_3/Ag	17.4 (15.2)	0.75 (0.69)	61 (55)	8.4 (6.1)	251
ITO/ZnO/Cs_2CO_3/P3HT:PCBM/MoO_x/Al	11.27 (10.83)	0.58 (0.56)	65.2 (61.7)	4.26 (3.74)	252
ITO/ZnO–Al/N719/P3HT:PCBM/WO_3/Al	10.46 (10.22)	0.61 (0.56)	60.00 (48.81)	3.83 (2.79)	199
ITO/ZnO/PEO/TQ1:$PC_{71}BM$/MoO_3/Ag	9.6 (8.69)	0.877 (0.864)	67 (60)	5.64 (4.50)	174
ITO/ZnO-ALD-ZnO/PTB7-F20:$PC_{71}BM$/PEDOT:PSS/Ag	17.9 (16.9)	0.672 (0.679)	65.9 (66.5)	7.96 (7.66)	151
ITO/ZnO/PEO/PDPPTPT:$PC_{70}BM$/MoO_3/Ag	14.5 (13.4)	0.78 (0.78)	62 (63)	7.04 (6.37)	250
ITO/ZnO/DPA-BA/P3HT:PCBM/MoO_3/Ag	8.34	0.61	54.6	2.78	254
ITO/ZnO/Cz-BA/P3HT:PCBM/MoO_3/Ag	8.29 (7.83)	0.62 (0.60)	56.1 (53.0)	2.88 (2.49)	254
ITO/ZnO/BBC/P3HT:PCBM/WO_3/Ag	9.00 (8.63)	0.58 (0.58)	55.6 (50.2)	2.90 (2.51)	255
ITO/ZnO/PEI/PTB7:$PC_{71}BM$/MoO_3/Al	17.19 (16.00)	0.73 (0.71)	69.6 (62.0)	8.76 (6.99)	87
ITO/ZnO/EDT/P3HT:$PC_{61}BM$/MoO_3/Ag	11.88 (11.24)	0.61 (0.59)	71 (63)	4.8 (3.8)	242
ITO/ZnO/[BMIM]BF_4/PTB7:$PC_{71}BM$/MoO_3/Ag	17.50	0.73	67.7	8.65	53
ITO/ZnO/[BzMIM]Cl/PTB7:$PC_{71}BM$/MoO_3/Ag	16.97 (16.09)	0.72 (0.72)	69.5 (64.8)	8.49 (7.51)	53
IITO/ZnO/[BMIM]BF_4/PTB7-Th:$PC_{71}BM$/MoO_3/Ag	17.43 (17.19)	0.78 (0.78)	70.3 (66.7)	9.56 (8.94)	53

several SAMs derived from benzoic acid or benzoyl chloride to tune the work function and surface properties of ZnO CBLs.[254,255] It was demonstrated that the benzoic acid interlayer could form a favorable interface dipole at the interface between the ZnO and the active layer, thus to passivate the ZnO surface traps and accordingly reduce the work function and facilitate electron transport.

Conjugated polyelectrolytes (CPEs) have been reported to serve as a cathode buffer layer between the cathodic electrode and the active layer in inverted PSCs to improve device performance by changing the electronic and orbital interactions at the interface.[45,51,88] CPEs have also been employed as efficient interlayer materials to modify ZnO CBLs.[205,206] Yang *et al.* reported the use of a thin layer (~5 nm) conjugated polyelectrolyte, poly[(9,9-bis(3′-(*N*,*N*-dimethylamino)propyl)-2,7-fluorene)-*alt*-2,7-(9,9-dioctylfluorene)] (PFN-Br), shown in Fig. 19b, on ZnO CBLs to reengineer the interface between ZnO and PBDT-DTNT:$PC_{71}BM$.[251] In their study, the inverted PSCs with a device architecture of ITO/ZnO/PFN-Br/PBDT-DTNT:$PC_{71}BM$/MoO_3/Ag showed a J_{sc} of 17.4 mA cm^{-2}, a V_{oc} of 0.75 V, a FF of 61% and an average PCE up to 8.4% was attained. The conduction band edge of ZnO was tuned from −4.46 eV to −4.08 eV (ZnO/PFN-Br) by using a PFN-Br thin layer, leading to an enhancement of the V_{oc} of the device. The enhanced J_{sc} and FF in the inverted PSCs with the PFN-Br interfacial layer were ascribed to the improved contact between the PFN-Br interfacial layer and the active layer, which was better than the interfacial layer formed between the naked ZnO layer and the active layer. As a result, over 37% enhancement in the PCE was obtained. Another conjugated polyelectrolyte (CPE), poly(9,9′-bis(6″-*N*,*N*,*N*-trimethylammoniumhexyl)fluorene-*co*-*alt*-phenylene), with bromide counterions (FPQ-Br, as shown in Fig. 19c) has also been successfully employed as an interlayer between ZnO and the active layer to improve the electron transport and interfacial contact.[250] Compared with the device based on a bare ZnO layer, J_{sc} increased by 11% and the PCE increased from 6.37% to 7.04% for the device with ZnO/CPE layers.

Woo *et al.* report an appreciable PCE enhancement in inverted PSCs by using an electron-rich polymer nano-layer (poly(ethyleneimine) (PEI)) modified ZnO CBL (Fig. 20a).[87] The thickness of the PEI nano-layer was controlled to be only 2 nm in view of its high insulting character. It has been demonstrated that the enhanced PCEs are due to the lowered conduction band energy of ZnO *via* the formation of an interfacial dipole layer at the interface between the ZnO layer and the PEI nano-layer (Fig. 20b). They also found that the PEI nano-layer could increase the surface roughness of ZnO, which noticeably decreases the series resistance of the device. As a result, the inverted PSCs with the structure of ITO/ZnO–PEI/PTB7:$PC_{71}BM$/MoO_3/Ag resulted in a PCE of up to 8.9%, while the devices using only the ZnO or PEI buffer layer show relatively low PCEs, 6.99% and 7.49%, respectively. The enhanced PCE mainly resulting from the increased J_{sc} and FF for devices with ZnO/PEI layers was attributed to the fast electron transport.

Ionic liquids (ILs) have been investigated to serve as a CBL material and as a surface modification layer to modify the ZnO buffer for inverted PSCs. Yu *et al.* reported a remarkable PCE exceeding 10% (10.15%) for the single-junction PTB7-Th:$PC_{71}BM$ inverted PSCs with a solution processed ZnO/[BMIM]BF_4 combined CBLs.[53] The PTB7:$PC_{71}BM$ inverted PSCs with the ZnO/[BMIM]BF_4 CBL achieved an average PCE of 8.71% (champion PCE of 9.12%), which is 15.2% (champion 21.4%) high compared to the control devices based on pure ZnO (PCE of 7.51%). The simultaneously enhanced J_{sc}, FF and PCEs were attributed to the decreased interfacial energy barrier due to the decreased work function of the cathode by forming spontaneous dipolar polarization at the interface. They demonstrated that the IL layer and the ZnO/IL combination layers with low work function, good optical transmittance, improved electron extraction and reduced resistance at the cathode interface, make excellent and general interfacial layers for inverted PSCs. It has been found that the [BzMIM]Cl or ZnO/[BzMIM]Cl combined CBL showed a similar improvement of the device performance than the inverted devices based on [BMIM]BF_4 or ZnO/[BMIM]BF_4 combined CBLs. Recently, Bai *et al.* developed a facial and general ethanedithiol (EDT) treatment method to passivate the surface defects and modulate the intragap states of ZnO CBLs

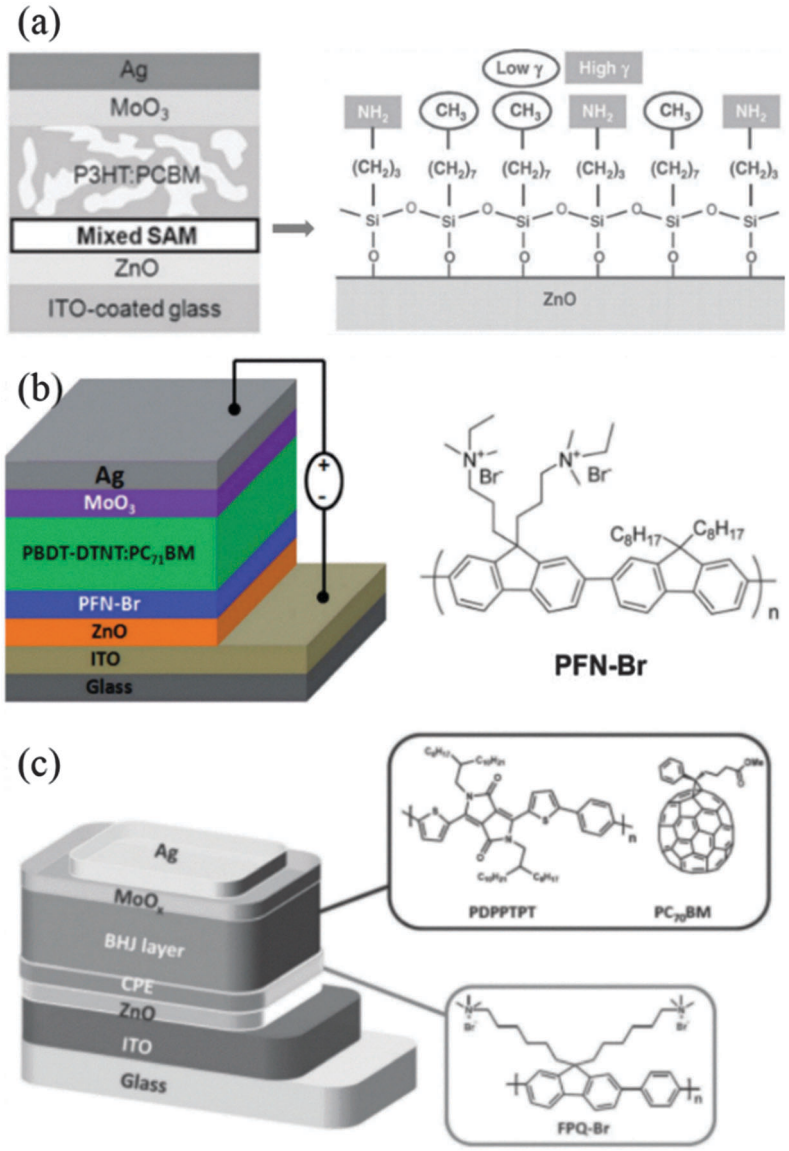

Fig. 19 Schematic illustrations of inverted device structures and chemical structures of ZnO surface modification materials including (a) mixed SAM.[241] Adapted with permission from ref. 241 Copyright 2010 Wiley-VCH Verlag GmbH & Co. KGaA. (b) poly[(9,9-bis(3′-(*N*,*N*-dimethylamino)propyl)-2,7-fluorene)-*alt*-2,7-(9,9-dioctylfluorene)] (PFN-Br).[251] Adapted with permission from ref. 251 Copyright 2012 The Royal Society of Chemistry. (c) Bromide counterions (FPQ-Br).[250] Adapted with permission from ref. 250 Copyright 2013 Wiley-VCH Verlag GmbH & Co. KGaA.

fabricated with solution-processing at low temperature (Fig. 21a).[242] They demonstrated that the covalent bonding of EDT molecules onto ZnO nanocrystals could effectively remove various surface defects of ZnO nanocrystal layers by forming zinc ethanedithiolates during the EDT treatment. Due to the chemical changes through EDT-passivation, the intragap states in pristine ZnO nanocrystals were modulated and a new intragap band was introduced (Fig. 21b and c), resulting in enhanced electron selectivity and improved electron transport properties to EDT-treated ZnO CBLs. As a result, the inverted devices with EDT-treated ZnO CBLs exhibited reduced charge recombination and enhanced charge extraction properties. The EDT treatment was also found to result in significant improvement of the ambient stability of the inverted PSCs. For the unencapsulated P3HT:PC61BM devices with EDT-treated ZnO CBLs, the PCE retained 90% of its original value after being exposed under dark and ambient conditions for 30 days. In contrast, the PCE of the control device with pure ZnO CBLs degraded to around 60% of the original value under the same conditions. The improved device stability was ascribed to the well-passivated EDT-treated ZnO films, which are less susceptible to oxygen and water molecules (as shown in Fig. 21d). Furthermore, it has been demonstrated that the EDT-passivation method is suitable for both colloidal nanocrystals and sol–gel derived ZnO films.[242]

Several kinds of metal oxides and salts, such as TiO_2,[136] Cs_2CO_3,[252] hafnium dioxide[149] and even ZnO[151,253] itself have been investigated to modify ZnO CBLs. Seo *et al.* reported that an ultrathin TiO_2 layer with a mean thickness of less than 3 nm

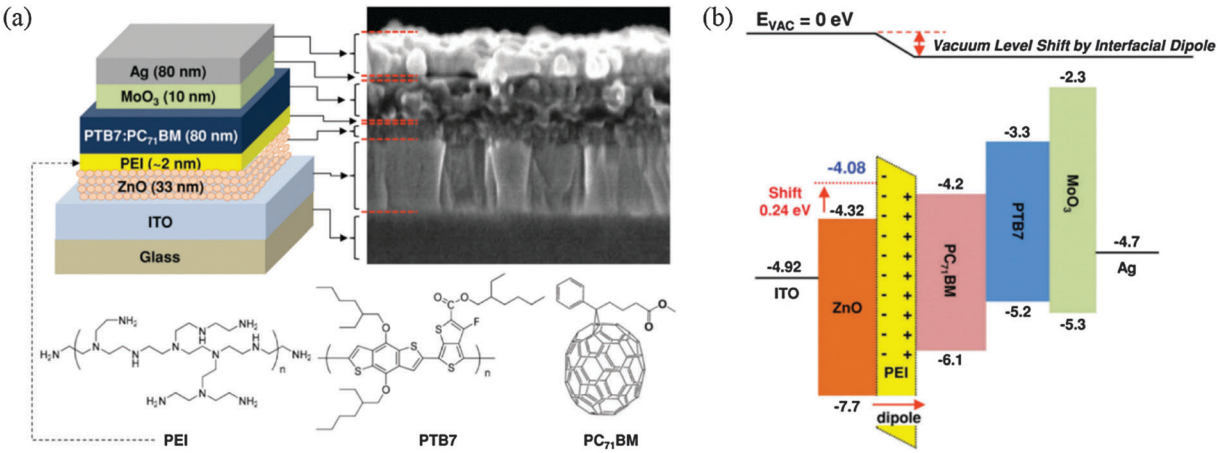

Fig. 20 (a) Inverted PSCs with PEI-coated ZnO CBLs: illustration of the device structure (top left), SEM image of the cross-section of the device (top right), and chemical structures of PEI, PTB7, and $PC_{71}BM$ (bottom). (b) Flat energy band diagram of the device with PEI-coated ZnO CBL where the conduction band energy of the ZnO CBL was lowered by 0.24 eV due to the dipole formation by the PEI nano-layer.[87] Adapted with permission from ref. 87 Copyright 2014 Wiley-VCH Verlag GmbH & Co. KGaA.

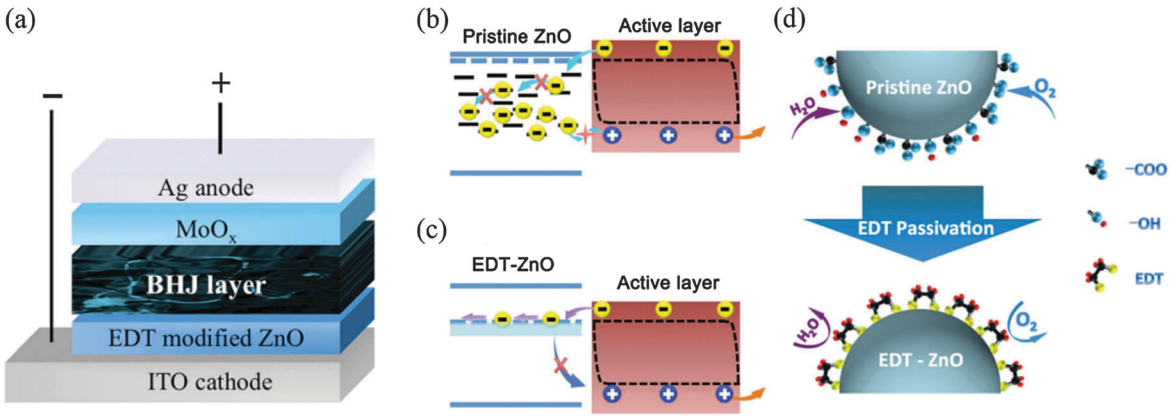

Fig. 21 (a) Schematic illustration of the inverted device structure with EDT modified ZnO CBLs. (b) Various intragap states of pristine ZnO layers, which act as recombination centres for photogenerated charges. (c) The intragap states are modified to a new intergap band, which facilitates electron transport in CBLs, thereby suppressing the interfacial bimolecular recombination and enhancing the charge extraction properties of the devices. (d) Schematic view showing that the various surface groups are removed and EDT molecules are covalently bound onto ZnO.[242] Adapted with permission from ref. 242 Copyright 2014 Wiley-VCH Verlag GmbH & Co. KGaA.

could slightly enhance the photovoltaic performance of inverted PSCs, while a thicker TiO_2 film resulted in reduced photovoltaic performance.[136] Based on the photoelectron spectroscopy study, it was suggested that the ultrathin TiO_2 layer could quench the recombination of electrons and holes on the surface of ZnO CBLs. Cheng *et al.* modified ZnO NP CBLs by coating a thin layer of Cs_2CO_3, using a solution process.[252] They demonstrated that the ZnO/Cs_2CO_3 bilayer presented enhanced electron-extraction and leakage-current-suppression abilities due to its modified energy level and improved surface morphology. As a result, about 40% enhancement in the PCE was obtained. More recently, Kim *et al.* reported that the wet-chemically prepared ripple-structured ZnO CBLs could be modified by depositing a very thin ZnO layer using the ALD method.[151] They found that a 1–2 nm ALD-ZnO layer can effectively quench the electron–hole recombination caused by surface defects of ZnO ripples, and thus enhance the J_{sc} and PCE of inverted devices. Modifying the ZnO CBL surface with a 0.6 nm ALD HfO_2 layer has also been reported to enhance the electron injection and hole-blocking, leading to the PCE increasing from 4.1% to 4.5%.[149] The R_{SH} of the devices increased significantly with the addition of the HfO_2 layer, while the R_S decreased. It was explained that the enhancement in the electron transport arose from the HfO_2 layer which passivated the ZnO CBL and reduced the defect states on the ZnO surface, thereby suppressing the loss of electrons caused by charge recombination at the defect sites. It should be noted that the deteriorated performance of devices with an HfO_2 layer thicker than 0.6 nm indicated that the enhancement in electron transport is reduced due to the insulating effect of the HfO_2 layer, which became dominant in the case of thick HfO_2. Besides the modification of the interface between ZnO and the active layer, the modification of the interface between ZnO and the ITO electrode has also been investigated to achieve more efficient collection and transport of electrons from the ZnO

layer to ITO.[256] Yoon *et al.* reported that inserting a nanoscopic copper hexadecafluorophthalocyanine (F16CuPc) nanowire film between the ZnO layer and the ITO electrode of inverted PSCs can increase the performance of inverted PSCs by enhancing interfacial electron transport.[256]

6. ZnO-based nanocomposite CBLs

6.1 ZnO/polymer nanocomposite CBLs

For low-temperature solution-processed ZnO CBLs, the general presence of high density defects, such as dangling bonds and surface groups, and poor spatial distribution of nanoparticles over a large area restrict their contribution to enhance the performance of inverted PSCs.[172,173] The development of uniform ZnO NP films with low density defects is essential to achieve high performance of inverted PSCs. Recently, polymer modified ZnO films, known as the so-called ZnO/polymer hybrids or nanocomposites, have been studied to meet such challenges.[173,174,257–260] For example, the ZnO/polymer composites, such as ZnO/poly(ethylene oxide) (PEO),[174] ZnO/poly(ethylene glycol) PEG,[258] ZnO/fullerene-end-capped poly(ethylene glycol) (C60-PEG),[261] ZnO/polyethylenimine (PEI),[260] ZnO/polyacrylic acid (PAA),[262] ZnO/poly(zinc diacrylate) (pZA),[257] ZnO/poly(diallyldimethylammonium chloride) (PDADMAC)[259] and ZnO/polyvinylpyrrolidone (PVP),[173,259] have been studied to serve as the efficient CBL in inverted PSCs to further improve the device performance. The improvement of photovoltaic parameters of inverted devices using ZnO/polymer hybrids or nanocomposite CBLs is summarized in Table 6.

Shao *et al.* reported that the poly(ethylene oxide) (PEO) modification to the ZnO NP surface could effectively passivate the surface traps, suppress the recombination loss of carriers, reduce the R_S as well as improve the electrical coupling of the ZnO/active layer.[174] For the inverted devices composed of TQ1:PCBM and PCDTBT:$PC_{71}BM$ active layers, the PCE of the devices using 0.05% PEO-modified ZnO NP (PEO/ZnO wt%) layer increased to 5.4% and 6.59% from 4.5% and 5.39% for the reference devices based on unmodified ZnO. However, when the PEO content was increased to 1 wt%, the device performance decreased due to the very rough surface of ZnO–PEO films. To effectively hybridize ZnO with a polymer, both the amount and molecular weight of the polymer should be tailored to achieve the desired interface and electrical properties of ZnO/polymer nanocomposite CBLs, as well as the device performance.[174,258] Hu *et al.* fabricated ZnO/poly(ethylene glycol) PEG hybrids as CBLs to improve the performance of inverted PSCs, as shown in Fig. 22a.[258] They demonstrated that the PEG can passivate the surface traps of ZnO NPs and thus suppressing the interfacial charge recombination, decreasing the work function and improving the energy level alignment between the $PC_{61}BM$ and ZnO. They suggested that the PEG chains wrapped around the ZnO surface could share their lone electron pairs of oxygen in the backbone with ZnO NPs, and thus passivate the shallow surface traps of ZnO. In their study, the effect of the molecular weight of PEG on the properties of ZnO–PEG CBLs and the performance of inverted PSCs has been investigated. It has been found that, compared to the devices with ZnO/PEG400 CBLs and ZnO/PEG20000 CBLs (with an average molecular weight of 400 and 20 000, respectively), the devices using ZnO/PEG6000 (with an average molecular weight of 6000) hybrids exhibited the best performance (PCE = 3.3%). This result was ascribed to the short backbone of PEG (*e.g.*, M_W = 400) containing less oxygen which could not effectively passivate ZnO surface traps. But the PEG with the long backbone (*e.g.*, M_W = 20 000) could lead to the formation of a charge transport barrier because of the insulating nature of PEG with the long backbone.[258] Recently, by *in situ* grown ZnO from amphiphilic fullerene-end-capped poly(ethylene glycol) (C60-PEG) at relatively low temperatures, Hu *et al.* employed this amphiphilic fullerene/ZnO hybrids (ZnO@C60-PEG) as CBLs to improve the charge selectivity of inverted PSCs.[261] They demonstrated that the C60-PEG could act as an n-dopant to the ZnO while the oxygen-rich PEG side chain of C60-PEG could passivate the defects of the ZnO. In addition, it was believed that the amphiphilic C60-PEG could facilitate the compatibility of the inorganic ZnO CBL and the organic active layer. As a result, compared to the pure ZnO, they demonstrated that the ZnO@C60-PEG possessed a decreased work function, less defects, and higher electron mobility, which could effectively reduce the recombination of carriers and enhance electron extraction. Consequently, the PCE of the inverted PSC based on the ZnO@C60-PEG CBL and with the PTB7:$PC_{71}BM$ active layer reached 8.0%. Due to the modification of C60-PEG to ZnO with fewer defects, the inverted PSCs with

Table 6 Non-exhaustive survey of inverted PSCs including ZnO/polymer hybrids or composite CBLs. The photovoltaic parameters are compared to those measured for a reference cell (values in parentheses), when available, made with a pristine ZnO CBL

Device architecture	J_{sc} [mA cm^{-2}]	V_{oc} [V]	FF [%]	PCE [%]	Ref.
ITO/ZnO–PVP/PDTG-TPD:$PC_{71}BM$/MoO_3/Ag	14.0	0.86	67.3	8.1	173
ITO/ZnO–pZA/P3HT:PCBM/MoO_3/Ag	9.21 (9.02)	0.58 (0.55)	61 (52)	3.26 (2.58)	257
ITO/ZnO–pZA/PTB7:$PC_{71}BM$/MoO_3/Ag	14.03 (13.83)	0.73 (0.72)	72 (67)	7.37 (6.67)	257
ITO/ZnO–PEG6000/P3HT:PCBM/PEDOT:PSS/Ag	10.19 (8.36)	0.581 (0.550)	55.9 (49.7)	3.3 (2.3)	258
ITO/ZnO–PSS/P3HT:PCBM/MoO_3/Al	1.77	0.45	54.00	0.42	259
ITO/ZnO–PVP/P3HT:PCBM/MoO_3/Al	9.62	0.59	40.00	1.71	259
ITO/ZnO–PDADMAC/P3HT:PCBM/MoO_3/Al	10.82 (0.25)	0.54 (0.59)	33.00 (58.20)	1.86 (0.10)	259
ITO/ZnO–PEO/TQ1:$PC_{71}BM$/MoO_3/Ag	9.6 (8.69)	0.877 (0.864)	67 (60)	5.64 (4.50)	174
ITO/ZnO–PEI/P3HT:PCBM/MoO_3/Ag	11.4 (10.3)	0.60 (0.60)	67 (60)	4.6 (3.7)	260
ITO/ZnO–PEI/PBDTTBO:$PC_{71}BM$/MoO_3/Ag	14.7 (13.3)	0.85 (0.85)	70 (65)	8.7 (7.3)	260
ITO/ZnO–PAA/PBDTTPD:$PC_{71}BM$/MoO_3/Ag	12.1 (11.9)	0.86 (0.84)	54 (46)	5.6 (4.6)	262
ITO/ZnO-C60-PEG/PTB7:$PC_{71}BM$/MoO_3/Ag	15.86 (15.51)	0.733 (0.724)	69.1 (61.4)	8.0 (6.9)	261

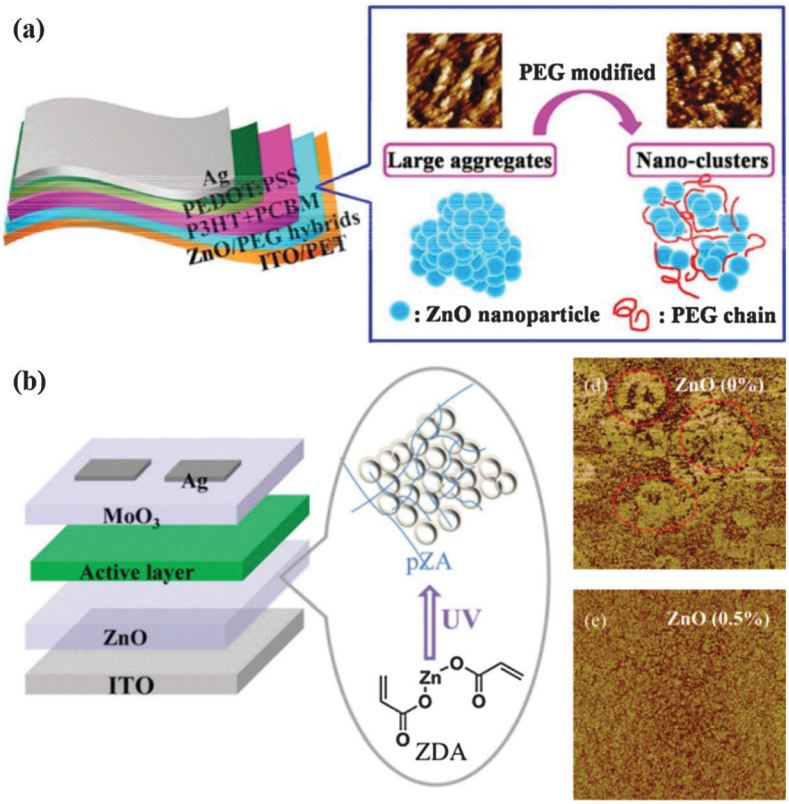

Fig. 22 (a) Schematic illustration of the inverted PSC with the ZnO/PEG hybrid film as the CBL. The inset is the AFM images and schematic diagrams of ZnO aggregates and PEG modified ZnO nano-clusters.[258] Adapted with permission from ref. 258 Copyright 2013 American Chemical Society. (b) Schematic diagram of an inverted PSC with ZnO/pZA CBL (left) and a brief processes in the fabrication of a pZA network (inset), and the AFM images of ZnO/pZA hybrid films with 0% and 0.5% pZA weight ratio to ZnO NPs (right), the scan size is 2 μm × 2 μm.[257] Adapted with permission from ref. 257 Copyright 2013 IOP Publishing.

ZnO@C60-PEG hybrid CBLs also exhibited better stability than the devices with bare ZnO CBLs.

Poly(zinc diacrylate) (pZA) was used to passivate the defects in ZnO CBLs, as shown in Fig. 22b.[257] By *in situ* cross-linking poly(zinc diacrylate) (pZA) on ZnO films with a 3D network, Wu *et al.* demonstrated that the incorporation of pZA into the ZnO NP layer could decrease the trap-assisted recombination rather than giving better energy alignment between the active layer and the ZnO interlayer.[257] Based on the pZA cross-linked ZnO CBL derived from ZnO NP solution containing 0.5 wt% zinc diacrylate (ZDA), the inverted PSCs composed of respective P3HT:PCBM and PTB7:$PC_{71}BM$ active layers achieved a PCE of 3.26% and 7.37%, respectively, while the PCE for the reference devices without pZA were 2.58% and 6.67% for P3HT:PCBM and PTB7:$PC_{71}BM$ active layers, respectively. The improvement in the device performance was attributed to the enhanced charge generation and transport. Polyvinylpyrrolidone (PVP) is yet another polymer studied for the preparation of ZnO/polymer nanocomposite CBLs for highly efficient inverted PSCs.[173,259] Small *et al.* reported the preparation and application of ZnO–PVP nanocomposite CBLs in inverted PSCs[173] and found that the ZnO–PVP nanocomposite films exhibited more uniform distribution of the ZnO nano-clusters in the polymer matrix in view of suppressing ZnO aggregation. The inverted devices with UV-ozone treated (10 min) ZnO–PVP nanocomposite CBLs and PDTG-TPD:$PC_{71}BM$ active layers showed a PCE of 8.1% with a J_{sc} of 14.0 mA cm^{-2}, a V_{oc} of 0.86 V, and a FF of 67.3%. It was suggested that the PVP acted as an organic capping molecule and a polymeric matrix, promoting the formation of ZnO electron-transporting nanocomposite films with uniform morphology. Tiwari *et al.* compared the effects of ZnO–polyelectrolytes [poly(diallyldimethylammonium chloride) (PDADMAC), poly(acrylic acid sodium salt) (PAS), poly-(4-styrenesulfonic acid) (PSS), and polyvinylpyrrolidone (PVP)] nanocomposite CBLs on the device performance.[259] They found that the combination of ZnO with PVP and PDADMAC gave the highest improvement in the PCEs. Besides serving as a matrix for suppressing ZnO aggregation and passivating the surface traps in ZnO films, it has also been found that the ZnO/polymer composite exhibited adjustable energy bands.[260] Chen *et al.* reported solution processed ZnO/polyethylenimine (PEI) nanocomposite electron transport layers for facilitating electron extraction in inverted PSCs.[260] They found that the energy bands of ZnO/PEI composites could be tuned considerably by varying the content of PEI, and thus forming a good electron transport layer. In addition, by adjusting the content of PEI, the structural order of ZnO in the ZnO/PEI films was adjusted to align perpendicularly to the ITO electrode, facilitating the electron transport vertically in ZnO/PEI nanocomposite films.[260]

It is worth noting that, a crucial issue for ZnO–polymer composites or organic-stabilized ZnO NP CBLs is the removal of polymers or organic surfactants so as to improve the electrical properties of ZnO CBLs as well as the device performance. This is because the insulating polymer or the organic surfactant will aggravate the charge transport by introducing additional resistance.[172,173] Ultraviolet-ozone (UVO) treatment is regarded as a promising approach to remove the polymer from the ZnO surface and to ensure a good electrical coupling between ZnO and the active layer in view of the act that UVO treatment did not alter the size, shape or distribution of ZnO NPs. Cho *et al.* suggested that UVO treatment could effectively remove the residual organic stabilizer molecules on the surface of ZnO NP films through an UV induced decomposition mechanism.[172] Small *et al.* investigated the UVO treatment duration on the performance of inverted solar cells with the ZnO–PVP composite film as the CBL and found that ZnO–PVP nanocomposite films with UVO treated for 10 min led to the highest enhancement in the device performance compared to the devices without UVO treatment.[173] It has been found that the UVO treatment removed the top PVP enabling the ZnO NPs to expose at the film surface, which was proven by both AFM (Fig. 23a–d) and X-ray photoelectron spectroscopy (XPS) characterization techniques. The enhanced device performance with UVO treated ZNO–PVP nanocomposite films was ascribed to the modified surface composition promoting charge collection. The UVO treatment time is a crucial factor that determines the morphology and electrical properties of ZNO–PVP nanocomposite films. It has been demonstrated that a too short time treatment results in an incomplete removal of the PVP from the top surface of ZnO–PVP composite films, while a too long time treatment may induces excess oxygen onto the ZnO surface, which will reduce the electron extraction efficiency.[173] Over all, polymer modified ZnO NP/polymer hybrids or composite films are more uniform and with low defects than the unmodified ZnO NP films. By choosing a suitable polymer or an organic surfactant material, adjusting the amount and molecular weight of the polymer, and employing an optimized UVO treatment process, one can expect to enhance the performance of ZnO/polymer composite CBLs as well as the device performance.

6.2 ZnO and oxide or titanate composite CBLs

The composites of ZnO and other oxides or titanates have also been studied as CBLs of inverted PSCs. Lan *et al.* studied the Ta_2O_5–ZnO composite films with varied compositions fabricated by sol–gel processing as the CBL for inverted polymer solar cells, and demonstrated enhanced PCE with excellent stability.[263] It was found that the CBLs incorporated with Ta_2O_5 exert two competing impacts on the solar cell performances. On one hand, the presence of Ta_2O_5 is likely to induce more positive charges around the Zn atom and form Ta–O–Zn bonding; it can reduce the surface charge recombination between the active layer and the Ta_2O_5–ZnO composite CBL, and result in high power conversion efficiency; however, on the other hand an excessive amount

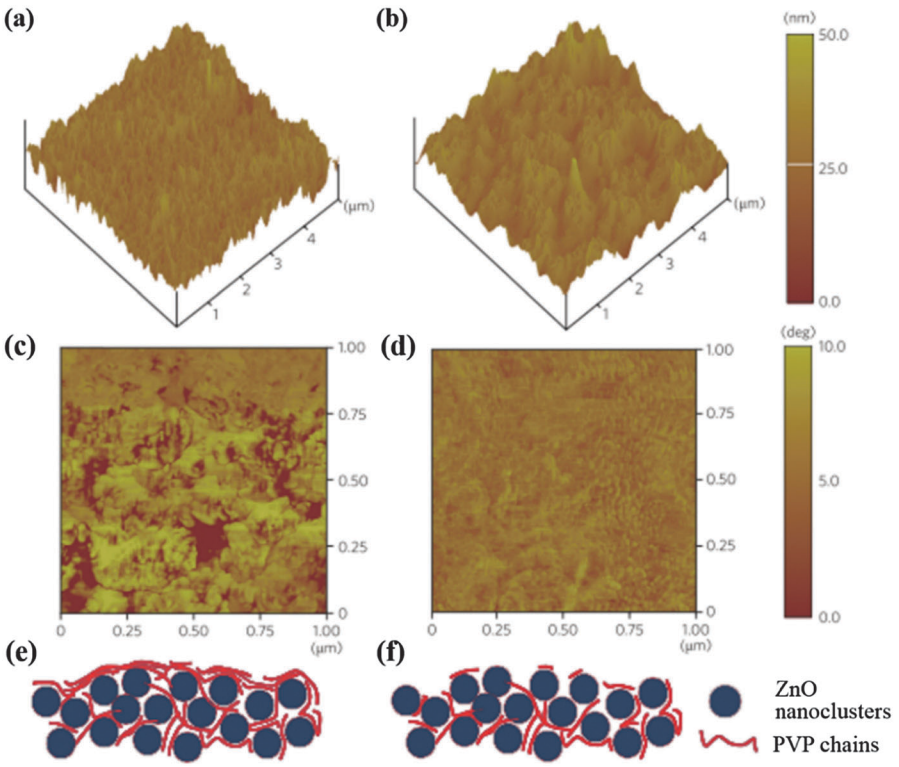

Fig. 23 Three-dimensional topography AFM images of (a) as-prepared and (b) 10 min UVO treated ZnO–PVP nanocomposite films. Phase images of (c) as-prepared and (d) 10 min UVO treated ZnO–PVP nanocomposite films. Schematic illustrations of (e) as-prepared and (f) 10 min UVO treated ZnO–PVP nanocomposite films.[173] Adapted with permission from ref. 173 Copyright 2011 Nature Publishing Group.

Table 7 Non-exhaustive survey of inverted polymer solar cells including a ZnO and oxide or titanate composite CBLs. The photovoltaic parameters are compared to those measured for a reference cell (values in parentheses) based on pristine ZnO CBLs

Device architecture	J_{sc} [mA cm^{-2}]	V_{oc} [V]	FF [%]	PCE [%]	Ref.
ITO/Ta_2O_5–ZnO/P3HT:PCBM/MoO_3/Ag	9.64 (9.49)	0.637 (0.636)	67.0 (61.3)	4.12 (3.70)	263
ITO/Ta_2O_5–ZnO/PSEHTT:$PC_{71}BM$/MoO_3/Ag	12.07 (12.04)	0.68 (0.67)	68.9 (65.6)	5.61 (5.29)	263
ITO/$SrTiO_3$: ZnO/P3HT:PCBM/PEDOT:PSS/Ag	10.08 (10.16)	0.63 (0.61)	64.7 (57.0)	4.10 (3.58)	98

of Ta_2O_5 would block the pathways of charge transport and lead to a drastic reduction in power conversion efficiency. In their results, the integration of 12–15% Ta_2O_5 into ZnO may result in the efficiency enhanced maximally for different active layers; the addition of excessive Ta_2O_5 would however lead to a dramatic decrease in the device performance, as per the photovoltaic parameters shown in Table 7. In addition, the inverted PSCs with Ta_2O_5–ZnO nanocomposite CBLs exhibited excellent long-term stability in air. In their work, the inverted PSCs with ZnO or Ta_2O_5–ZnO nanocomposite CBLs retained almost 100% of their original PCEs after being exposed under ambient conditions for 42 days without encapsulation.

In another work also done by Lan *et al.*, dual phase $SrTiO_3$: ZnO nanocomposite films with varied composition ratios were fabricated by sol–gel processing and applied as CBLs in inverted PSCs, and demonstrated enhanced device performance.[98] In their work, when the $SrTiO_3$: ZnO nanocomposite CBLs were assembled into the solar cell, the device properties including incident photon-to-current conversion efficiency (IPCE), power conversion efficiency, and electron mobility were investigated systematically. $SrTiO_3$ in CBLs was found to be amorphous or quasi-amorphous. Although more detailed experiments are needed, $SrTiO_3$ is more likely to have some local ordering structure with aligned TiO_6 octohedra, *i.e.*, a quasi-amorphous phase, and thus possesses spontaneous polarization. It has been demonstrated that the localized polar molecules $SrTiO_3$ in the nanocomposite CBL are in random orientations under the dark conditions or open circuit voltage conditions (Fig. 24a), while a self-built electric field on the interface between the active layer and CBL was generated by electron and hole transfer to the opposite direction and there is a net interface dipole directed away from the cathodic buffer layer under illumination (Fig. 24b). It was suggested that such a spontaneous polarization is likely to induce a self-built electric field to prevent electron recombination on the interface of the active layer and the CBL, which shows an enhancement of FF of device performance. As a result, an enhancement in PCE from 3.58% to 4.1% was achieved for the device with $SrTiO_3$: ZnO of 90 : 10 CBL and P3HT:PCBM active layer.[98] Fig. 24c shows the *I–V* curves of inverted devices with various $SrTiO_3$: ZnO nanocomposite CBLs. It was suggested that a further improvement of the solar cell performance could be expected by improving the crystallinity of both $SrTiO_3$ and ZnO.

7. Concluding remarks

PSCs are complex devices, so far high performance can only be achieved when all the following requirements are met: (1) a good p-type polymer donor and n-type fullerene derivative acceptor with the desired electronic structure, (2) a bulk heterojunction with the desired micro and nanostructures, and (3) interfaces between different layers for efficient charge separation and transport. Inverted PSCs introduce a cathode buffer layer of electron transport but hole blocking material, and thus demand extra efforts to understand and engineer both the interface and the material in terms of chemistry, crystallinity, morphology, surface roughness and contacts, chemical and physical stability, and electrical and electronic properties.

To achieve high power conversion efficiency, long-term device stability and compatible with the low-cost roll-to-roll manufacturing, much more efforts in the aspect of developing new materials, improving chemical and physical properties of interfaces, and low cost scalable processing are required. Further fundamental understanding and innovation and engineering of CBLs are an

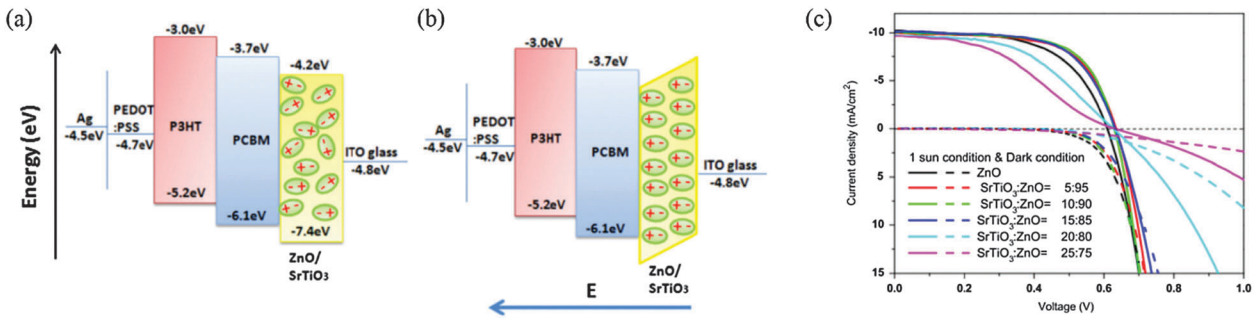

Fig. 24 Schematic energy level diagrams of inverted PSCs with $SrTiO_3$: ZnO composite CBLs. (a) The inverted device is under open circuit conditions, and there is no net interface dipole. (b) The inverted device is under illumination, and the electron field was generated by electron and hole transfer to the opposite direction and there is a net interface dipole directed away from the CBL. (c) *I–V* curves of inverted PSCs with various $SrTiO_3$: ZnO composite CBLs.[98] Adapted with permission from ref. 98 Copyright 2014 Elsevier.

important aspect for the achievement of highly efficient inverted PSCs. ZnO is the most extensively investigated material serving as CBLs in inverted PSCs due to its relatively high electron mobility, high transparency, ease of fabrication by solution-based processing at low temperature, good chemical stability and low cost.

The role of ZnO CBLs in an inverted PSC is to collect and transport electrons and block holes. The contact between ZnO CBLs and the polymer active layer can significantly affect the performance of inverted polymer solar cells. The contact quality relies on both the preparation method and the post-treatment, which can influence the properties of ZnO CBLs in terms of morphology, thickness and transmittance, and the surface state. Doping and surface modification are effective ways to tailor the electronic, optical and chemical properties of the ZnO CBL and thus to improve the photovoltaic performance of the inverted PSCs. To further improve the efficiency of inverted PSCs, some specific considerations with regard to the ZnO-based CBL are listed as follows:

(1) Development of ZnO-based CBLs with dense packing, a large surface area and high transmittance. A dense and homogenous surface of ZnO CBLs favors the formation of an intimate contact between ZnO CBLs and the BHJ photoactive layer, and thus lowers the contact resistance and decreases the series resistance (R_S) of the device. In addition, the dense surface also makes the ZnO layer having better electrical properties and higher transmittance. The large surface area of ZnO CBLs can enlarge the ZnO/BHJ active layer contact area, thus providing larger electron extraction interface and enabling more electrodes to penetrate into the BHJ active layer so as to reduce the charge transport distance and increase the J_{sc} of devices.

(2) Doping ZnO for higher conductivity and appropriate energy level. Appropriate doping can enhance the electrical conductivity of ZnO and thus improve the photovoltaic performance of inverted PSCs.

(3) Development of interfacial materials for the surface modification of ZnO-based CBLs, for instance the functional fullerene based SAMs, with appropriate surface energy and improved interfacial properties. The surface modification of ZnO-based CBL helps to reduce the charge recombination and improve the charge transport at the interface by passivating the surface defects, tuning the surface energy and work function, and may thus lead to improved photovoltaic performance of the inverted devices.

Abbreviations

AALD	Atmospheric atomic layer deposition
ABL	Anode buffer layer
AFM	Atomic force microscopy
ALD	Atomic layer deposition
AM	Air mass
AZO	Aluminum-doped zinc oxide
BHJ	Bulk heterojunction
CBL	Cathode buffer layer
C60	Fullerene
C60-COOH	2-(*p*-Carboxyphenyl)-*N*-methylpyrrolidino-C60
C60-PEG	Fullerene-end-capped poly(ethylene glycol)
CBD	Chemical bath deposition
C-PCBSD	Cross-linked [6,6]-phenyl-C61-butyric styryl endron ester
CPE	Conjugated polyelectrolyte
CuPc	Copper phthalocyanine
deZn	Diethylzinc
ECD	Electrochemical deposition
ECL	Electron collection layer (ECL)
ED	Electro-deposition
EPBT	Energy payback time
ESL	Electron selective layer
ETL	Electron transport layer
FF	Fill factor
FTO	Fluorinated tin oxide
GO	Graphene oxide
GZO	Gallium-doped zinc oxide
HCL	Hole collection layer
HOMO	The highest occupied molecular orbital
HSL	Hole selective layer
HTL	Hole transport layer
$IC_{60}BA$	Indene-C60 bisadduct
$IC_{60}MA$	Indene-C60 monoadduct
$IC_{70}BA$	Indene-C70 bisadduct
$IC_{70}MA$	Indene-C70 monoadduct
ITO	Indium tin oxide
IZO	Indium doped zinc oxide
i-ZnO	Intrinsic ZnO
J_{sc}	Short circuit current density
LUMO	The lowest unoccupied molecular orbital
MEA	Methoxyethoxyacetic acid
MoO_3	Molybdenum oxide
MPCVD	Mist pyrolysis chemical vapor deposition
NF	Nanofiber
NP	Nanoparticle
NR	Nanorod
NW	Nanowire
P3HT	Poly(3-hexylthiophene)
PCE	Power conversion efficiency
PCBM	Methyl[6,6]-phenyl-C60-butyrate
$PC_{71}BM$	Methyl[6,6]-phenyl-C70-butyrate
PCDTBT	Poly[2,6-(4,4-bis-(2-ethylhexyl)-4*H*-cyclopenta[2,1-*b*;3,4-*b*′]dithiophene)-*alt*-4,7-(2,1,3-benzothiadiazole)]
PDTG-TPD	Poly(thieno[3,4-*c*]pyrrole-4,6-dione-*co*-dithienogermole)
PDADMAC	Poly(diallyldimethylammonium chloride)
PEDOT:PSS	Poly(3,4-ethylenedioxithiophene):poly(styrene sulfonic acid)
PEG	Poly(ethylene glycol)
PEI	Polyethylenimine
PEN	Polyethylene naphthalate
PEO	Poly(ethylene oxide)
PES	Polyethersulfone

PET	Polyethylene terephthalate
PSC	Polymer solar cell
PsiF-DBT	Poly[(2,7-dioctylsi-lafluorene)-2,7-diyl-*alt*-(4,7-bis(2-thienyl)-2,1,3-benzothiadiaz-ole)-5,5′-diyl]
PVP	Poly(vinyl pyrrolidone)
pZA	Poly(zinc diacrylate)
R_S	Series resistance
R_{SH}	Shunt resistance
RF	Radio-frequency
RMS	Root-mean-square
SAM	Self-assembled monolayer
SEM	Scanning electron microscopy
SP	Spray-pyrolysis
TiO_2	Titanium oxide
T_R	Relative optical transmittance
UPS	Ultraviolet photoelectron spectroscopy
UV	Ultraviolet
UVO	Ultraviolet-ozone
UV-Vis	Ultraviolet-visible
V_{oc}	Open circuit voltage
XPS	X-ray photoelectron spectroscopy
XRD	X-ray diffraction
ZDA	Zinc diacrylate
$Zn(OAC)_2$	Zinc acetate
ZnO	Zinc oxide

Acknowledgements

This work was financially supported in part by the National Natural Science Foundation of China (No. 21373144, 51503136), Natural Science Foundation of Jiangsu Province of China (BK20140353, BK20150007, BK20130287) and China Post-doctoral Science Foundation (2014M561704). The work was also supported by the National Science Foundation of the U.S. (DMR-1035196 and DMR-1505902), Intel Research Lab, and the University of Washington TGIF.

Notes and references

1 T. Hisatomi, J. Kubota and K. Domen, *Chem. Soc. Rev.*, 2014, **43**, 7520–7535.
2 X. Chen, C. Li, M. Gratzel, R. Kostecki and S. S. Mao, *Chem. Soc. Rev.*, 2012, **41**, 7909–7937.
3 H. M. Chen, C. K. Chen, R. S. Liu, L. Zhang, J. Zhang and D. P. Wilkinson, *Chem. Soc. Rev.*, 2012, **41**, 5654–5671.
4 P. Pinel, C. A. Cruickshank, I. Beausoleil-Morrison and A. Wills, *Renewable Sustainable Energy Rev.*, 2011, **15**, 3341–3359.
5 A. F. B. Braga, S. P. Moreira, P. R. Zampieri, J. M. G. Bacchin and P. R. Mei, *Sol. Energy Mater. Sol. Cells*, 2008, **92**, 418–424.
6 Z. Zou, J. Ye, K. Sayama and H. Arakawa, *Nature*, 2001, **414**, 625–627.
7 J. Huang, Z. Yin and Q. Zheng, *Energy Environ. Sci.*, 2011, **4**, 3861–3877.
8 F. He and L. Yu, *J. Phys. Chem. Lett.*, 2011, **2**, 3102–3113.
9 Y. J. Cheng, S. H. Yang and C. S. Hsu, *Chem. Rev.*, 2009, **109**, 5868–5923.
10 M. A. Green, *Phys. E*, 2002, **14**, 65–70.
11 G. Li, V. Shrotriya, J. Huang, Y. Yao, T. Moriarty, K. Emery and Y. Yang, *Nat. Mater.*, 2005, **4**, 864–868.
12 S. K. Hau, H.-L. Yip and A. K. Y. Jen, *Polym. Rev.*, 2010, **50**, 474–510.
13 R. Po, C. Carbonera, A. Bernardi and N. Camaioni, *Energy Environ. Sci.*, 2011, **4**, 285–310.
14 G. Li, R. Zhu and Y. Yang, *Nat. Photonics*, 2012, **6**, 153–161.
15 S. B. Darling and F. You, *RSC Adv.*, 2013, **3**, 17633–17648.
16 S. Lizin, S. Van Passel, E. De Schepper, W. Maes, L. Lutsen, J. Manca and D. Vanderzande, *Energy Environ. Sci.*, 2013, **6**, 3136–3149.
17 S. Tomoki, U. Tokiyoshi, H. Yuuki, F. Akihiko and Y. Katsumi, *J. Phys. D: Appl. Phys.*, 2004, **37**, 847–850.
18 G. Yu, J. Gao, J. C. Hummelen, F. Wudl and A. J. Heeger, *Science*, 1995, **270**, 1789–1791.
19 H. Zeng, X. Zhu, Y. Liang and X. Guo, *Polymers*, 2015, **7**, 333–372.
20 B. C. Thompson and J. M. J. Fréchet, *Angew. Chem., Int. Ed.*, 2008, **47**, 58–77.
21 L.-M. Chen, Z. Hong, G. Li and Y. Yang, *Adv. Mater.*, 2009, **21**, 1434–1449.
22 S. Zhang, L. Ye, W. Zhao, D. Liu, H. Yao and J. Hou, *Macromolecules*, 2014, **47**, 4653–4659.
23 L. Ye, S. Zhang, W. Zhao, H. Yao and J. Hou, *Chem. Mater.*, 2014, **26**, 3603–3605.
24 T. L. Nguyen, H. Choi, S. J. Ko, M. A. Uddin, B. Walker, S. Yum, J. E. Jeong, M. H. Yun, T. J. Shin, S. Hwang, J. Y. Kim and H. Y. Woo, *Energy Environ. Sci.*, 2014, **7**, 3040–3051.
25 J. You, L. Dou, K. Yoshimura, T. Kato, K. Ohya, T. Moriarty, K. Emery, C.-C. Chen, J. Gao, G. Li and Y. Yang, *Nat. Commun.*, 2013, **4**, 1–10.
26 K. Kawano, R. Pacios, D. Poplavskyy, J. Nelson, D. D. C. Bradley and J. R. Durrant, *Sol. Energy Mater. Sol. Cells*, 2006, **90**, 3520–3530.
27 M. P. de Jong, L. J. van Ijzendoorn and M. J. A. de Voigt, *Appl. Phys. Lett.*, 2000, **77**, 2255–2257.
28 K. W. Wong, H. L. Yip, Y. Luo, K. Y. Wong, W. M. Lau, K. H. Low, H. F. Chow, Z. Q. Gao, W. L. Yeung and C. C. Chang, *Appl. Phys. Lett.*, 2002, **80**, 2788–2790.
29 Y. Sun, J. H. Seo, C. J. Takacs, J. Seifter and A. J. Heeger, *Adv. Mater.*, 2011, **23**, 1679–1683.
30 H. Cao, W. He, Y. Mao, X. Lin, K. Ishikawa, J. H. Dickerson and W. P. Hess, *J. Power Sources*, 2014, **264**, 168–183.
31 M. S. White, D. C. Olson, S. E. Shaheen, N. Kopidakis and D. S. Ginley, *Appl. Phys. Lett.*, 2006, **89**, 143517.
32 S. K. Hau, H.-L. Yip, N. S. Baek, J. Zou, K. O'Malley and A. K. Y. Jen, *Appl. Phys. Lett.*, 2008, **92**, 253301.
33 T. Yang, W. Cai, D. Qin, E. Wang, L. Lan, X. Gong, J. Peng and Y. Cao, *J. Phys. Chem. C*, 2010, **114**, 6849–6853.
34 F. Zhang, X. Xu, W. Tang, J. Zhang, Z. Zhuo, J. Wang, J. Wang, Z. Xu and Y. Wang, *Sol. Energy Mater. Sol. Cells*, 2011, **95**, 1785–1799.

35 C.-Y. Li, T.-C. Wen, T.-H. Lee, T.-F. Guo, J.-C.-A. Huang, Y.-C. Lin and Y.-J. Hsu, *J. Mater. Chem.*, 2009, **19**, 1643–1647.
36 J.-H. Huang, H.-Y. Wei, K.-C. Huang, C.-L. Chen, R.-R. Wang, F.-C. Chen, K.-C. Ho and C.-W. Chu, *Energy Environ. Sci.*, 2010, **3**, 654–658.
37 H.-L. Yip and A. K. Y. Jen, *Energy Environ. Sci.*, 2012, **5**, 5994–6011.
38 Z. Yin, Q. Zheng, S.-C. Chen and D. Cai, *ACS Appl. Mater. Interfaces*, 2013, **5**, 9015–9025.
39 C. Girotto, B. P. Rand, S. Steudel, J. Genoe and P. Heremans, *Org. Electron.*, 2009, **10**, 735–740.
40 K. Frederik C, *Org. Electron.*, 2009, **10**, 761–768.
41 M. R. Lilliedal, A. J. Medford, M. V. Madsen, K. Norrman and F. C. Krebs, *Sol. Energy Mater. Sol. Cells*, 2010, **94**, 2018–2031.
42 Z. Xu, L.-M. Chen, G. Yang, C.-H. Huang, J. Hou, Y. Wu, G. Li, C.-S. Hsu and Y. Yang, *Adv. Funct. Mater.*, 2009, **19**, 1227–1234.
43 S. Schumann, R. Da Campo, B. Illy, A. C. Cruickshank, M. A. McLachlan, M. P. Ryan, D. J. Riley, D. W. McComb and T. S. Jones, *J. Mater. Chem.*, 2011, **21**, 2381–2386.
44 L.-M. Chen, Z. Xu, Z. Hong and Y. Yang, *J. Mater. Chem.*, 2010, **20**, 2575–2598.
45 Z. He, C. Zhong, S. Su, M. Xu, H. Wu and Y. Cao, *Nat. Photonics*, 2012, **6**, 591–595.
46 J. Kong, I. W. Hwang and K. Lee, *Adv. Mater.*, 2014, **26**, 6275–6283.
47 L. K. Jagadamma, M. Al-Senani, A. El-Labban, I. Gereige, G. O. Ngongang Ndjawa, J. C. D. Faria, T. Kim, K. Zhao, F. Cruciani, D. H. Anjum, M. A. McLachlan, P. M. Beaujuge and A. Amassian, *Adv. Energy Mater.*, 2015, **5**, 1500204.
48 Z. Yin, Q. Zheng, S.-C. Chen, D. Cai, L. Zhou and J. Zhang, *Adv. Energy Mater.*, 2014, **4**, 1301404.
49 S. H. Liao, H. J. Jhuo, P. N. Yeh, Y. S. Cheng, Y. L. Li, Y. H. Lee, S. Sharma and S. A. Chen, *Sci. Rep.*, 2014, **4**, 6813.
50 P. Li, X. Li, C. Sun, G. Wang, J. Li, T. Jiu and J. Fang, *Sol. Energy Mater. Sol. Cells*, 2014, **126**, 36–41.
51 Z. He, B. Xiao, F. Liu, H. Wu, Y. Yang, S. Xiao, C. Wang, T. P. Russell and Y. Cao, *Nat. Photonics*, 2015, **9**, 174–179.
52 Y. Liu, J. Zhao, Z. Li, C. Mu, W. Ma, H. Hu, K. Jiang, H. Lin, H. Ade and H. Yan, *Nat. Commun.*, 2014, **5**, 5293.
53 W. Yu, L. Huang, D. Yang, P. Fu, L. Zhou, J. Zhang and C. Li, *J. Mater. Chem. A*, 2015, **3**, 10660–10665.
54 X. Ouyang, R. Peng, L. Ai, X. Zhang and Z. Ge, *Nat. Photonics*, 2015, **9**, 520–524.
55 M. Jørgensen, K. Norrman, S. A. Gevorgyan, T. Tromholt, B. Andreasen and F. C. Krebs, *Adv. Mater.*, 2012, **24**, 580–612.
56 R. R. Søndergaard, M. Hösel and F. C. Krebs, *J. Polym. Sci., Part B: Polym. Phys.*, 2013, **51**, 16–34.
57 H. Zhou, Q. Chen, G. Li, S. Luo, T.-B. Song, H.-S. Duan, Z. Hong, J. You, Y. Liu and Y. Yang, *Science*, 2014, **345**, 542–546.
58 N. J. Jeon, J. H. Noh, Y. C. Kim, W. S. Yang, S. Ryu and S. I. Seok, *Nat. Mater.*, 2014, **13**, 897–903.
59 Q. Lin, A. Armin, R. C. R. Nagiri, P. L. Burn and P. Meredith, *Nat. Photonics*, 2015, **9**, 106–112.
60 J. T. Wang, J. M. Ball, E. M. Barea, A. Abate, J. A. Alexander-Webber, J. Huang, M. Saliba, I. Mora-Sero, J. Bisquert, H. J. Snaith and R. J. Nicholas, *Nano Lett.*, 2014, **14**, 724–730.
61 S. Ryu, J. H. Noh, N. J. Jeon, Y. Chan Kim, W. S. Yang, J. Seo and S. I. Seok, *Energy Environ. Sci.*, 2014, **7**, 2614.
62 M. Liu, M. B. Johnston and H. J. Snaith, *Nature*, 2013, **501**, 395–398.
63 J. Burschka, N. Pellet, S. J. Moon, R. Humphry-Baker, P. Gao, M. K. Nazeeruddin and M. Gratzel, *Nature*, 2013, **499**, 316–319.
64 S. Ye, W. Sun, Y. Li, W. Yan, H. Peng, Z. Bian, Z. Liu and C. Huang, *Nano Lett.*, 2015, **15**, 3723–3728.
65 C. Tao, S. Neutzner, L. Colella, S. Marras, A. R. Srimath Kandada, M. Gandini, M. D. Bastiani, G. Pace, L. Manna, M. Caironi, C. Bertarelli and A. Petrozza, *Energy Environ. Sci.*, 2015, **8**, 2365–2370.
66 W. S. Yang, J. H. Noh, N. J. Jeon, Y. C. Kim, S. Ryu, J. Seo and S. I. Seok, *Science*, 2015, **348**, 1234–1237.
67 J. Shi, X. Xu, D. Li and Q. Meng, *Small*, 2015, **11**, 2472–2486.
68 J. Cao, J. Yin, S. F. Yuan, Y. Zhao, J. Li and N. F. Zheng, *Nanoscale*, 2015, **7**, 9443–9447.
69 N. Aristidou, I. Sanchez-Molina, T. Chotchuangchutchaval, M. Brown, L. Martinez, T. Rath and S. A. Haque, *Angew. Chem.*, 2015, **54**, 8208–8212.
70 S. Guarnera, A. Abate, W. Zhang, J. M. Foster, G. Richardson, A. Petrozza and H. J. Snaith, *J. Phys. Chem. Lett.*, 2015, **6**, 432–437.
71 H. Choi, C. K. Mai, H. B. Kim, J. Jeong, S. Song, G. C. Bazan, J. Y. Kim and A. J. Heeger, *Nat. Commun.*, 2015, **6**, 7348.
72 X. Dong, X. Fang, M. Lv, B. Lin, S. Zhang, J. Ding and N. Yuan, *J. Mater. Chem. A*, 2015, **3**, 5360–5367.
73 H. Choi, J. W. Cho, M.-S. Kang and J. Ko, *Chem. Commun.*, 2015, **51**, 9305–9308.
74 J. Gong, S. B. Darling and F. You, *Energy Environ. Sci.*, 2015, **8**, 1953–1968.
75 N. Espinosa, L. Serrano-Luján, A. Urbina and F. C. Krebs, *Sol. Energy Mater. Sol. Cells*, 2015, **137**, 303–310.
76 A. K. K. Kyaw, X. W. Sun, C. Y. Jiang, G. Q. Lo, D. W. Zhao and D. L. Kwong, *Appl. Phys. Lett.*, 2008, **93**, 221107.
77 J.-P. Liu, K.-L. Choy and X.-H. Hou, *J. Mater. Chem.*, 2011, **21**, 1966–1969.
78 T. Z. Oo, R. D. Chandra, N. Yantara, R. R. Prabhakar, L. H. Wong, N. Mathews and S. G. Mhaisalkar, *Org. Electron.*, 2012, **13**, 870–874.
79 S. K. Hau, H.-L. Yip, O. Acton, N. S. Baek, H. Ma and A. K. Y. Jen, *J. Mater. Chem.*, 2008, **18**, 5113–5119.
80 T. Kuwabara, H. Sugiyama, T. Yamaguchi and K. Takahashi, *Thin Solid Films*, 2009, **517**, 3766–3769.
81 I. Sasajima, S. Uesaka, T. Kuwabara, T. Yamaguchi and K. Takahashi, *Org. Electron.*, 2011, **12**, 113–118.
82 Y.-J. Kang, C. S. Kim, D. S. You, S. H. Jung, K. Lim, D.-G. Kim, J.-K. Kim, S. H. Kim, Y.-R. Shin, S.-H. Kwon and J.-W. Kang, *Appl. Phys. Lett.*, 2011, **99**, 073308.

83 Y. Zhou, H. Cheun, J. W. J. Potscavage, C. Fuentes-Hernandez, S.-J. Kim and B. Kippelen, *J. Mater. Chem.*, 2010, **20**, 6189–6194.
84 O. Wiranwetchayan, Z. Liang, Q. Zhang, G. Cao and P. Singjai, *Mater. Sci. Appl.*, 2011, **2**, 1697–1701.
85 Y. Zhu, X. Xu, L. Zhang, J. Chen and Y. Cao, *Sol. Energy Mater. Sol. Cells*, 2012, **97**, 83–88.
86 M. Jin Tan, S. Zhong, R. Wang, Z. Zhang, V. Chellappan and W. Chen, *Appl. Phys. Lett.*, 2013, **103**, 063303.
87 S. Woo, W. Hyun Kim, H. Kim, Y. Yi, H.-K. Lyu and Y. Kim, *Adv. Energy Mater.*, 2014, **4**, 1301692.
88 R. Xia, D.-S. Leem, T. Kirchartz, S. Spencer, C. Murphy, Z. He, H. Wu, S. Su, Y. Cao, J. S. Kim, J. C. deMello, D. D. C. Bradley and J. Nelson, *Adv. Energy Mater.*, 2013, **3**, 718–723.
89 Z. Tang, W. Tress, Q. Bao, M. J. Jafari, J. Bergqvist, T. Ederth, M. R. Andersson and O. Inganäs, *Adv. Energy Mater.*, 2014, **4**, 1400643.
90 T. Kuwabara, M. Nakamoto, Y. Kawahara, T. Yamaguchi and K. Takahashi, *J. Appl. Phys.*, 2009, **105**, 124513–124516.
91 J.-J. Zhu, Z.-Q. Xu, G.-Q. Fan, S.-T. Lee, Y.-Q. Li and J.-X. Tang, *Org. Electron.*, 2011, **12**, 2151–2158.
92 J.-J. Zhu, G.-Q. Fan, H.-X. Wei, Y.-Q. Li, S.-T. Lee and J.-X. Tang, *CrystEngComm*, 2012, **14**, 8090–8096.
93 G. Li, C. W. Chu, V. Shrotriya, J. Huang and Y. Yang, *Appl. Phys. Lett.*, 2006, **88**, 253503.
94 H.-H. Liao, L.-M. Chen, Z. Xu, G. Li and Y. Yang, *Appl. Phys. Lett.*, 2008, **92**, 173303.
95 Y.-I. Lee, J.-H. Youn, M.-S. Ryu, J. Kim, H.-T. Moon and J. Jang, *Sol. Energy Mater. Sol. Cells*, 2011, **95**, 3276–3280.
96 H. Bin Yang, Y. Qian Dong, X. Wang, S. Yun Khoo, B. Liu and C. Ming Li, *Sol. Energy Mater. Sol. Cells*, 2013, **117**, 214–218.
97 J. W. Kim, Y. H. Suh, C. L. Lee, Y. S. Kim and W. B. Kim, *Nanoscale*, 2015, **7**, 4367–4371.
98 J.-L. Lan, Z. Liang, Y.-H. Yang, F. S. Ohuchi, S. A. Jenekhe and G. Cao, *Nano Energy*, 2014, **4**, 140–149.
99 J. Liu, S. Shao, G. Fang, B. Meng, Z. Xie and L. Wang, *Adv. Mater.*, 2012, **24**, 2774–2779.
100 M. R. Rajesh Menon, M. V. Maheshkumar, K. Sreekumar, C. Sudha Kartha and K. P. Vijayakumar, *Sol. Energy Mater. Sol. Cells*, 2010, **94**, 2212–2217.
101 M. R. R. Menon, M. V. Maheshkumar, K. Sreekumar, C. S. Kartha and K. P. Vijayakumar, *Phys. Status Solidi A*, 2012, **209**, 199–203.
102 X. Chen, J. Yang, L. Y. X. C. Haley, J. Lu, F. Zhu and K. P. Loh, *Org. Electron.*, 2010, **11**, 1942–1946.
103 K. Sun, H. Zhang and J. Ouyang, *J. Mater. Chem.*, 2011, **21**, 18339–18346.
104 K. Sun, B. Zhao, A. Kumar, K. Zeng and J. Ouyang, *ACS Appl. Mater. Interfaces*, 2012, **4**, 2009–2017.
105 A. Li, R. Nie, X. Deng, H. Wei, S. Zheng, Y. Li, J. Tang and K.-Y. Wong, *Appl. Phys. Lett.*, 2014, **104**, 123303.
106 Q. Zhang, D. Zhang, X. Li, X. Liu, W. Zhang, L. Han and J. Fang, *Chem. Commun.*, 2015, **51**, 10182–10185.
107 C. Y. Jiang, X. W. Sun, D. W. Zhao, A. K. K. Kyaw and Y. N. Li, *Sol. Energy Mater. Sol. Cells*, 2010, **94**, 1618–1621.
108 M. P. Nikiforov, J. Strzalka, Z. Jiang and S. B. Darling, *Phys. Chem. Chem. Phys.*, 2013, **15**, 13052–13060.
109 X. Wan, G. Long, L. Huang and Y. Chen, *Adv. Mater.*, 2011, **23**, 5342–5358.
110 J. Liu, Y. Xue, Y. Gao, D. Yu, M. Durstock and L. Dai, *Adv. Mater.*, 2012, **24**, 2228–2233.
111 J. Liu, M. Durstock and L. Dai, *Energy Environ. Sci.*, 2014, **7**, 1297–1306.
112 Y. W. Heo, D. P. Norton, L. C. Tien, Y. Kwon, B. S. Kang, F. Ren, S. J. Pearton and J. R. LaRoche, *Mater. Sci. Eng., R*, 2004, **47**, 1–47.
113 K. Ellmer, *J. Phys. D: Appl. Phys.*, 2001, **34**, 3097–3108.
114 S. H. Liao, H. J. Jhuo, Y. S. Cheng and S. A. Chen, *Adv. Mater.*, 2013, **25**, 4766–4771.
115 F. C. Krebs, J. Fyenbo, D. M. Tanenbaum, S. A. Gevorgyan, R. Andriessen, B. van Remoortere, Y. Galagan and M. Jorgensen, *Energy Environ. Sci.*, 2011, **4**, 4116–4123.
116 F. C. Krebs, T. Tromholt and M. Jorgensen, *Nanoscale*, 2010, **2**, 873–886.
117 F. C. Krebs, J. Fyenbo and M. Jorgensen, *J. Mater. Chem.*, 2010, **20**, 8994–9001.
118 F. C. Krebs, T. D. Nielsen, J. Fyenbo, M. Wadstrom and M. S. Pedersen, *Energy Environ. Sci.*, 2010, **3**, 512–525.
119 F. C. Krebs, S. A. Gevorgyan and J. Alstrup, *J. Mater. Chem.*, 2009, **19**, 5442–5451.
120 G. D. Spyropoulos, P. Kubis, N. Li, D. Baran, L. Lucera, M. Salvador, T. Ameri, M. M. Voigt, F. C. Krebs and C. J. Brabec, *Energy Environ. Sci.*, 2014, **7**, 3284–3290.
121 R. Steim, F. R. Kogler and C. J. Brabec, *J. Mater. Chem.*, 2010, **20**, 2499–2512.
122 R. Po, M. Maggini and N. Camaioni, *J. Phys. Chem. C*, 2010, **114**, 695–706.
123 W. Cai, X. Gong and Y. Cao, *Sol. Energy Mater. Sol. Cells*, 2010, **94**, 114–127.
124 Y.-Y. Lai, Y.-J. Cheng and C.-S. Hsu, *Energy Environ. Sci.*, 2014, **7**, 1866–1883.
125 F. Wang, Z. a. Tan and Y. Li, *Energy Environ. Sci.*, 2015, **8**, 1059–1091.
126 I. Etxebarria, J. Ajuria and R. Pacios, *Org. Electron.*, 2015, **19**, 34–60.
127 C.-C. Chueh, C.-Z. Li and A. K. Y. Jen, *Energy Environ. Sci.*, 2015, **8**, 1160–1189.
128 A. Manor, E. A. Katz, T. Tromholt and F. C. Krebs, *Sol. Energy Mater. Sol. Cells*, 2012, **98**, 491–493.
129 J.-C. Wang, W.-T. Weng, M.-Y. Tsai, M.-K. Lee, S.-F. Horng, T.-P. Perng, C.-C. Kei, C.-C. Yu and H.-F. Meng, *J. Mater. Chem.*, 2010, **20**, 862–866.
130 J. Sun, Y. Zhu, X. Xu, L. Lan, L. Zhang, P. Cai, J. Chen, J. Peng and Y. Cao, *J. Phys. Chem. C*, 2012, **116**, 14188–14198.
131 A. Moliton and J.-M. Nunzi, *Polym. Int.*, 2006, **55**, 583–600.
132 Z. Liang, Q. Zhang, O. Wiranwetchayan, J. Xi, Z. Yang, K. Park, C. Li and G. Cao, *Adv. Funct. Mater.*, 2012, **22**, 2194–2201.
133 T. Kuwabara, Y. Kawahara, T. Yamaguchi and K. Takahashi, *ACS Appl. Mater. Interfaces*, 2009, **1**, 2107–2110.

134 M.-Y. Liu, C.-H. Chang, C.-H. Chang, K.-H. Tsai, J.-S. Huang, C.-Y. Chou, I.-J. Wang, P.-S. Wang, C.-Y. Lee, C.-H. Chao, C.-L. Yeh, C.-I. Wu and C.-F. Lin, *Thin Solid Films*, 2010, **518**, 4964–4969.
135 H.-J. Park, K.-H. Lee, B. Kumar, K.-S. Shin, S.-W. Jeong and S.-W. Kim, *J. Nanoelectron. Optoelectron.*, 2010, **5**, 135–138.
136 H. O. Seo, S.-Y. Park, W. H. Shim, K.-D. Kim, K. H. Lee, M. Y. Jo, J. H. Kim, E. Lee, D.-W. Kim, Y. D. Kim and D. C. Lim, *J. Phys. Chem. C*, 2011, **115**, 21517–21520.
137 C. Zhang, H. You, Z. Lin and Y. Hao, *Jpn. J. Appl. Phys.*, 2011, **50**, 082302.
138 D. C. Lim, W. H. Shim, K.-D. Kim, H. O. Seo, J.-H. Lim, Y. Jeong, Y. D. Kim and K. H. Lee, *Sol. Energy Mater. Sol. Cells*, 2011, **95**, 3036–3040.
139 N. Sekine, C.-H. Chou, W. L. Kwan and Y. Yang, *Org. Electron.*, 2009, **10**, 1473–1477.
140 L. K. Jagadamma, M. Abdelsamie, A. El Labban, E. Aresu, G. O. Ngongang Ndjawa, D. H. Anjum, D. Cha, P. M. Beaujuge and A. Amassian, *J. Mater. Chem. A*, 2014, **2**, 13321–13331.
141 X. Bao, A. Yang, Y. Yang, T. Wang, L. Sun, N. Wang and L. Han, *Phys. B*, 2014, **432**, 1–4.
142 H.-Y. Park, D. Lim, K.-D. Kim and S.-Y. Jang, *J. Mater. Chem. A*, 2013, **1**, 6327–6334.
143 S. K. Hau, H.-L. Yip, J. Zou and A. K. Y. Jen, *Org. Electron.*, 2009, **10**, 1401–1407.
144 S. Chen, C. E. Small, C. M. Amb, J. Subbiah, T.-h. Lai, S.-W. Tsang, J. R. Manders, J. R. Reynolds and F. So, *Adv. Energy Mater.*, 2012, **2**, 1333–1337.
145 M. J. Tan, S. Zhong, J. Li, Z. Chen and W. Chen, *ACS Appl. Mater. Interfaces*, 2013, **5**, 4696–4701.
146 W. Qin, X. Xu, D. Liu, C. Ma, L. Yang, S. Yin, F. Zhang and J. Wei, *J. Renewable Sustainable Energy*, 2013, **5**, 053106.
147 S. Park, S. J. Tark, J. S. Lee, H. Lim and D. Kim, *Sol. Energy Mater. Sol. Cells*, 2009, **93**, 1020–1023.
148 H. Cheun, C. Fuentes-Hernandez, Y. Zhou, W. J. Potscavage, S.-J. Kim, J. Shim, A. Dindar and B. Kippelen, *J. Phys. Chem. C*, 2010, **114**, 20713–20718.
149 C.-Y. Chang and F.-Y. Tsai, *J. Mater. Chem.*, 2011, **21**, 5710–5715.
150 R. L. Z. Hoye, D. Muñoz-Rojas, D. C. Iza, K. P. Musselman and J. L. MacManus-Driscoll, *Sol. Energy Mater. Sol. Cells*, 2013, **116**, 197–202.
151 K. D. Kim, D. C. Lim, J. Hu, J. D. Kwon, M. G. Jeong, H. O. Seo, J. Y. Lee, K. Y. Jang, J. H. Lim, K. H. Lee, Y. Jeong, Y. D. Kim and S. Cho, *ACS Appl. Mater. Interfaces*, 2013, **5**, 8718–8723.
152 N. O. V. Plank, M. E. Welland, J. L. MacManus-Driscoll and L. Schmidt-Mende, *Thin Solid Films*, 2008, **516**, 7218–7222.
153 Y.-J. Noh, S.-I. Na and S.-S. Kim, *Sol. Energy Mater. Sol. Cells*, 2013, **117**, 139–144.
154 Z. Hu, J. Zhang and Y. Zhu, *Sol. Energy Mater. Sol. Cells*, 2013, **117**, 610–616.
155 K.-S. Shin, H.-J. Park, B. Kumar, K.-K. Kim, S.-G. Ihn and S.-W. Kim, *J. Mater. Chem.*, 2011, **21**, 12274–12279.
156 S.-G. Ihn, K.-S. Shin, M.-J. Jin, X. Bulliard, S. Yun, Y. Suk Choi, Y. Kim, J.-H. Park, M. Sim, M. Kim, K. Cho, T. Sang Kim, D. Choi, J.-Y. Choi, W. Choi and S.-W. Kim, *Sol. Energy Mater. Sol. Cells*, 2011, **95**, 1610–1614.
157 F. Zhu, X. Chen, L. Zhou, J. Zhou, J. Yang, S. Huang and Z. Sun, *Thin Solid Films*, 2014, **551**, 131–135.
158 F. Zhu, X. Chen, J. Zhou, Z. Lu, Y. Chen, S. Huang and Z. Sun, *Mater. Res. Express*, 2014, **1**, 025020.
159 J.-H. Lee, S. Yoshikawa and T. Sagawa, *Sol. Energy Mater. Sol. Cells*, 2014, **127**, 111–121.
160 Y. Lare, A. Godoy, L. Cattin, K. Jondo, T. Abachi, F. R. Diaz, M. Morsli, K. Napo, M. A. del Valle and J. C. Bernède, *Appl. Surf. Sci.*, 2009, **255**, 6615–6619.
161 M. Ohyama, H. Kouzuka and T. Yoko, *Thin Solid Films*, 1997, **306**, 78–85.
162 T. Stubhan, H. Oh, L. Pinna, J. Krantz, I. Litzov and C. J. Brabec, *Org. Electron.*, 2011, **12**, 1539–1543.
163 L. Znaidi, *Mater. Sci. Eng., B*, 2010, **174**, 18–30.
164 B. S. Ong, C. Li, Y. Li, Y. Wu and R. Loutfy, *J. Am. Chem. Soc.*, 2007, **129**, 2750–2751.
165 C. Jiang, R. R. Lunt, P. M. Duxbury and P. P. Zhang, *RSC Adv.*, 2014, **4**, 3604–3610.
166 P. Morvillo, R. Diana, A. Mucci, E. Bobeico, R. Ricciardi and C. Minarini, *Sol. Energy Mater. Sol. Cells*, 2015, **141**, 210–217.
167 Z. Lin, J. Chang, C. Jiang, J. Zhang, J. Wu and C. Zhu, *RSC Adv.*, 2014, **4**, 6646–6651.
168 B. A. MacLeod, B. J. Tremolet de Villers, P. Schulz, P. F. Ndione, H. Kim, A. J. Giordano, K. Zhu, S. R. Marder, S. Graham, J. J. Berry, A. Kahn and D. C. Olson, *Energy Environ. Sci.*, 2015, **8**, 592–601.
169 S. K. Hau, Y.-J. Cheng, H.-L. Yip, Y. Zhang, H. Ma and A. K. Y. Jen, *ACS Appl. Mater. Interfaces*, 2010, **2**, 1892–1902.
170 A. L. Roest, J. J. Kelly, D. Vanmaekelbergh and E. A. Meulenkamp, *Phys. Rev. Lett.*, 2002, **89**, 036801.
171 P. Li, T. Jiu, G. Tang, G. Wang, J. Li, X. Li and J. Fang, *ACS Appl. Mater. Interfaces*, 2014, **6**, 18172–18179.
172 J. M. Cho, S.-W. Kwak, H. Aqoma, J. W. Kim, W. S. Shin, S.-J. Moon, S.-Y. Jang and J. Jo, *Org. Electron.*, 2014, **15**, 1942–1950.
173 C. E. Small, S. Chen, J. Subbiah, C. M. Amb, S.-W. Tsang, T.-H. Lai, J. R. Reynolds and F. So, *Nat. Photonics*, 2012, **6**, 115–120.
174 S. Shao, K. Zheng, T. Pullerits and F. Zhang, *ACS Appl. Mater. Interfaces*, 2012, **5**, 380–385.
175 Y. Chen, Z. Hu, Z. Zhong, W. Shi, J. Peng, J. Wang and Y. Cao, *J. Phys. Chem. C*, 2014, **118**, 21819–21825.
176 I. A. Kowalik, E. Guziewicz, K. Kopalko, S. Yatsunenko, A. Wójcik-Głodowska, M. Godlewski, P. Dłużewski, E. Łusakowska and W. Paszkowicz, *J. Cryst. Growth*, 2009, **311**, 1096–1101.
177 S. Oh, I. Jang, S.-G. Oh and S. S. Im, *Sol. Energy*, 2015, **114**, 32–38.
178 X. Yu, X. Yu, Z. Hu, J. Zhang, G. Zhao and Y. Zhao, *Mater. Lett.*, 2013, **108**, 50–53.
179 Z. Ma, Z. Tang, E. Wang, M. R. Andersson, O. Inganäs and F. Zhang, *J. Phys. Chem. C*, 2012, **116**, 24462–24468.
180 R. B. Ambade, S. B. Ambade, R. S. Mane and S. H. Lee, *ACS Appl. Mater. Interfaces*, 2015, **7**, 7951–7960.

181 S. Wilken, J. Parisi and H. Borchert, *J. Phys. Chem. C*, 2014, **118**, 19672–19682.
182 F. Verbakel, S. C. J. Meskers and R. A. J. Janssen, *J. Appl. Phys.*, 2007, **102**, 083701.
183 A. Sharma, M. Ionescu, G. G. Andersson and D. A. Lewis, *Sol. Energy Mater. Sol. Cells*, 2013, **115**, 64–70.
184 A. Sharma, J. B. Franklin, B. Singh, G. G. Andersson and D. A. Lewis, *Org. Electron.*, 2015, **24**, 131–136.
185 S. Loser, B. Valle, K. A. Luck, C. K. Song, G. Ogien, M. C. Hersam, K. D. Singer and T. J. Marks, *Adv. Energy Mater.*, 2014, **4**, 1301938.
186 S. O'Brien, L. H. K. Koh and G. M. Crean, *Thin Solid Films*, 2008, **516**, 1391–1395.
187 S. Kamaruddin, K.-Y. Chan, H.-K. Yow, M. Zainizan Sahdan, H. Saim and D. Knipp, *Appl. Phys. A: Mater. Sci. Process.*, 2011, **104**, 263–268.
188 Y. Li, L. Xu, X. Li, X. Shen and A. Wang, *Appl. Surf. Sci.*, 2010, **256**, 4543–4547.
189 K. P. Bhuvana, J. Elanchezhiyan, N. Gopalakrishnan and T. Balasubramanian, *J. Alloys Compd.*, 2009, **473**, 534–537.
190 X. Yu, Z.-Y. Hu, Z.-H. Huang, X.-M. Yu, J.-J. Zhang, G.-S. Zhao and Y. Zhao, *Chin. Phys. B*, 2013, **22**, 118801.
191 X. Yu, X. Yu, J. Zhang, Z. Hu, G. Zhao and Y. Zhao, *Sol. Energy Mater. Sol. Cells*, 2014, **121**, 28–34.
192 H. Oh, J. Krantz, I. Litzov, T. Stubhan, L. Pinna and C. J. Brabec, *Sol. Energy Mater. Sol. Cells*, 2011, **95**, 2194–2199.
193 K.-S. Shin, K.-H. Lee, H. H. Lee, D. Choi and S.-W. Kim, *J. Phys. Chem. C*, 2010, **114**, 15782–15785.
194 K. Aung Ko Ko, S. Xiaowei, Z. De Wei, T. Swee Tiam, Y. Divayana and H. V. Demir, *IEEE J. Sel. Top. Quantum Electron.*, 2010, **16**, 1700–1706.
195 J. Alstrup, M. Jørgensen, A. J. Medford and F. C. Krebs, *ACS Appl. Mater. Interfaces*, 2010, **2**, 2819–2827.
196 R. Søndergaard, M. Helgesen, M. Jørgensen and F. C. Krebs, *Adv. Energy Mater.*, 2011, **1**, 68–71.
197 S. Trost, K. Zilberberg, A. Behrendt, A. Polywka, P. Görrn, P. Reckers, J. Maibach, T. Mayer and T. Riedl, *Adv. Energy Mater.*, 2013, **3**, 1437–1444.
198 S.-W. Cho, Y. T. Kim, W. H. Shim, S.-Y. Park, K.-D. Kim, H. O. Seo, N. K. Dey, J.-H. Lim, Y. Jeong, K. H. Lee, Y. D. Kim and D. C. Lim, *Appl. Phys. Lett.*, 2011, **98**, 023102.
199 A. Gadisa, Y. Liu, E. T. Samulski and R. Lopez, *Appl. Phys. Lett.*, 2012, **100**, 253903.
200 M. Thambidurai, J. Y. Kim, J. Song, Y. Ko, H.-J. Song, C.-M. Kang, N. Muthukumarasamy, D. Velauthapillai and C. Lee, *J. Mater. Chem. C*, 2013, **1**, 8161.
201 O. Pachoumi, C. Li, Y. Vaynzof, K. K. Banger and H. Sirringhaus, *Adv. Energy Mater.*, 2013, **3**, 1428–1436.
202 T. Stubhan, M. Salinas, A. Ebel, F. C. Krebs, A. Hirsch, M. Halik and C. J. Brabec, *Adv. Energy Mater.*, 2012, **2**, 532–535.
203 S. H. Tsai, S. T. Ho, H. J. Jhuo, C. R. Ho, S. A. Chen and J.-H. He, *Appl. Phys. Lett.*, 2013, **102**, 253111.
204 J. Piris, N. Kopidakis, D. C. Olson, S. E. Shaheen, D. S. Ginley and G. Rumbles, *Adv. Funct. Mater.*, 2007, **17**, 3849–3857.
205 B. A. MacLeod, P. Schulz, S. R. Cowan, A. Garcia, D. S. Ginley, A. Kahn and D. C. Olson, *Adv. Energy Mater.*, 2014, **4**, 1400073.
206 M. Lenes, L. J. A. Koster, V. D. Mihailetchi and P. W. M. Blom, *Appl. Phys. Lett.*, 2006, **88**, 243502.
207 D. W. Sievers, V. Shrotriya and Y. Yang, *J. Appl. Phys.*, 2006, **100**, 114509.
208 T. Kirchartz, T. Agostinelli, M. Campoy-Quiles, W. Gong and J. Nelson, *J. Phys. Chem. Lett.*, 2012, **3**, 3470–3475.
209 W. L. Ma, C. Y. Yang, X. Gong, K. Lee and A. J. Heeger, *Adv. Funct. Mater.*, 2005, **15**, 1617–1622.
210 D.-H. Ko, J. R. Tumbleston, W. Schenck, R. Lopez and E. T. Samulski, *J. Phys. Chem. C*, 2011, **115**, 4247–4254.
211 J. M. Lee, J. Lim, N. Lee, H. I. Park, K. E. Lee, T. Jeon, S. A. Nam, J. Kim, J. Shin and S. O. Kim, *Adv. Mater.*, 2014, **27**, 1519–1525.
212 S.-H. Jeong, H. Choi, J. Y. Kim and T.-W. Lee, *Part. Part. Syst. Charact.*, 2014, **32**, 164–175.
213 C. H. Chou and F. C. Chen, *Nanoscale*, 2014, **6**, 8444–8458.
214 S.-J. Ko, H. Choi, W. Lee, T. Kim, B. R. Lee, J.-W. Jung, J.-R. Jeong, M. H. Song, J. C. Lee, H. Y. Woo and J. Y. Kim, *Energy Environ. Sci.*, 2013, **6**, 1949–1955.
215 J. Li, L. Zuo, H. Pan, H. Jiang, T. Liang, Y. Shi, H. Chen and M. Xu, *J. Mater. Chem. A*, 2013, **1**, 2379–2386.
216 L. Müller-Meskamp, Y. H. Kim, T. Roch, S. Hofmann, R. Scholz, S. Eckardt, K. Leo and A. F. Lasagni, *Adv. Mater.*, 2012, **24**, 906–910.
217 K. Takanezawa, K. Hirota, Q.-S. Wei, K. Tajima and K. Hashimoto, *J. Phys. Chem. C*, 2007, **111**, 7218–7223.
218 C.-Y. Chou, J.-S. Huang, C.-H. Wu, C.-Y. Lee and C.-F. Lin, *Sol. Energy Mater. Sol. Cells*, 2009, **93**, 1608–1612.
219 M. Law, L. E. Greene, J. C. Johnson, R. Saykally and P. Yang, *Nat. Mater.*, 2005, **4**, 455–459.
220 M. Wang, Y. Li, H. Huang, E. D. Peterson, W. Nie, W. Zhou, W. Zeng, W. Huang, G. Fang, N. Sun, X. Zhao and D. L. Carroll, *Appl. Phys. Lett.*, 2011, **98**, 103305.
221 N. K. Elumalai, T. M. Jin, V. Chellappan, R. Jose, S. K. Palaniswamy, S. Jayaraman, H. K. Raut and S. Ramakrishna, *ACS Appl. Mater. Interfaces*, 2013, **5**, 9396–9404.
222 K. Takanezawa, K. Tajima and K. Hashimoto, *Appl. Phys. Lett.*, 2008, **93**, 063308.
223 R. Thitima, C. Patcharee, S. Takashi and Y. Susumu, *Solid-State Electron.*, 2009, **53**, 176–180.
224 Y. Hames, Z. Alpaslan, A. Kösemen, S. E. San and Y. Yerli, *Sol. Energy*, 2010, **84**, 426–431.
225 S. Yodyingyong, X. Zhou, Q. Zhang, D. Triampo, J. Xi, K. Park, B. Limketkai and G. Cao, *J. Phys. Chem. C*, 2010, **114**, 21851–21855.
226 J.-S. Huang, C.-Y. Chou and C.-F. Lin, *Sol. Energy Mater. Sol. Cells*, 2010, **94**, 182–186.
227 K. H. Lee, B. Kumar, H.-J. Park and S.-W. Kim, *Nanoscale Res. Lett.*, 2010, **5**, 1908–1912.
228 Z. Yuan, J. Yu, N. Wang and Y. Jiang, *J. Mater. Sci.: Mater. Electron.*, 2011, **22**, 1730–1735.
229 Y.-M. Sung, F.-C. Hsu, C.-T. Chen, W.-F. Su and Y.-F. Chen, *Sol. Energy Mater. Sol. Cells*, 2012, **98**, 103–109.
230 M. Ahmadi, K. Mirabbaszadeh and M. Ketabchi, *Electron. Mater. Lett.*, 2013, **9**, 729–734.

231 K. Sung Hyun, P. Sung Hwak, L. Kyoung II, K. Seon Min and C. Jin Woo, *Inorganic/organic heterojunction solar cell fabricated with ZnO nanowires, IEEE*, 2010, pp. 001636–001638.
232 J. Ajuria, I. Etxebarria, E. Azaceta, R. Tena-Zaera, N. Fernandez-Montcada, E. Palomares and R. Pacios, *Phys. Chem. Chem. Phys.*, 2011, **13**, 20871–20876.
233 H. Woo Choi, K.-S. Lee, N. David Theodore and T. L. Alford, *Sol. Energy Mater. Sol. Cells*, 2013, **117**, 273–278.
234 D. C. Olson, J. Piris, R. T. Collins, S. E. Shaheen and D. S. Ginley, *Thin Solid Films*, 2006, **496**, 26–29.
235 Z. Hu, J. Zhang, Y. Liu, Y. Li, X. Zhang and Y. Zhao, *Synth. Met.*, 2011, **161**, 2174–2178.
236 Z. Hu, J. Zhang, Y. Liu, Z. Hao, X. Zhang and Y. Zhao, *Sol. Energy Mater. Sol. Cells*, 2011, **95**, 2126–2130.
237 Z. Liang, R. Gao, J.-L. Lan, O. Wiranwetchayan, Q. Zhang, C. Li and G. Cao, *Sol. Energy Mater. Sol. Cells*, 2013, **117**, 34–40.
238 Y.-C. Ho, P.-Y. Ho, H.-C. Lee, S.-K. Chang, Y.-R. Hong and C.-F. Lin, *Sol. Energy Mater. Sol. Cells*, 2015, **132**, 570–577.
239 P. P. Boix, J. Ajuria, I. Etxebarria, R. Pacios, G. Garcia-Belmonte and J. Bisquert, *J. Phys. Chem. Lett.*, 2011, **2**, 407–411.
240 A. Manor, E. A. Katz, T. Tromholt and F. C. Krebs, *Adv. Energy Mater.*, 2011, **1**, 836–843.
241 X. Bulliard, S.-G. Ihn, S. Yun, Y. Kim, D. Choi, J.-Y. Choi, M. Kim, M. Sim, J.-H. Park, W. Choi and K. Cho, *Adv. Funct. Mater.*, 2010, **20**, 4381–4387.
242 S. Bai, Y. Jin, X. Liang, Z. Ye, Z. Wu, B. Sun, Z. Ma, Z. Tang, J. Wang, U. Würfel, F. Gao and F. Zhang, *Adv. Energy Mater.*, 2015, **5**, 1401606.
243 J. J. Intemann, K. Yao, Y.-X. Li, H.-L. Yip, Y.-X. Xu, P.-W. Liang, C.-C. Chueh, F.-Z. Ding, X. Yang, X. Li, Y. Chen and A. K. Y. Jen, *Adv. Funct. Mater.*, 2013, **24**, 1465–1473.
244 S. K. Hau, H.-L. Yip, H. Ma and A. K. Y. Jen, *Appl. Phys. Lett.*, 2008, **93**, 233304.
245 H.-L. Yip, S. K. Hau, N. S. Baek, H. Ma and A. K. Y. Jen, *Adv. Mater.*, 2008, **20**, 2376–2382.
246 C.-H. Hsieh, Y.-J. Cheng, P.-J. Li, C.-H. Chen, M. Dubosc, R.-M. Liang and C.-S. Hsu, *J. Am. Chem. Soc.*, 2010, **132**, 4887–4893.
247 S. Cho, K. D. Kim, J. Heo, J. Y. Lee, G. Cha, B. Y. Seo, Y. D. Kim, Y. S. Kim, S. Y. Choi and D. C. Lim, *Sci. Rep.*, 2014, **4**, 4306.
248 T. Tromholt, M. V. Madsen, J. E. Carlé, M. Helgesen and F. C. Krebs, *J. Mater. Chem.*, 2012, **22**, 7592.
249 Y.-J. Cheng, C.-H. Hsieh, Y. He, C.-S. Hsu and Y. Li, *J. Am. Chem. Soc.*, 2010, **132**, 17381–17383.
250 J. Jo, J. R. Pouliot, D. Wynands, S. D. Collins, J. Y. Kim, T. L. Nguyen, H. Y. Woo, Y. Sun, M. Leclerc and A. J. Heeger, *Adv. Mater.*, 2013, **25**, 4783–4788.
251 T. Yang, M. Wang, C. Duan, X. Hu, L. Huang, J. Peng, F. Huang and X. Gong, *Energy Environ. Sci.*, 2012, **5**, 8208–8214.
252 G. Cheng, W.-Y. Tong, K.-H. Low and C.-M. Che, *Sol. Energy Mater. Sol. Cells*, 2012, **103**, 164–170.
253 K.-D. Kim, D. C. Lim, M.-G. Jeong, H. O. Seo, B. Y. Seo, J. Y. Lee, Y. Song, S. Cho, J.-H. Lim and Y. D. Kim, *Bull. Korean Chem. Soc.*, 2014, **35**, 353–356.
254 S. I. Yoo, T. T. Do, Y. E. Ha, M. Y. Jo, J. Park, Y.-C. Kang and J. H. Kim, *Bull. Korean Chem. Soc.*, 2014, **35**, 569–574.
255 Y. E. Ha, M. Y. Jo, J. Park, Y.-C. Kang, S.-J. Moon and J. H. Kim, *Synth. Met.*, 2014, **187**, 113–117.
256 S. M. Yoon, S. J. Lou, S. Loser, J. Smith, L. X. Chen, A. Facchetti and T. Marks, *Nano Lett.*, 2012, **12**, 6315–6321.
257 Z. Wu, T. Song, Z. Xia, H. Wei and B. Sun, *Nanotechnology*, 2013, **24**, 484012.
258 T. Hu, F. Li, K. Yuan and Y. Chen, *ACS Appl. Mater. Interfaces*, 2013, **5**, 5763–5770.
259 J. P. Tiwari, S. Pillai, S. Parakh, F. Ali, A. Sharma and S. Chand, *Appl. Phys. Lett.*, 2014, **104**, 041114.
260 H. C. Chen, S. W. Lin, J. M. Jiang, Y. W. Su and K. H. Wei, *ACS Appl. Mater. Interfaces*, 2015, **7**, 6273–6281.
261 T. Hu, L. Chen, K. Yuan and Y. Chen, *Nanoscale*, 2015, **7**, 9194–9203.
262 M. Eita, A. E. Labban, F. Cruciani, A. Usman, P. M. Beaujuge and O. F. Mohammed, *Adv. Funct. Mater.*, 2015, **25**, 1558–1564.
263 J.-L. Lan, S.-J. Cherng, Y.-H. Yang, Q. Zhang, S. Subramaniyan, F. S. Ohuchi, S. A. Jenekhe and G. Cao, *J. Mater. Chem. A*, 2014, **2**, 9361–9370.

